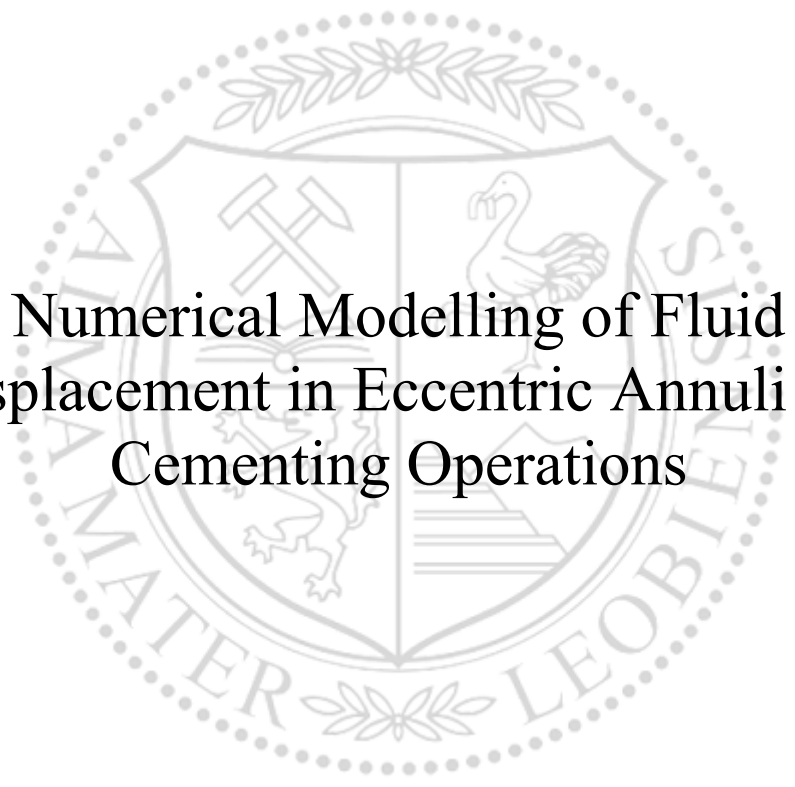




Chair of Drilling and Completion Engineering

Master's Thesis



Numerical Modelling of Fluid
Displacement in Eccentric Annuli for
Cementing Operations

Anass Al Didi

May 2022



AFFIDAVIT

I declare on oath that I wrote this thesis independently, did not use other than the specified sources and aids, and did not otherwise use any unauthorized aids.

I declare that I have read, understood, and complied with the guidelines of the senate of the Montanuniversität Leoben for "Good Scientific Practice".

Furthermore, I declare that the electronic and printed version of the submitted thesis are identical, both, formally and with regard to content.

Date 16.05.2022

A handwritten signature in blue ink, appearing to read 'Anas', written over a horizontal line.

Signature Author
Anass Al Didi

Anass Al Didi
Master Thesis 2022
Petroleum Engineering

Numerical Modelling of Fluid Displacement in Eccentric Annuli for Cementing Operations

Supervisor: Prof. Kris Ravi

Chair of Drilling and Completions Engineering

*To my grandmother for her endless support and encouragement,
you are dearly missed.*

Acknowledgments

I would like to express my sincere gratitude to my supervisor Prof. Kris Ravi for his invaluable guidance and encouragement that helped me throughout my research.

This work would not have been possible without the constant support of my family and girlfriend, thank you very much.

Abstract

Cement plays an integral role in maintaining well integrity throughout the life cycle of a well. Successful cementing jobs provide good zonal isolation and ensure strong bonding of cement to the casing and formation. The cementing job success is mainly governed by the fluid displacement efficiency and the degree of contamination with other wellbore fluids. However, displacing fluids downhole over long distances is a complex task that requires understanding of mud-spacer-cement interactions, their rheological behavior, as well as frictional pressure losses and flow regimes.

Computational Fluid Dynamics (CFD) has been proven to be a powerful tool for modelling fluid behavior in numerous industries. The use of CFD allows us to model these complexities in a precise and reliable manner, and it can provide tailored solutions for individual cementing jobs to ensure maximum job efficiency and safety. In this study, a state-of-the-art CFD model was created using Ansys Fluent software to examine the displacement efficiency of a cementing job under different conditions in eccentric annuli. The CFD model was validated in single phase simulations using two sets of experimental data. The parameters studied include fluid density and rheology, casing eccentricity, flow rate, wellbore deviation, and casing rotation. The effect of each parameter was analyzed and the data was compiled to provide guidelines for efficient fluid displacement. This study stressed the importance of maintaining density and viscosity hierarchies between the displacing and displaced fluids. The drastic effect of eccentricity on the displacement process was shown, as well as possible solutions to counteract this effect by optimizing fluid properties and flowrates. Furthermore, casing rotation proved to be a valuable tool that enhances the displacement efficiency and can partly mitigate the negative effects of high eccentricity.

The CFD model proved to be an invaluable resource for optimizing the cement placement process and can be utilized in a variety of ways to provide specialized solutions for each cementing job.

Zusammenfassung

Zement spielt eine wesentliche Rolle bei der Aufrechterhaltung der Bohrlochintegrität während des gesamten Lebenszyklus eines Bohrlochs. Erfolgreiche Zementierungsarbeiten sorgen für eine gute Zonenisolierung und stellen eine starke Bindung des Zements an die Verrohrung und Formation sicher. Der Erfolg der Zementarbeit wird hauptsächlich durch die Flüssigkeitsverdrängungseffizienz und den Grad der Verunreinigung mit anderen Bohrlochflüssigkeiten bestimmt. Das Verdrängen von Flüssigkeiten im Bohrloch über große Entfernungen ist jedoch eine komplexe Aufgabe, die ein Verständnis der Wechselwirkungen zwischen Schlamm, Abstandshalter und Zement, deren rheologischen Verhalten sowie von Reibungsdruckverlusten und Strömungsregimen erfordert.

Computational Fluid Dynamics (CFD) hat sich in zahlreichen Branchen als leistungsstarkes Werkzeug zur Modellierung des Fluidverhaltens erwiesen. Der Einsatz von CFD ermöglicht es uns, diese Komplexitäten präzise und zuverlässig zu modellieren und maßgeschneiderte Lösungen für einzelne Zementierungsaufgaben bereitzustellen, um maximale Arbeitseffizienz und -sicherheit zu gewährleisten. In dieser Studie wurde ein hochmodernes CFD-Modell mit der Ansys Fluent-Software erstellt, um die Verdrängungseffizienz einer Zementierungsaufgabe unter verschiedenen Bedingungen in exzentrischen Ringräumen zu untersuchen. Das CFD-Modell wurde in einphasigen Simulationen unter Verwendung von zwei Sätzen experimenteller Daten validiert. Zu den untersuchten Parametern gehören Fluidichte und -rheologie, Verrohrungsexzentrizität, Durchflussrate, Bohrlochabweichung und Verrohrungsrotation. Die Wirkung jedes Parameters wurde analysiert und die Daten wurden zusammengestellt, um Richtlinien für eine effiziente Flüssigkeitsverdrängung bereitzustellen. Diese Studie betonte die Bedeutung der Aufrechterhaltung von Dichte- und Viskositätshierarchien zwischen den verdrängenden und verdrängten Fluiden. Der drastische Einfluss der Exzentrizität auf den Verdrängungsvorgang wurde gezeigt, sowie mögliche Lösungen, um diesem Effekt durch Optimierung der Fluideigenschaften und Durchflussraten entgegenzuwirken. Darüber hinaus erwies sich die Gehäuserotation als wertvolles Werkzeug, das die Verdrängungseffizienz verbessert und die negativen Auswirkungen einer hohen Exzentrizität teilweise mildern kann.

Das CFD-Modell hat sich als sehr nützliche Ressource für die Optimierung des Zementierungsvorgangs erwiesen und kann auf vielfältige Weise genutzt werden, um spezialisierte Lösungen für jede Zementierungsaufgabe bereitzustellen.

Table of Contents

Acknowledgments	3
Abstract	5
Zusammenfassung	6
Table of Contents	7
Chapter 1	9
Introduction	
1.1 Background and Context	9
1.2 Project Objectives	10
1.3 Achievements	10
1.4 Overview of Dissertation	11
Chapter 2	13
Literature Review	
2.1 Cementing Overview	13
2.1.1 Well Parameters	15
2.1.2 Fluid Displacement	17
2.2 Cement Slurry Design	20
2.3 Cement Evaluation	22
2.3.1 Hydraulic Testing	23
2.3.2 Well Logging:	23
2.4 Displacement Efficiency	25
2.4.1 Fluid Properties	26
2.4.2 Pipe Eccentricity	28
2.4.3 Pipe Movement	29
2.4.4 Flow Regime	30
2.5 Experimental Work and Empirical Correlations:	31
2.6 Displacement Models:	39
Chapter 3	43
Computational Fluid Dynamics	
3.1 Governing Equations:	46
3.1.1 Conservation of Mass:	48
3.1.2 Conservation of Momentum:	48
3.1.3 Conservation of Energy:	49
3.1.4 Constitutive Relations:	50
3.2 Discretization Methods:	52

3.2.1	Finite Difference Method (FDM):	52
3.2.2	Finite Volume Method (FVM):	55
Chapter 4	57
Computational Domain		
4.1	Mesh Nomenclature:	57
4.2	Structured Grids:	58
4.3	Unstructured Grids:	59
4.4	Mesh Quality:	60
4.5	Mesh Generation:	61
4.6	Grid Convergence Study	64
Chapter 5	65
Single Phase Validation Simulations		
5.1	Model Validation: Pressure Drop	67
5.2	Model Validation: Velocity	70
Chapter 6	75
Multiphase Displacement Results and Discussion		
6.1	Eccentricity:	75
6.2	Density Vertical:	77
6.3	Density Horizontal:	80
6.4	Viscosity:	82
6.5	Flowrate:	84
6.6	Casing Rotation:	86
Chapter 7	89
Conclusion		
7.1	Summary	89
7.2	Future Work	90
References	91

Chapter 1

Introduction

1.1 Background and Context

Well integrity plays a crucial role in various operations such as drilling and production operations. The NORSOK Standard D-010 defines well integrity as “the application of technical, operational and organizational solutions to reduce the risk of uncontrolled release of formation fluids throughout the life cycle of the well”. This well integrity must be maintained throughout the entire life cycle of a well. One of the most important elements that work to ensure well integrity is cement. Cement acts as a well barrier element not only during the operational phase but also at the end of the well life cycle during plugging and abandonment.

The cementing operation is an integral part of any well. The cement is normally pumped down the string and up the annular space between the casing and borehole wall where it will set. Several steps ensure the success of the cement job. Most of these steps are related to cement slurry placement and effective mud displacement. An essential part of the cementing job is the proper and complete removal of the drilling mud that is present in the annular space. The main technique is to use a spacer fluid with modified rheological properties to improve mud displacement. This efficient mud removal is critical to not compromise cement sheath strength, obtain a strong bond of cement with formation and casing, and zonal isolation. However, poor displacements can lead to major problems in well integrity, as well as environmental issues such as contamination of freshwater aquifers and leakage to the surface.

Optimizing the fluid displacement requires understanding mud-spacer-cement interactions, flow patterns and properties, and frictional pressure losses. These factors are largely influenced by the fluids' density and rheology, wellbore geometry, casing

eccentricity, fluid volumes, and pump flow rates. The goal is to have a stable and flat fluid interface for optimal displacement. Incompatibility of these working parameters will lead to channeling, intermixing of fluids, and thus an inefficient displacement. Casing eccentricity is also a major problem, especially in highly deviated wells. The casing will normally not be completely centered in the wellbore and based on the degree of eccentricity, the fluid will have a higher displacement on the wide side and possibly bypass the narrower side.

All these complexities are difficult to account for in typical empirical and analytical solutions. This is why the industry still encounters poor cement jobs even after implementing proper techniques and best practices. This is where Computational Fluid Dynamics (CFD) comes into play. CFD models allow more accurate modeling of all these interactions to ensure the highest quality cement job. These models can account for the aforementioned complexities to provide better guidelines on cement placement.

1.2 Project Objectives

The main objective of this thesis is to evaluate the efficiency and effectiveness of the cement placement by numerical simulation using the Ansys Fluent CFD software. This simulator will also act as a “digital twin” for the experimental flow loop setup where the operating parameters and results from the simulations and experiments can be cross-checked and validated. To achieve this goal, the following sub-objectives must be completed:

- Develop a comprehensive literature review on the challenges faced during cement placement and the factors affecting it. In addition, proper modeling techniques will be reviewed to obtain accurate and reliable CFD simulations.
- Develop a reliable numerical model using Ansys Fluent and validate this model using available experimental work, analytical models, and literature.
- Run simulations for numerous test cases by varying fluid density and rheology, pump rates, casing eccentricity, and casing rotation. The data will be compiled and analyzed to examine the effect of each parameter and to give insight into how to optimize cement placement.

1.3 Achievements

In this work, a state-of-the-art CFD model was created using well-known software to make it more accessible. This model was validated against several sets of experimental data to ensure its accuracy and reliability. This model can simulate an

extensive range of fluid displacement processes and is ideal in its current state for lab-scale experiments and simulations. It serves as the digital twin for an experimental flow loop setup and will be thoroughly validated in future works. Furthermore, the model could serve as the base for more advanced models that are able to simulate larger-scale dimensions similar to typical well sizes.

1.4 Overview of Dissertation

This work starts with an overview of oilfield cementing operations. It goes through the basic procedures and the most important parameters affecting them. In addition, it includes a thorough overview of fluid displacement modeling techniques including empirical, analytical, and numerical modeling. After that, a section is devoted to the vast field of Computational Fluid Dynamics (CFD) and the general schemes and equations that govern it. This concludes the literature review. What follows is the generation of the computational domain and the setup of the CFD model. Then, the single-phase validation simulations of the CFD model against experimental data are shown and discussed. Finally, the multiphase displacement simulations are presented, the results are analyzed, and guidelines for optimizing the fluid displacement process are discussed.

Chapter 2

Literature Review

2.1 Cementing Overview

Drilling a well is typically done in stages. After reaching the planned depth of each stage, casing is run into the well to secure the wellbore. This casing is cemented to create a bond between the casing and borehole wall which secures the casing and allows for drilling of subsequent sections. Each subsequent casing is smaller in diameter than the previous one. The last and smallest casing is typically the production casing which runs directly into the reservoir. The cement provides structural support to the casing strings that support the weight of all subsequent strings. Furthermore, the well runs through different formations that might be fluid-bearing. Thus, the cement is essential to prevent communication of these formations or the leaking of hydrocarbons from the target formation to the surface and shallower freshwater aquifers (Liu, 2021). The drilling process also involves destructive rock cutting which induces a lot of shocks and vibrations that can cause severe damage to the downhole equipment. The cement provides extra support to the casing to protect it from these shock loads. Fig. 1 below shows the typical schematic of a well with the numerous cased and cemented sections (Sevillano et al., 2016).

Cementing operations are split into two main branches: primary cementing and remedial cementing. Primary cementing is the process of mixing a certain volume of cement slurry and pumping it down the well and up the annulus where it will set between the casing and borehole wall. A sufficient column of cement can firmly bond the casing to the borehole. Remedial cementing, on the other hand, is normally done to fix problems associated with the primary cementing job. It is best to avoid such remedial cementing jobs through thorough planning, design, and execution of the

primary cementing job. This would yield the most economic and successful cementing job. According to Mitchell and Lake, 2006, the main objectives of a cementing job include:

- Provide a hydraulic seal.
- Provide zonal isolation for different oil, gas, and water-bearing zones.
- Prevent blowouts
- Seal off lost circulation and thief zones.
- Protect water aquifers.
- Provide structural support for the casing.
- Protect casing from corrosion.

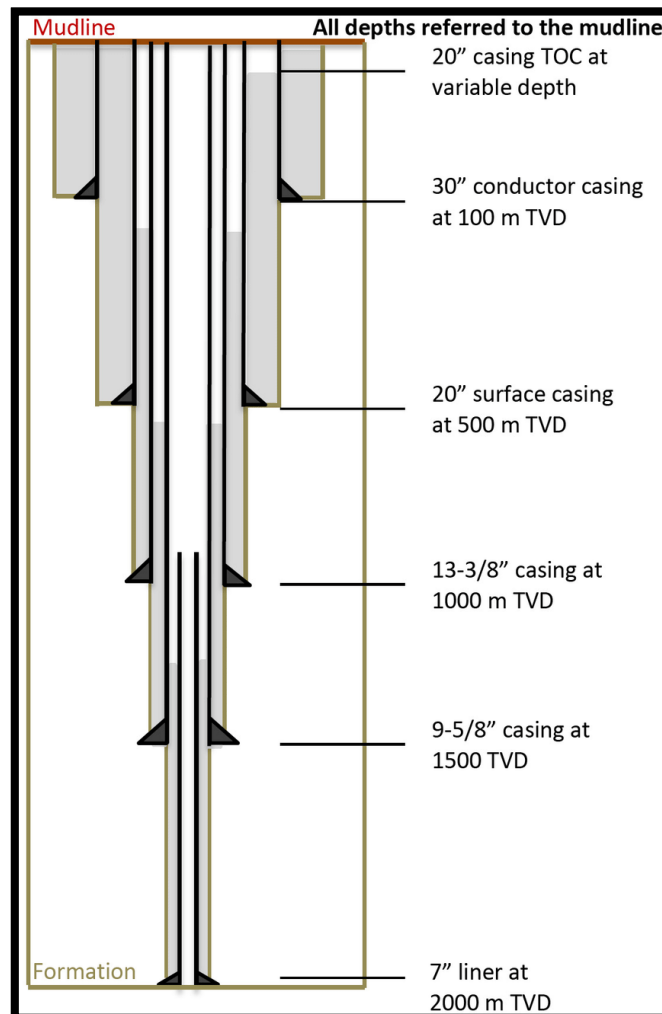


Figure 1. Typical Well Schematic (Sevillano et al., 2016)

Mitchell and Larry, 2006, further defined five steps that are required to ensure a successful cement placement and fulfill the objectives mentioned above:

1. Analyze the well parameters, define the requirements of the well, and design the cement placement to ensure an adequate job throughout the lifecycle of the well.
2. Calculate slurry composition and do laboratory testing to ensure it meets all requirements.
3. Calculate the volume of fluid needed, then mix and pump the slurry into the annulus.
4. Monitor the job in real-time, compare with a plan, and adjust as necessary.
5. Evaluate the results, compare with the plan, and apply lessons learned for future jobs.

2.1.1 Well Parameters

The design of the cement job requires very thorough planning and consideration of each well's unique parameters that will have a great impact on the success of the cement job.

2.1.1.1 Well depth

The depth of the well will influence the volume of fluids to be handled, the hydrostatic pressure to overcome, the frictional pressures, the formation fracture pressure, and the temperature. All these parameters are directly involved in the design of the cement slurry. The depth also influences the hole and casing sizes used, and with very deep wells, HPHT conditions pose a significant challenge.

2.1.1.2 Wellbore geometry

The wellbore geometry influences the amount of cement required to create an adequate cement interval. The hole size, casing size, washouts, and casing determine the annular volume and amount of fluid needed. The hole size (including washouts and casing) can be measured in a variety of ways, which involve using different types of calipers.

These sizes also determine the diameter of the annular space which has an impact on the effectiveness of the mud displacement. Smaller annular spaces restrict the flow

and make it more difficult to displace the fluids in the wellbore. A minimum annular space of 0.75 to 1.5 inches is generally recommended.

Furthermore, the inclination angle of the wellbore is an aspect of major importance. Highly deviated wells can be problematic because the casing is likely not centered in the hole. This eccentricity creates different velocity profiles on the wide and narrow sides of the annulus which can lead to channeling and inefficient displacement. This problem can be overcome by using centralizers on the casing to keep it centered in the borehole. However, adding too many centralizers also creates the problem of excess drag and might lead to stuck pipe. There is always a trade-off to be done to ensure the most efficient cement job.

2.1.1.3 Temperature

There are 3 temperatures to consider for the cementing job, the bottom hole circulating temperature (BHCT), the bottom hole static temperature (BHST), and the temperature differential (temperature difference between top and bottom of cement). These temperatures can be measured by temperature probes that are circulated with the fluids. The BHCT is the temperature the cement encounters while it is being circulated. This temperature affects slurry thickening time, fluid loss, settling, rheology, and setting time. The BHST is the temperature when the fluids are not in motion in the wellbore. This influences the compressive strength development and the integrity of the cement sheath throughout the lifecycle of the well. The temperature differential is influential when there exists a large cement interval, and the temperature varies greatly between the top and bottom of the cement interval. To cater for this temperature differential, two cement slurry designs are typically required to ensure an efficient cement job considering both temperatures. Downhole temperature recorders are recommended to be used to accurately measure downhole temperatures. The cementing job should be designed based on actual downhole circulating temperature to ensure the optimum cost and displacement efficiency are achieved.

2.1.1.4 Formation Pressures

Estimations of pore pressure, fracture pressure, and information about the rock characteristics must be known for the design of the cement job. These parameters are normally determined by analogy, and then validated during the drilling phase. These pressures are reflected in the density of the drilling mud which is determined and limited by the pore pressure and fracture gradient. The range between these two

pressures is known as the “mud window”. To maintain safe operations and ensure the success of the cementing job, the hydrostatic pressure of the wellbore fluids (cement, drilling fluid, spacer...etc) in addition to the friction pressure created by the fluids’ movement must not exceed the fracture pressure of the weakest formation. The fracture pressure is the pressure at which the formation will break down. If this happens, then we will have lost circulation and the cement will be partially or completely lost into the formation resulting in an ineffective seal and compromising the well integrity.

2.1.1.5 Formation Characteristics

The compatibility of the cement slurry with the formations exposed to it must be assessed. For example, some shales are sensitive to fresh water and can create a sloughing problem. To counter this problem, special precautions have to be taken such as increasing the salinity of the water used. Other considerations also have to be accounted for such as swelling clays, high pH fluids, formations containing flowing fluids, corrosive fluids, high-pressure fluids, or other complex features that can influence the properties of the cement slurry and its integrity.

2.1.2 Fluid Displacement

The most common practice for primary cementing jobs is the two-plug displacement technique (Nelson, 2012). The casing is lowered into the borehole after completing drilling of a section. The drilling fluid might fill the inside of the casing while it is being lowered. The main purpose of this cementing job is to displace the drilling fluid from the inside of the casing and annulus (to a pre-determined depth) and replace it with cement. However, cement slurries and drilling fluids are typically chemically incompatible. If the two fluids are mixed and commingled, this can lead to creating a highly viscous and gelled fluid that hinders the proper placement of the cement slurry. For this reason, chemical and physical practices are employed to ensure the fluids remain separated. Chemical washes and spacer fluids need to be pumped before the cement slurry to clean the wellbore and provide an adequate fluid interface for the displacement process. In addition, wiper plugs are used to physically separate the fluids pumped inside the casing. Two plugs are used: the top plug separates the cement slurry from the displacement fluid (typically drilling fluid, water, or brine), and the bottom plug separates the cement slurry from the drilling fluid or spacer fluids below. The bottom is designed to rupture which creates a pathway for the cement

slurry into the annulus. The top plug does not rupture, so when the cement slurry is pumped completely, the top plug creates a hydraulic seal between the annulus and casing interior. Finally, the crew waits on cement (WOC) which means waiting for the cement to set and develop compressive strength. Fig. 2 below is an illustration of how this process works.

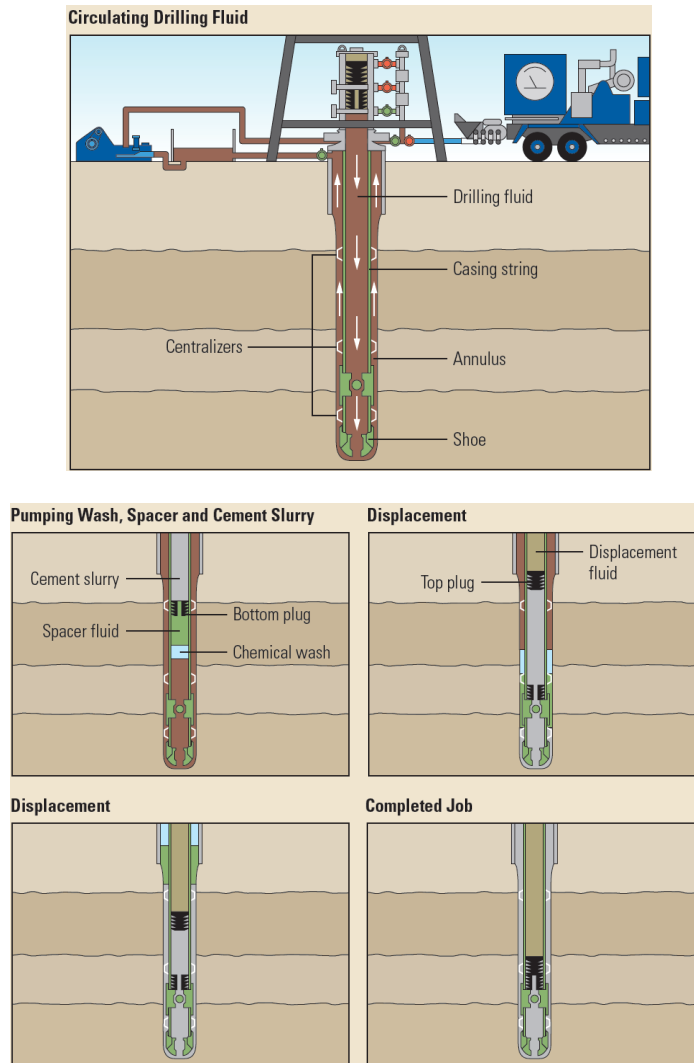


Figure 2. Primary cementing job with two-plug technique (Nelson, 2012)

Numerous factors contribute to the success or failure of a cementing job. A decent number of these factors relate to the properties of the fluids pumped through the wellbore and their condition. For this reason, there exist practices and guidelines that aim at providing the best conditions for the cement placement process. These factors include:

2.1.2.1 Mud Conditioning

The condition of the drilling fluid plays a vital role in the efficiency of the cement placement process. After drilling stops and the drilling fluid is at rest, pockets of gelled fluid typically form. This gelled fluid increases the complexity of the displacement and needs to be broken up to re-establish adequate drilling fluid mobility. Therefore, it is recommended to circulate the drilling fluid at least 2-3 borehole volumes after running the casing and before commencing the cementing operation (Mitchell and Larry, 2006). This results in a low gel strength fluid which is easier to displace. It also cleans out cutting and other debris and reduced bottom hole temperature. Pipe movement i.e., reciprocation and rotation, also assists in breaking gelled pockets and enhancing fluid mobility. Additionally, hole cleaning can be enhanced by varying the drilling fluid pumping rates. The following steps are helpful for conditioning the mud for a cement job:

- Don't allow the drilling fluid to be static for extended periods of time, especially under high temperatures. Keep circulating whenever possible until the displacement process begins.
- Condition the borehole by circulating an appropriate volume of drilling fluid until equilibrium is reached.
- Vary the flow properties of the drilling fluids for optimum cuttings removal and fluid mobility.
- Regularly conduct gel strength tests and account for downhole pressure and temperature conditions to develop an accurate model for the gel development of the drilling fluid.
- In highly deviated wellbores, a higher viscosity drilling fluid might be needed to ensure that the gelled drilling fluid and cuttings do not settle on the bottom side of the annulus.

2.1.2.2 Spacers and Washes

Spacers and chemical flushes/washes are important because they separate the typically incompatible drilling fluid and cement slurry, thus creating a favorable fluid interface for efficient displacement. They can be designed to displace water-based and oil-based drilling fluids. In addition to aiding in the removal of gelled drilling fluid to pave the way for a better cement bond, spacer fluids can serve numerous needs. For instance, weighted spacer fluids can assist with well control. Reactive spacer fluids can increase the effectiveness of the removal of gelled drilling fluids. A vital role of the spacer fluid is to create interfaces of drilling fluid/spacer and spacer/cement. It is

necessary also to thoroughly plan pumping the spacer in terms of optimum pump rates, the volume of spacer needed, and contact time at each point in the well to achieve the best displacement (Liu, 2021).

Chemical flushes also serve to separate the drilling fluid and cement slurry, but they have the added benefit of thinning and dispersing drilling fluid particles. They can also be designed to displace water-based and oil-based drilling fluids. These flushes assist in preparing both the formation and the casing for the cementing job. Flushes also go by the name of washes or pre-flushes.

2.1.2.3 Displacement Fluid

This fluid is used to displace the cement slurry from the casing interior into the annulus. The displacement fluids typically used are drilling fluid, completion fluid, or water. For maximum efficiency and simplicity, the displacement fluid used should be the one needed for the next operation in the borehole, otherwise the fluid used needs to be fully circulated out of the well before commencing the next operation. Additionally, this fluid can be heated to reduce the setting time of cement where cold formations are encountered.

2.2 Cement Slurry Design

The design of the cement slurry should meet the demands of each particular well as the conditions of these wells can vary significantly. The cement slurry can be modified to desired specifications by adding and mixing in chemical compounds commonly known as additives. Cement slurry design is influenced by many parameters including:

- Well depth
- Quality of mix water
- BHCT
- BHST
- Fluid-loss control
- Flow regime
- Drilling fluid's hydrostatic pressure
- Type of drilling fluid (water-based/oil-based)
- Settling and free water
- Gas migration potential

The additives typically have a primary effect which is desirable and beneficial for the cement slurry. However, most chemical additives also have a secondary effect which

can be either beneficial or harmful for the cement slurry placement. This leads to the use of various additives to counter the negative side effects of other additives and ensure that we get the beneficial factor of each additive used. This trade-off interaction between the additives serves as the basis for cement slurry design. We cannot measure accurately the interaction of these additives with the cement and each other, but we can measure their physical effect on the cement slurry performance properties. The slurry performance properties typically measure include compressive strength, thickening time, fluid loss, rheology, free fluid, and slurry stability. The ideal slurry must maintain a stable density for hydrostatic control, have negligible measurable free water, provide proper fluid-loss control, and contain sufficient retarders to ensure proper placement.

The additives used for cement slurry modification fall into broad categories. The main categories will be explained in the following section (Liu, 2021).

Accelerators: these chemical compounds reduce the thickening time of the cement slurry which is the time required for the cement slurry to solidify. They can also increase the rate of compressive strength development of the cement slurry. Accelerators are useful when we are dealing with a low-density cement slurry or when the formations exposed to the slurry have low temperatures. Typical accelerators include Calcium Chloride (CCl₂), Sodium Chloride (NaCl), Potassium Chloride (KCl)...etc.

Retarders: these chemical compounds are the opposite of accelerators which means they increase the thickening time of the cement slurry. The cement typically used for oilfield purposes does not have a sufficient thickening time if the BHCT exceeds 38°C (100°F). Thus, retarders are required to increase the thickening time of these cement slurries to sufficient values. Typical retarders include Lignosulfonates, Cellulose derivatives, Hydroxycarboxylic acids...etc.

Lightweight Additives/Extenders: Cement slurries without additives normally have a slurry density exceeding 15 ppg. However, weak formations with low fracture pressures are commonly encountered in all parts of the world. This creates a fractured formation and severe lost circulation problem if these high-density slurries are used. Thus, these lightweight additives decrease the density of the cement slurry to maintain the fluid hydrostatic pressure below the formation fracture pressure during cement placement.

Foaming Agents: foamed cement is created by adding when nitrogen (most commonly used) is injected at high pressure into a cement slurry that consists of a foam stabilizer and a foaming agent. Nitrogen is typically used which is considered inert and does not

affect the cement hydration process. Foamed cement provides plenty of advantages which include:

- Lightweight slurry
- Excellent strength to density ratio
- Enhances mud removal
- Prevents gas migration
- Improves zonal isolation
- Provides fluid-loss control
- Stable at high temperatures

The disadvantage associated with foamed cement is that its operation is more complex than a typical cement slurry and it requires additional specialized cementing equipment.

Weighting Agents: these agents are required when a high-density cement slurry is needed to control high-pressure wells. They are normally required for densities above 17 ppg. These agents should also be chemically inert and should not interfere with logging tools. Typical weighting agents include Hematite (Fe_2O_3) and Barite (BaSO_4).

Dispersants: these are also referred to as friction reducers. They are used to improve the rheological properties of the cement slurry. Using dispersants results in lowering the frictional pressure exerted when pumping the cement slurry. This leads to several advantages:

- Reduces surface pumping pressure required to pump the cement slurry.
- Reduces surface horsepower required to pump the cement slurry.
- Reduces pressure exerted on the formation, thus preventing lost circulation.

Fluid-loss-control Additives: these additives work to ensure a sufficient volume of fluid remains in the cement slurry so as not to alter its properties. Cement slurries with no fluid-loss control additives normally exhibit an API fluid loss that would be considered excessive if permeable formations are encountered or in the case of long cement columns. Therefore, these additives are required to reduce this fluid loss value to acceptable levels to ensure that the cement slurry properties remain unaltered.

2.3 Cement Evaluation

After the cement has set and the cementing job is completed, the integrity and quality of the cement sheath must be evaluated. Hydraulic testing and well logging are

common techniques to ensure that the cement sheath meets the planned design criteria.

2.3.1 Hydraulic Testing

Pressure testing is the most used hydraulic testing technique to evaluate the integrity of the cement sheath. The first step is to perform a casing pressure test which aims at verifying the mechanical integrity of the casing string. Then, the casing shoe is drilled out. The driller would then increase the casing internal pressure until it goes beyond the maximum pressure encountered in the next drilling phase, this is known as a pressure integrity test. If there is no leakage, the test is successful, and the cement is considered as properly sealing. The wellbore pressures are continuously monitored throughout the life of a well to evaluate the integrity of the cement sheath. Fig.3 below is a basic representation of how a pressure test works.

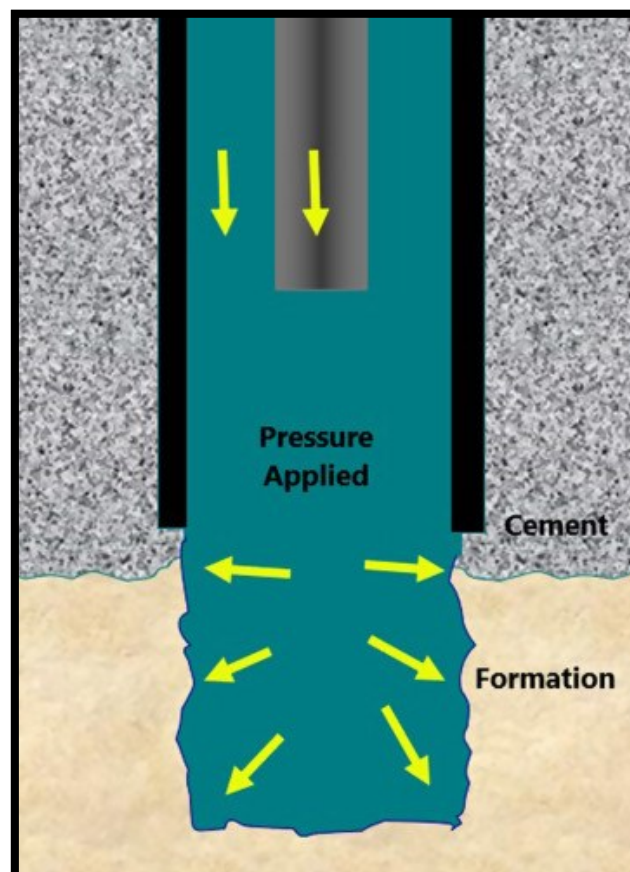


Figure 3. Pressure test (Harris, 2021)

2.3.2 Well Logging:

Logging consists of lowering a measuring device into the borehole, taking measurements, and plotting these measurements versus depth. Several well logs can

be used to examine the integrity and quality of the cement job. The most widely used logs include:

2.3.2.1 Temperature logs

These logs can give an indication on the location of the top of cement in the annulus. The cement hydration process is an exothermic reaction that causes an elevated temperature in its surroundings. By examining the temperature log, one can look for a deviation from the normal temperature gradient which is caused by the cement hydration process. However, the log must be run in the time window when the hydration reaction is taking place for the log to be effective. Furthermore, there is significant uncertainty associated with determining the exact top of cement using this method. A solution might be to make several runs to compare and average the measurements for a better estimation of the top of cement (Benge, 2015). Fig. 4 below shows a typical temperature log where you can spot the deviation from the normal gradient corresponding to the presence of cement.

2.3.2.2 Cement Bond Log (CBL)

The cement-casing and cement-formation interfaces can be analyzed with the help of data acquired from acoustic and ultrasonic logging. These logs provide information about the cement sheath and how well it bonds to the formation and casing. The most common of these logs is the CBL. The CBL consists of a logging tool run in the casing that transmits an acoustic signal, and the reflected amplitude from this signal is measured and presented in the log. The attenuation of the reflected signal gives a direct indication of the cement-casing bond integrity. Furthermore, an acoustic log presents the waveforms of the reflected signal detected. This log can give a qualitative assessment of the cement sheath, casing, and formation. Fig. 5 below shows a typical CBL used to evaluate the quality of a cement job (Nelson, 2012).

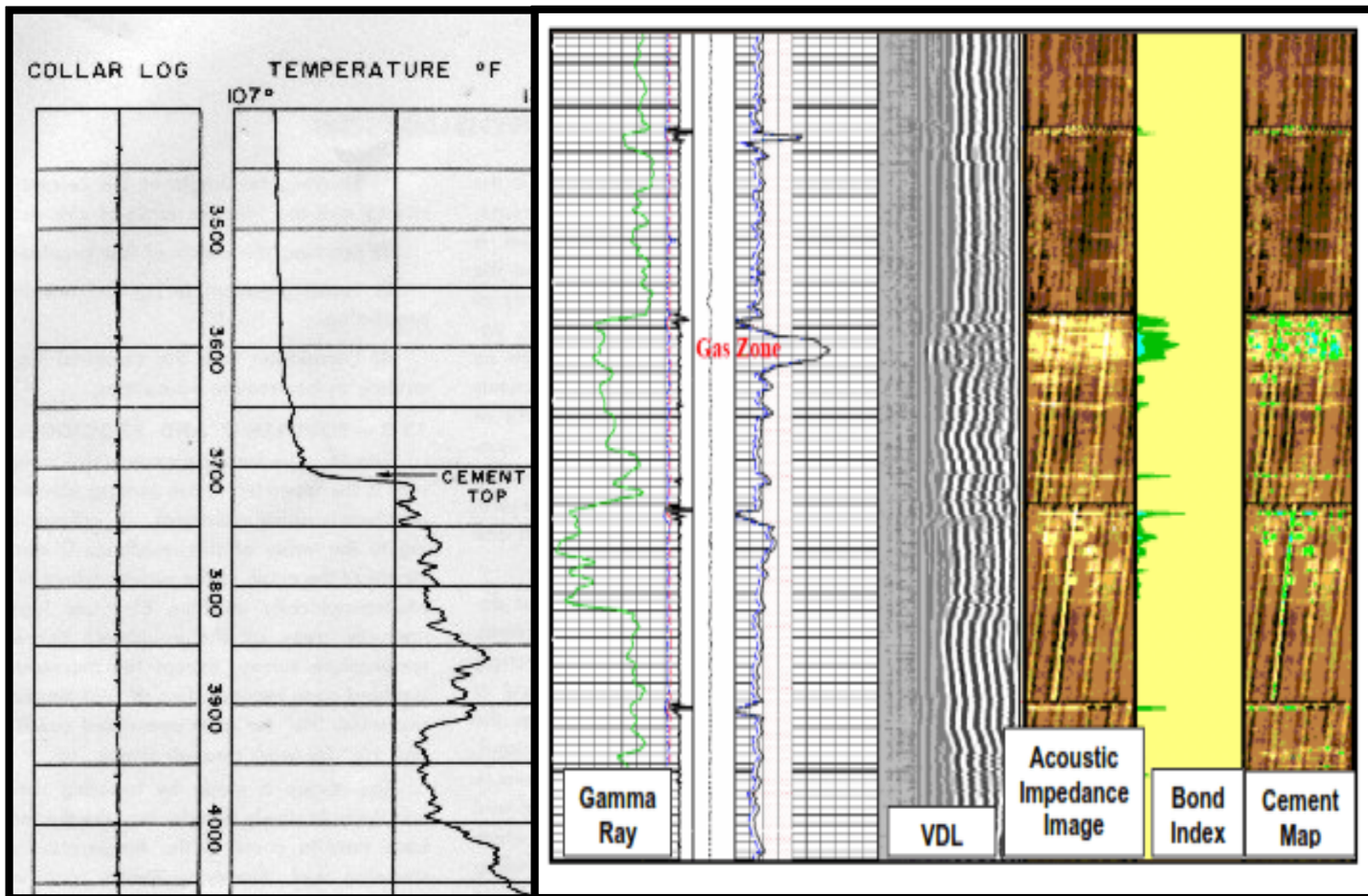


Figure 5. Temperature Log (Crain, 2006)

Figure 4. Cement Bond Log (Drilling Manual, 2021)

2.4 Displacement Efficiency

The displacement efficiency is defined by Liu, 2021 as “the percentage of the annular volume that is occupied by cement.” As discussed before, one of the essential factors to achieve a successful cementing job is the effective removal of the drilling fluid from the wellbore. Thus, efficient fluid displacement and cement placement is a procedure that requires thorough planning and understanding. A high displacement efficiency is associated with a flat and stable drilling fluid/spacer/cement interface which ensures that the cement will satisfy its intended functions. However, low displacement efficiencies are associated with instable drilling fluid/spacer/cement interfaces, excessive mixing, and cement contamination. This results in a poor cementing job which compromises the well integrity. Fig. 6 below shows varying displacement

efficiencies to illustrate its effect on the cement sheath where we can see equal distribution in (A), and then different instabilities and channeling behaviors that have adverse effects on the success of the cementing job.

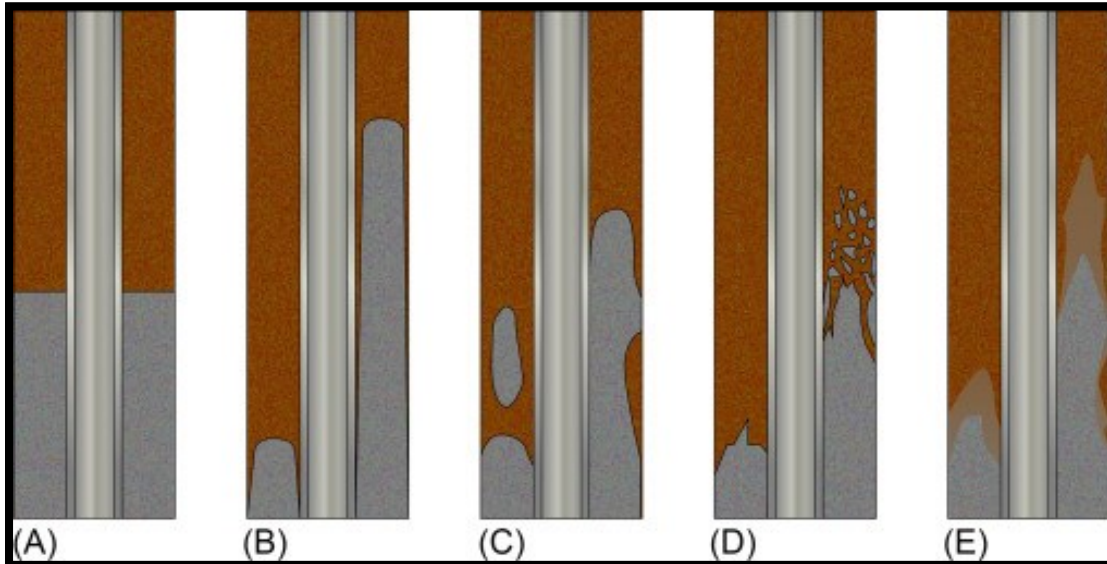


Figure 6. Displacement efficiency illustration (Dai, 2021)

There are several factors that affect the displacement efficiency. The main variables directly affecting the quality and reliability of the cementing job will be discussed below. They include but are not limited to:

- Fluid density, rheology, and composition
- Fluid velocity (pumping rate) and circulating times
- Pipe Eccentricity
- Pipe Movement
- Hole Inclination
- Fluid Losses and Lost Circulation

2.4.1 Fluid Properties

Density: studies have shown that the buoyant force resulting from the density difference between the mud, spacer and cement has less impact on the displacement than expected. These studies were conducted on test setups in a vertical position with eccentric pipes. Increasing the density difference did not seem beneficial to counter the reduced mobility of the drilling fluid on the narrow side of the annulus. However, other experiments on inclined annuli showed that a higher density of the displacing fluid assisted in displacing the bypassed drilling fluid on the narrow side of the annulus. In highly inclined wellbores, a higher density difference between the displaced and

displacing fluids at low flow rates increases the buoyancy of the displaced fluid. This assists the heavier displacing fluid in moving down from the wider annular gap to the narrow one, thus resulting in a higher displacement efficiency. In a similar manner, the heavier displacing fluid in a horizontal wellbore will be pushed down by gravity from wider annular side on top to the narrow side on the bottom, which results in removing the displaced fluid on the narrow side and increasing the displacement efficiency. Therefore, the effect of density on displacement efficiency is minimal in vertical wellbores as long as the density hierarchy is maintained. However, in highly inclined and horizontal wellbores, we observe a buoyancy-dominated flow and the effect of increased density on the displacement efficiency becomes apparent (Foroushan et al, 2021).

Rheology: as discussed before, the drilling fluid must be properly conditioned before commencing the cementing operation. This is due to the fact that the drilling fluid is designed to facilitate the drilling operation, which does not necessarily mean that it is optimized for drilling fluid displacement and cement placement. The rheological properties of the drilling fluid, which are apparent viscosity, yield strength, and gel strength, should be optimized to facilitate the removal of the drilling fluid in the cementing phase after completing drilling of a section. This means preventing excessive filter cake formation and build-up of gelled drilling fluid. Several efforts have been made to study the effect of these properties on the displacement efficiency. These studies have concluded that a high viscosity ratio, which is the ratio of the viscosity of the displacing fluid to the viscosity of the displaced fluid, increases the displacement efficiency. In addition, the gel strength of the mud should be low enough to allow it to be broken up and displaced by the displacing fluid. The yield strength of the mud and spacer should also be low to avoid trapping the fluids in the narrow annular side. Fig. below shows the effect of rheology (represented by the power-law index n) on the velocity profile of the fluids and the displacement efficiency.

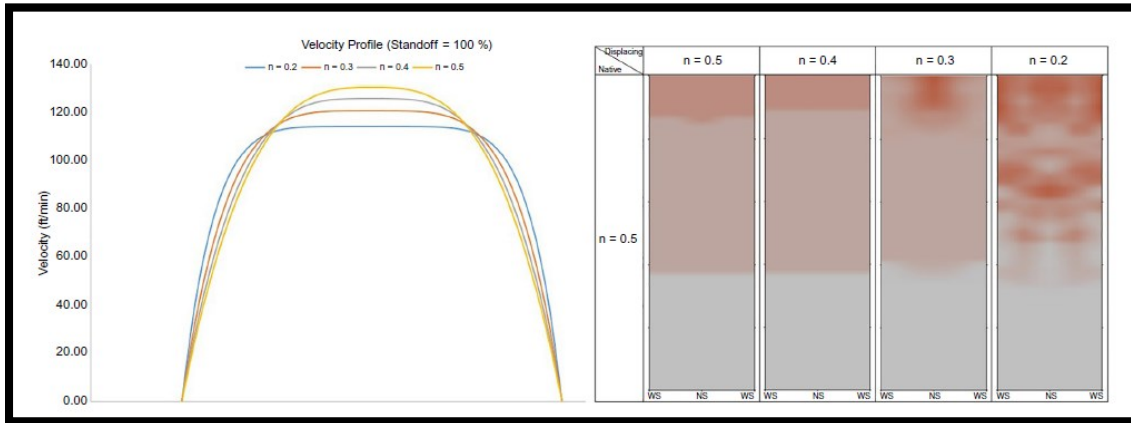


Figure 7. Effect of power law index on velocity profile and displacement efficiency (Foroushan et al, 2021)

2.4.2 Pipe Eccentricity

Pipe eccentricity or stand-off is defined as the minimum radial distance between the pipe and the borehole wall. Centralization of the pipe or casing is typically defined in terms of the stand-off ratio (SOR), this SOR is illustrated in Fig. 7 below.

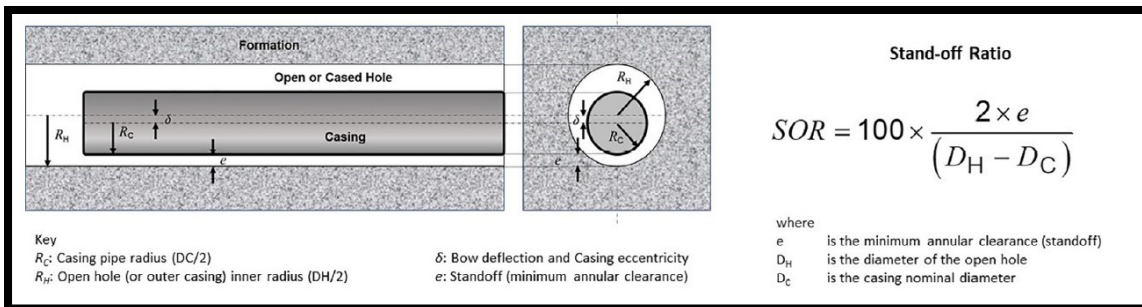


Figure 8. Pipe Stand-Off Ratio Definition (Liu, 2021)

Due to the eccentricity, the cement will tend to have higher annular velocities in the wider gap and lower velocities in the narrow gap. This will have a significant impact on the efficiency of the mud removal on the narrow side of the annulus. This detrimental effect can be visualized in Fig. 8 below using the 3D annular velocity profiles of the fluids during the displacement process. This emphasizes the need to keep the highest possible stand-off. The use of centralizers is usually employed to keep the casing concentric to a certain extent. However, these centralizers induce a significant drag force that may be problematic. Even with centralizers, this issue appears to be still difficult as the casing can sag and bend between the centralizers resulting in a non-uniform stand-off at different locations in the well. Thus, it is of utmost importance to consider the effect of eccentricity on the cementing job because it can lead to major

issues such as mud channels which result in an inadequate bond between the casing/borehole and cement.

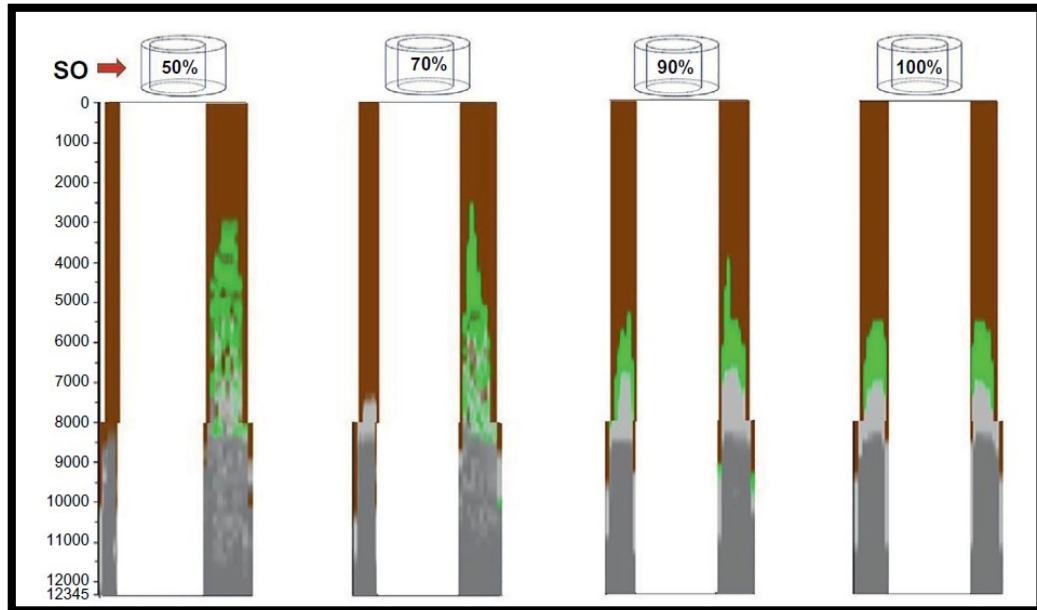


Figure 9. Visualization on the effect of casing eccentricity on displacement efficiency (Liu, 2021)

2.4.3 Pipe Movement

Several researchers investigated the idea that pipe movement, reciprocation, and rotation, assisted in improving the displacement process. Experimental studies have shown that rotating the casing while cementing has a beneficial impact on the displacement efficiency and reduces the need for remedial cementing jobs. It was seen that casing rotation has a negligible impact in concentric annuli, whereas its impact on displacement efficiency is substantial in eccentric annuli. The pipe rotation increases the displacement efficiency because it can assist in balancing the flow in the annulus by exerting shear forces on the stuck mud pockets on the narrow annular side, thus increasing the mobility of the drilling fluid on the narrow side. However, careful consideration should be put into the design and number of centralizers used if the casing is to be rotated during the cementing job. This is important because of the torque limitations of surface equipment and connections especially in highly deviated and horizontal wells where torque increases greatly. Furthermore, the casing rotation will also affect the equivalent circulating density (ECD) which should be accounted for to avoid fracturing the formation and lost circulation. In addition, casing reciprocation can also enhance displacement efficiency although not as effectively as casing

rotation. The reciprocation can also assist in breaking gelled drilling fluid and increasing the mobility of stuck pockets, especially on the narrower side of the annulus. Fig. 9 below shows the impact of casing rotation on the displacement efficiency where we can see how the fluid interface is more uniform and stable when we increase the casing rotational speed.

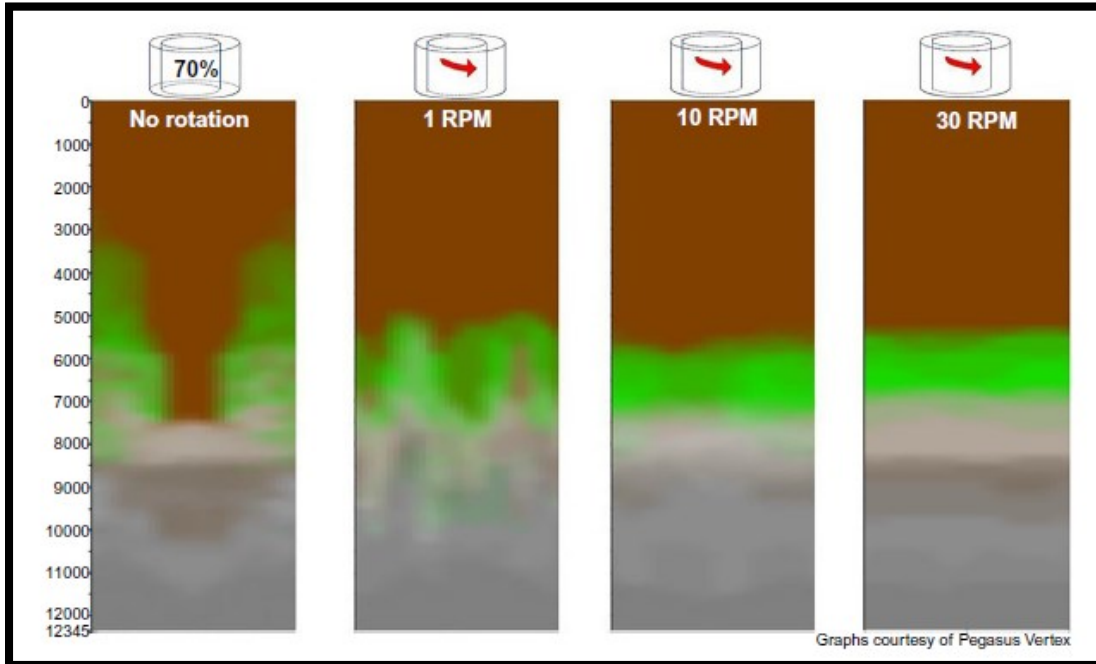


Figure 10. Effect of casing rotation on displacement efficiency (Liu, 2021)

2.4.4 Flow Regime

Several researchers have studied the effect of laminar and turbulent flows on the displacement process. Parker et al. showed that efficient displacements can be achieved at low flow rates as long as there is enough density, viscosity, and gel strength difference between the displacing and displaced fluid. For these identical fluids, increasing the flow rate further resulted in decreasing the displacement efficiency (Parker et al, 1965). However, other researchers have suggested that pumping the displacing fluid in turbulent flow would enhance the displacement efficiency if the contact time of the fluid was sufficient. But pumping the displacing fluid in turbulent regime does not necessarily mean that the displaced fluid is also experiencing turbulent flow. The displaced fluid might need greater pressure drops than produced by the turbulent displacing fluid for efficient displacement. Furthermore, eccentric annuli require higher flow rates than concentric ones to achieve turbulent flow throughout the whole annulus. Increasing the flow rate might lead to unstable interfaces and increase fluid fingering and intermixing. These high flow rates might

also be a problem in terms of formation fracture pressures and lost circulation. So, thinning the cement to allow for turbulent flow might not be efficient as it might not be able to displace the more viscous mud which leads to inefficient displacements (Foroushan et al, 2021). Thus, it can be concluded that varying solely the flow regime is not a direct influencer on the quality of the cement job. But the most important parameter is to establish an adequate density and viscosity hierarchy which in turn will lead to efficient displacements.

2.5 Experimental Work and Empirical Correlations:

Numerous researchers have conducted experimental work to attempt to create a set of rules and correlations that can assist in the cement placement process. These correlations have provided important guidelines for good cementing jobs over the years. However, they are often not easily extrapolated to operating conditions outside the range at which their studies were made. In the next section, I will discuss some of the work done in this area. To begin with, Lockyear et al, 1990, attempted to create a set of rules that can predict the fluid behavior under all conditions. Lockyear et al. defined 3 conditions that must be satisfied for successful cement placement.

1. **Mud Displacement:** the gelled mud must be broken down before pumping the cement so that the mud can flow in the entire annulus. If the pipe is not being rotated or reciprocated, the only force acting on the mud is the frictional pressure drop. Thus, to break down the gelled mud, the wall shear stress (τ_w) generated by this frictional pressure drop should be greater than the mud's gel strength (τ_g). The wall shear stress in annuli can be expressed as follows:

$$\tau_w = \frac{b}{2}(\Delta P)$$

This results in the following general rule:

$$\frac{b}{2}(\Delta P) > \tau_g$$

where b is the width of the narrow annular gap, and ΔP is the frictional pressure drop. The wall shear stress can be increased either by decreasing the eccentricity (which increases b), or by increasing the flow rate (which increases

the pressure drop). The gel strength of the mud (τ_g) can also be decreased by circulating and conditioning the mud before the casing is run in the hole.

- 2. Yield Stress:** after breaking down the gelled mud, the mud will be able to flow throughout the entire annulus. But now, we need to consider the yield stress of the fluids to be able to pump them. Here we have 2 main forces: the frictional pressure drop, and the hydrostatic pressure drop caused by the density differences between the fluids. Fig. 11 below shows the displacement of fluid A by fluid B in an inclined wellbore. As mentioned previously, the fluid will take the path of least resistance. So, fluid B will flow faster on the wider side of the annulus which leaves fluid A stuck or moving slowly on the narrower side. To ensure that fluid A will also move in the narrow side of the annulus, the wall shear stress (τ_w), caused by both frictional and hydrostatic pressure drops, should exceed the yield stress of fluid A. This translates into the following equation:

$$|\Delta P + (\rho_B - \rho_A)g \cos \theta| > \frac{2\tau_{yA}}{b}$$

This equation can be rearranged into a dimensionless form:

$$\left| \frac{\Delta P}{\frac{2\tau_{yA}}{b}} + \frac{(\rho_B - \rho_A)g \cos \theta}{\frac{2\tau_{yA}}{b}} \right| > 1$$

which means:

$$\left| \frac{\text{pressure}}{\text{yield}} + \frac{\text{density}}{\text{yield}} \right| > 1$$

Fluid A will be able to flow in the narrow side of the annulus if the above inequality is satisfied.

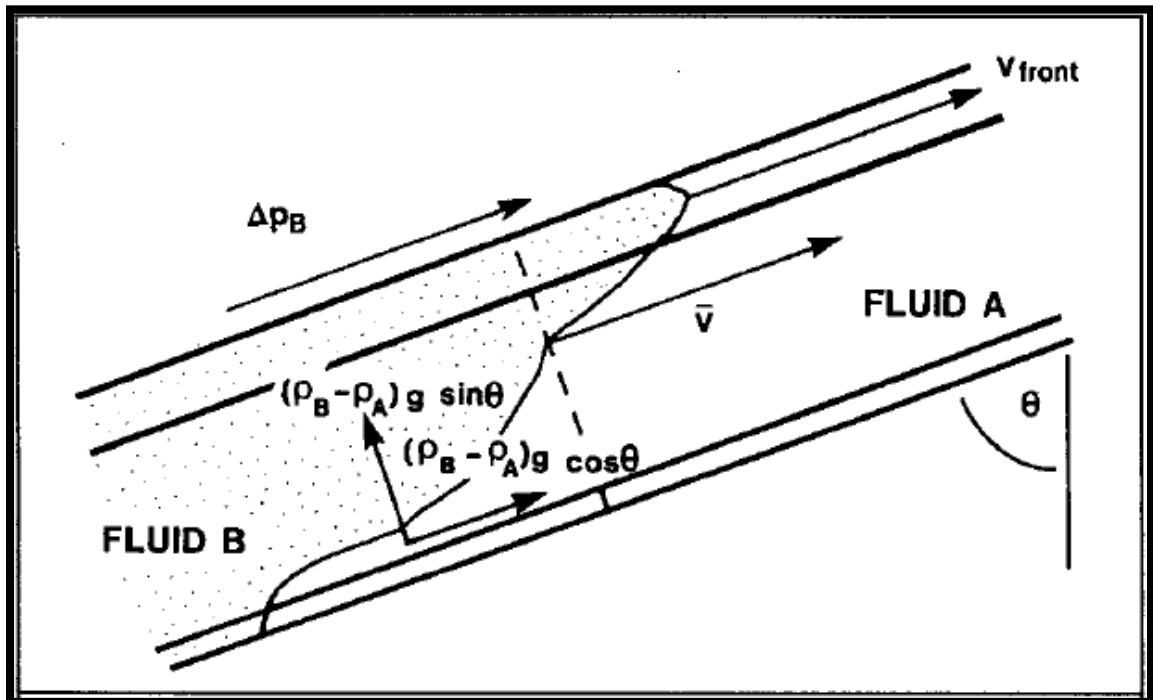


Figure 11. Forces acting on the fluids during displacement in an eccentric inclined annulus (Lockyear et al, 1990)

3. **Channeling:** a third crucial aspect of a successful cementing job is to eliminate channeling and intermixing of the pumped fluids. This can be done by controlling the operating parameters to achieve a stable interface between the fluids. The most important requirements for achieving a stable interface are the density and viscosity hierarchies, i.e., the displacing fluid must have a higher density and viscosity than the displaced fluid. If these hierarchies are not maintained, the interface will be considerably unstable and would result in intermixing and channeling of the displacing fluid. Fig. 12 below shows the possible mechanisms involved in displacing a heavier fluid with a lighter fluid in an eccentric vertical wellbore. The lighter fluid has the tendency to move up the wide side of the annulus creating channels. This leads to the heavier fluid on the narrow side dropping downwards and mixing into the wider side where it is carried by the higher velocity flow.

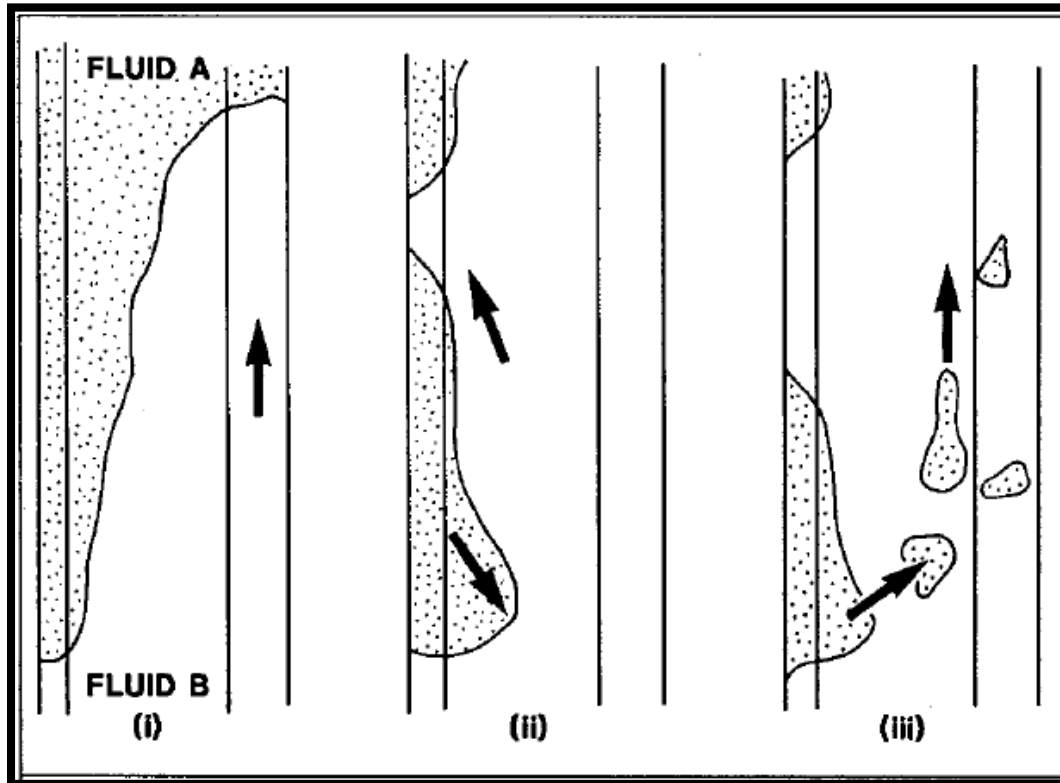


Figure 12. Illustration of channeling and mixing during displacement between a denser fluid (Fluid A) and a lighter fluid (Fluid B) (Lockyear et al, 1990).

Another general rule was suggested by Couturier et al, 1990, that assists in the fluid displacement in eccentric annuli. This rule was to achieve a higher velocity of the displaced fluid in the narrow annular gap than that of the displacing fluid in the wide annular gap. This translates to the following equation:

$$\left(\frac{dp}{dl}\right)_1 + \rho_1 g \cos \theta < \left(\frac{dp}{dl}\right)_2 + \rho_2 g \cos \theta$$

where $\frac{dp}{dl}$ is the frictional pressure gradient, and the subscripts "1" and "2" represent the displaced fluid and the displacing fluid, respectively.

Kroken et al, 1996, developed a requirement for horizontal and near-horizontal wells. They suggested that the buoyancy forces must exceed the inertial forces so that the displacing fluid is able to move to the narrow lower sections of the annulus and displace the displaced fluid. This translates to the Froude number being less than unity, as per the following equation:

$$\frac{1}{Fr^2} = \frac{gd_o(\rho_2 - \rho_1)}{\rho_1 \bar{v}^2} > 1$$

where d_o is the wellbore diameter, and \bar{v} is the average velocity.

Numerous experimental setups have been created to study this fluid displacement process and the parameters affecting it, I will introduce some of them in the following section. The University of Tulsa houses a Displacement and Mixing Facility where Foroushan et al, 2020, conducted experiments for fluid displacement in annuli. Fig. 13 shows an illustration of the facility and test section, while Table 1 shows the specifications of the test section. The facility consisted of two tanks for mixing the displaced and displacing fluids. The fluids were circulated through different lines to the test section by using 3-way pneumatic valves. The test section consisted of an outer acrylic pipe and an inner aluminum pipe that simulated an annulus. The inclination of the test setup was adjustable to any angle between 0 and 90 degrees, and the eccentricity was also adjustable using in-house centralizers. The density and rheological properties of the fluid were varied using Xanthan Gum and Cesium Formate brine with water. The density ratio of the fluids ranged from 1.06 to 1.35, and the Herschel-Bulkley model was used for rheology. They did experiments in laminar flow regime only where the mean velocity ranged from 0.18 m/s to 0.8 m/s. They evaluated the displacement efficiency using a camera placed 17 ft away from the inlet with a camera coverage of 2 ft. The camera recorded videos of the displacement fluids which were dyed in different colors. However, this evaluation was only two-dimensional because only one camera was used.

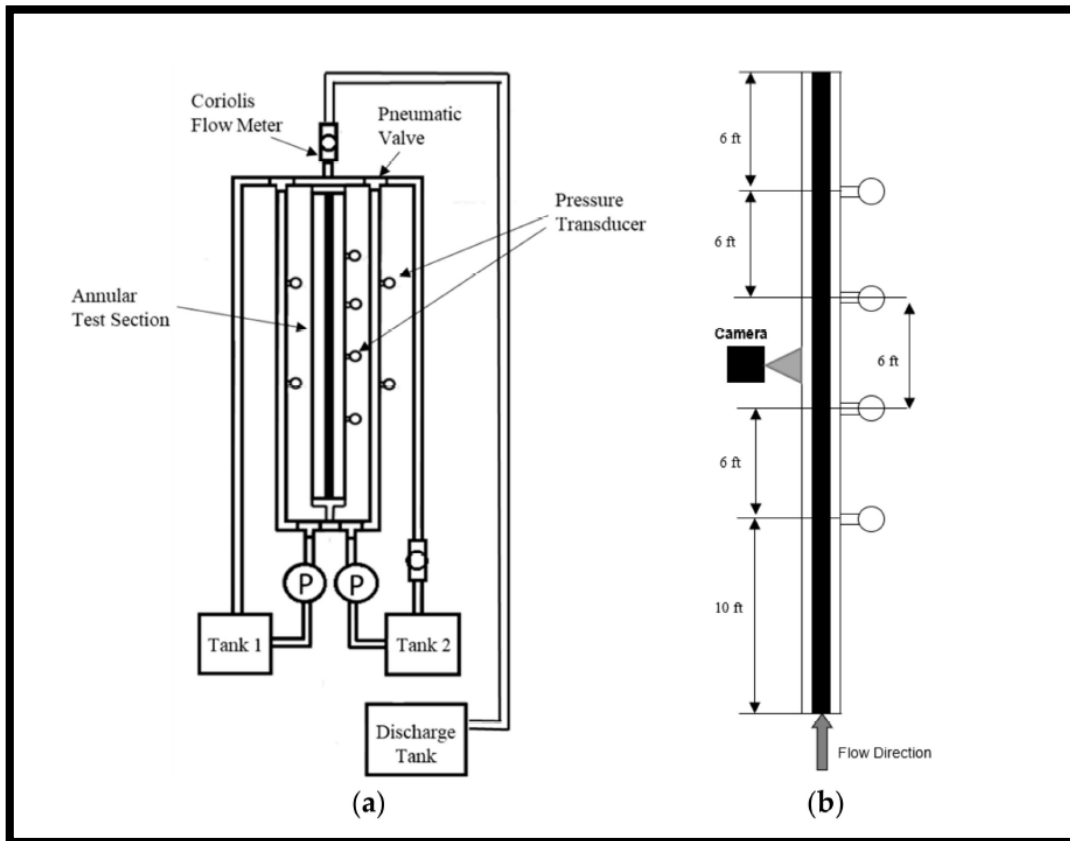


Figure 13. Illustration of testing facility (a) and test section (b) (Foroushan et al., 2020)

Table 1. Test section specifications.

Test section length (ft)	34
OD of inner pipe (inch)	2.5
ID of outer pipe (inch)	3
Reservoir and discharge tank volume (gallon)	50
Camera location from inlet (ft)	17

Furthermore, Ravi et al, 1992, built an experimental setup to study the mechanism behind erosion of partially dehydrated gelled (PDG) drilling fluid and filter cake. They defined PDG drilling fluid as “the drilling fluid which, in addition to developing gel strength in the absence of shear, has also lost a portion of its water (fluid).” The main aim was to define the erodibility of this partially dehydrated gelled (PDG) drilling fluid to develop guidelines in order to improve the removal of drilling fluid and filter cake during a cementing job. An illustration of their experimental setup is shown in Fig. 14 below. It consisted of a 2” inner pipe inside a 5” outer pipe. The pipes are surrounded by a permeable simulated formation. This formation was placed inside a containment

casing which is placed in a water bath. The water bath and heating jacket can be used for temperature control as desired. In the sealed space between the two pipes, pressure ports were installed which were then connected to differential pressure transducers. They conducted a 4-day experimental procedure to study the removal of PDG drilling fluid from the annulus during the cementing job. The procedure consisted of:

Day 1: calibration of the wellbore by pumping water in turbulent flow. After that, drilling fluid was circulated for 10 minutes at 2 and 4 bbl/min. Then the filtrate valve was opened, and the drilling fluid was circulated for 3 hours at 3 different flow rates. This was followed by a shut-off period with a 100 psi differential pressure into the formation, during which filtrate samples were collected.

Day 2: after shutting down for 18 hours, drilling fluid was circulated again until a steady state was reached. Then the drilling fluid was circulated further at different flow rates. After circulation, the wellbore was shut off again with a 100 psi differential pressure, and filtrate samples were collected.

Day 3-4: the same procedure as for day 2 was followed. But after circulation, a spacer fluid was pumped in the wellbore followed by a cement slurry. The cement was left to cure for 48 hours, and then it was cut into sections and photographed for evaluation.

After several experiments were conducted where the pressure drop was being measured, they were able to come up with some valuable conclusions. It was seen that the PDG drilling fluid and filter cake can be eroded if the pressure drop in the annulus surpasses a certain threshold. This pressure drop can be related to shear stress at the wall. They also proposed an adhesion-shear stress mechanism to describe the erosion. The PDG drilling fluid and filter cake are packed with particles, and the surface forces causing adhesion of the particles to each other can be expressed as the yield stress of these packed particles. Thus, they proposed that erosion of the PDG drilling fluid and filter cake will occur if the wall shear stress exceeds the yield stress of the packed particles in fluid and filter cake. They further defined erodibility of a drilling fluid for practical applications, where it was considered inversely proportional to wall shear stress. So, they proposed an equation for the calculation of erodibility by using the minimum required wall shear stress and a proportionality constant. This allowed them to provide some guidelines and recommendations to improve the removal of PDG drilling fluid and filter cake during cementing jobs.

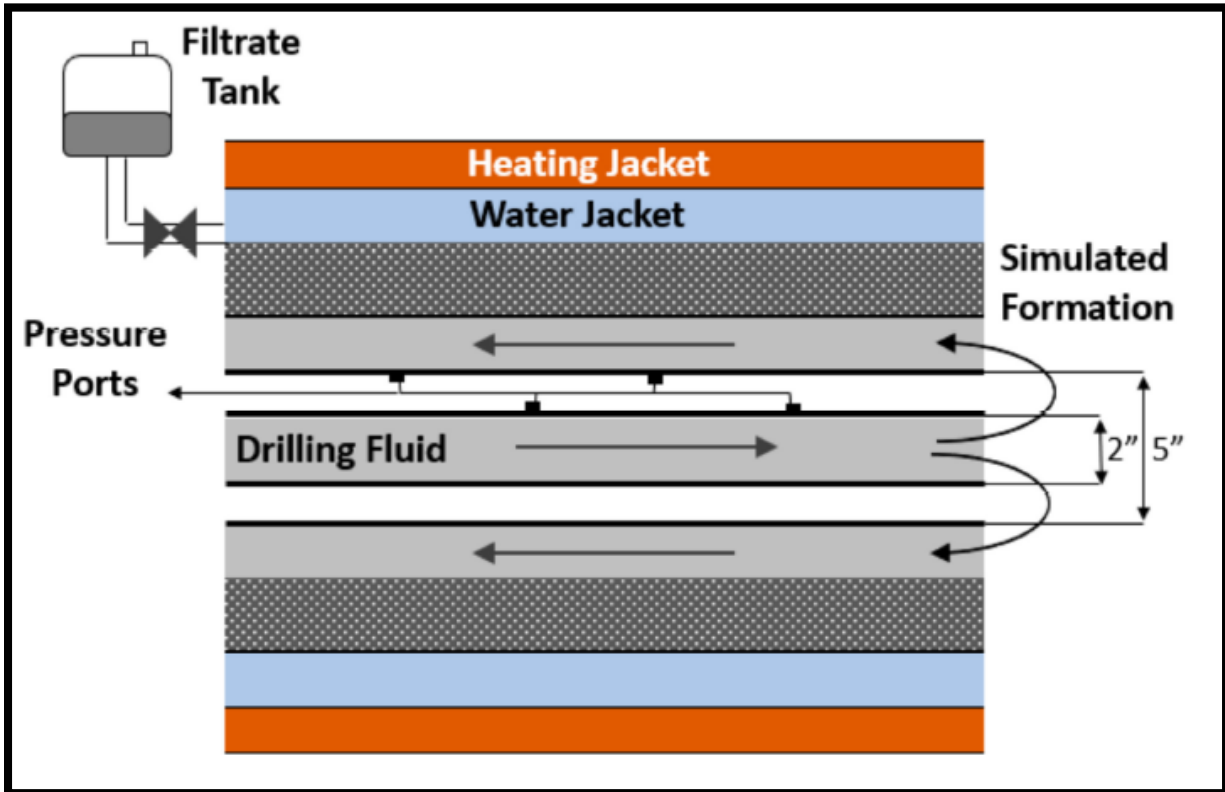


Figure 14. Illustration of experimental setup for measurement of erodability of PDG drilling fluid (Ravi et al, 1992).

Another experimental setup was developed by Biezen et al, 2000, for similar purposes. They aimed at studying the erodibility and removal efficiency of drilling fluids in a horizontal wellbore. So, they conducted experiments where spacer fluids are displacing drilling fluids, both in concentric and 20% eccentric annuli. Fig. 15 below shows the experimental setup, consisting of a 5" ID outer pipe and a 3" OD inner pipe creating an 8.5 ft annulus. The setup had a hollow core section around the annulus to simulate the filter cake buildup and filtrate collection. A heating jacket was also applied to control the temperature of the assembly. Several parameters were tracked to analyze the displacement including pressure, temperature, flow rate, and mainly electrical conductivity. Two conductivity probes were installed, one on the wide side of

the annulus and the other on the narrow side.

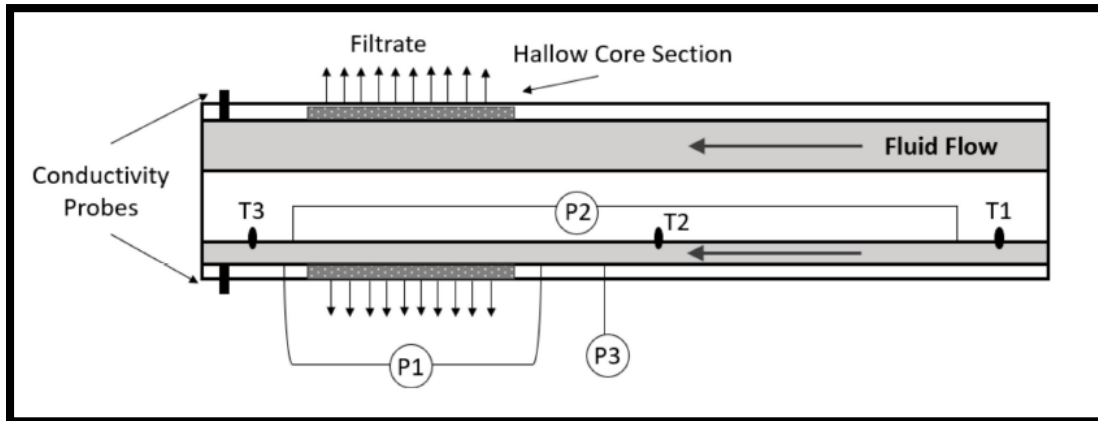


Figure 15. Schematic of conductivity measurement experimental setup (Biezen et al, 2000)

The experimental procedure was planned for 3 days which include:

Day 1: the drilling fluid was first mixed and heated, then circulated through the setup. After circulation, there was an overnight shut-in period with constant temperature and no applied pressure.

Day 2: the same procedure as Day 1 was followed. But at the end of this day, the wellbore was shut-in for 24 hours at static pressure and temperature. So, filter cake started to build up inside the annulus, and filtrate was collected from outside the core.

Day 3: a spacer fluid was pumped through the annulus at increasing flow rates to remove the drilling fluid. The conductivity probes were able to capture when the spacer fluid removed the drilling fluid at the end of the test setup by the sudden spike in conductivity. The remaining filter cake and gelled fluid were visually inspected, and X-ray diffraction method was used to analyze any residue.

2.6 Displacement Models:

Extensive work has been done on the development of a general analytical model that allows the estimation of displacement efficiency and the determination of the main parameters affecting it. The physical phenomenon to be modelled is the displacement of one non-Newtonian fluid by another, each having different properties, in an annulus of varying eccentricity and inclination. Mclean et al, 1967, developed an analytical early on where they divided an eccentric annulus into multiple sectors as shown in Fig. 16 below. Each sector would then be treated as concentric annulus on its own for the calculation of the flow parameters. An example of sector C is shown in Fig. 16 where the inner radius becomes that fitted for the sector, and the outer radius remains as the

original borehole radius. The calculations are then made assuming the sector as a concentric annulus made from the above-mentioned radii.

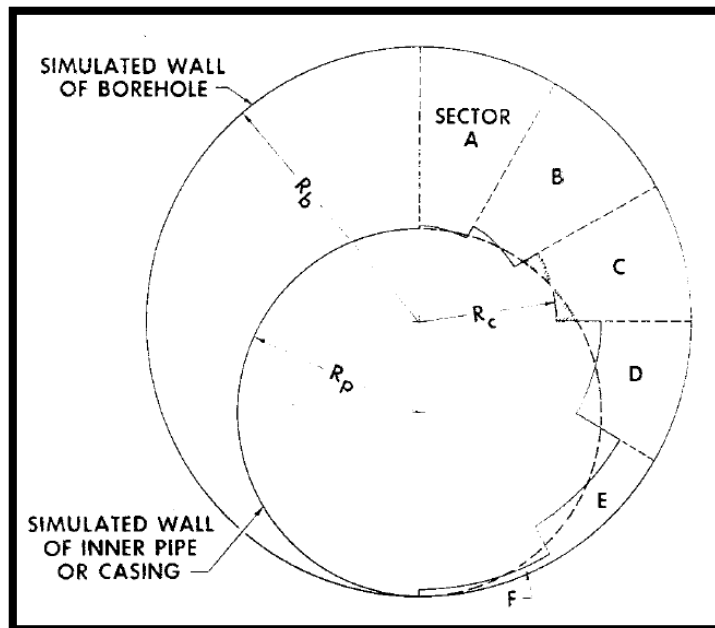


Figure 16. Sector division of an eccentric annulus (Mclean et al, 1967)

Beirute and Flumerfelt, 1977, developed a mathematical model to represent the displacement of drilling fluids by cement slurries, but only in a laminar flow profile. The model describes the rheological properties of the fluids using the Robertson-Stiff model. The model accounted for and was to study the effect of varying fluid properties, well geometry, and displacement flow rates. Fig. 16 below shows how the displacement process is assumed to take place. It is assumed that a stable front of the displacing fluid is moving through the displaced fluid in a laminar flow regime. For calculating the displacement efficiency, the position of the displacing front should be established at any time throughout the displacement process. The solution they obtained was approximate. They utilized several assumptions including:

- Interfacial forces between the fluids are neglected.
- Diffusive and convective mixing between the fluids at the interface is negligible.
- A constant rate displacement is used (Flow rate is constant at all cross sections).
- The displacement occurs under quasi-steady conditions.
- The velocity in the z direction is the only important component of velocity.
- The velocity gradient in z-direction is negligible compared to that in the radial direction.

An important problem created by the approximate nature of the solution is that the calculated volume of fluid displaced is not necessarily equal to the volume of fluid entering the system. Thus, the solution may suffer from mass balance inconsistencies. To counteract this issue, they introduced a correction factor to account for this effect when calculating the displaced volume. Another problem that was caused by the approximate solution is that situations may arise where the calculated shear stress of the fluids is negative. In such cases, they set the value of the shear stress to zero and assumed that the displacement front is flat in the regions where the negative values are encountered. The validity of the physics behind this assumption is discussed in other works. Their studies concluded that that higher density and viscosity ratios (ratio of displacing fluid to displaced fluid) lead to higher displacement efficiencies. The yield stress of the displacing fluid is directly proportional to displacement efficiency, while the yield stress of the displaced fluid is inversely proportional. Furthermore, they concluded that increasing the displacement flow rate will result in more channeling and decrease the displacement efficiency. Thus, and slow and stable displacement is desirable which will result in a flat displacement front.

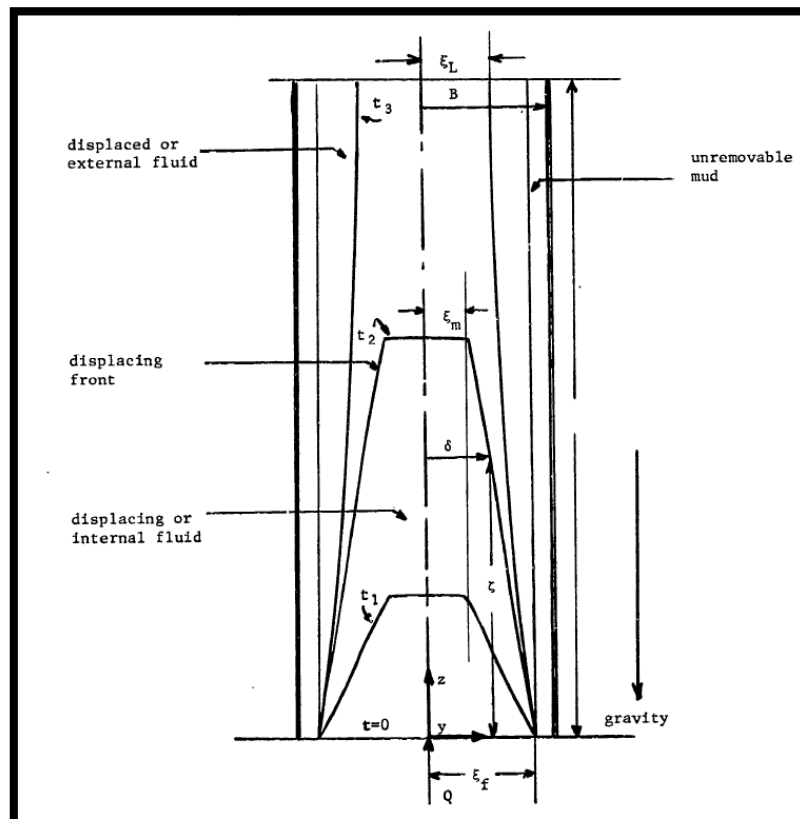


Figure 17. Displacement process as depicted by Beirute and Flumerfelt, 1977.

Foroushan et al, 2018, also developed an analytical model to study the displacement process in a vertical eccentric annulus. They developed the model in two steps. The

first step was to build a model to calculate single-phase fluid flow in an eccentric annulus. Then, the model was expanded to include a multiphase system of two fluids taking into account fluid interface calculations. The model was developed by considering the flow of a single fluid inside an unwrapped eccentric annulus as seen in Fig.18 below. The case of an eccentric annulus can be translated into an unwrapped eccentric annulus using the following equations of the parameters shown in Fig. 19:

$$R(z) = \varepsilon \cos \theta + \sqrt{R^2 - (\varepsilon \sin \theta)^2}$$

$$H(z) = R(z) - R1$$

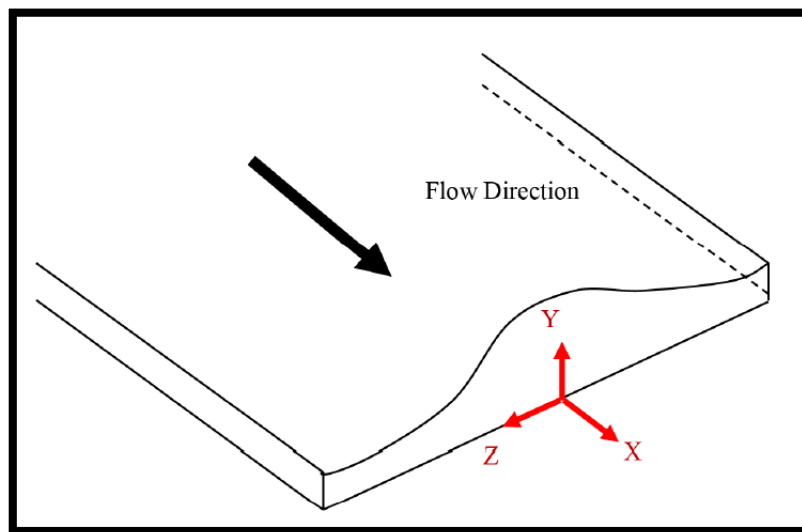


Figure 18. Unwrapped eccentric annulus (Foroushan et al, 2018)

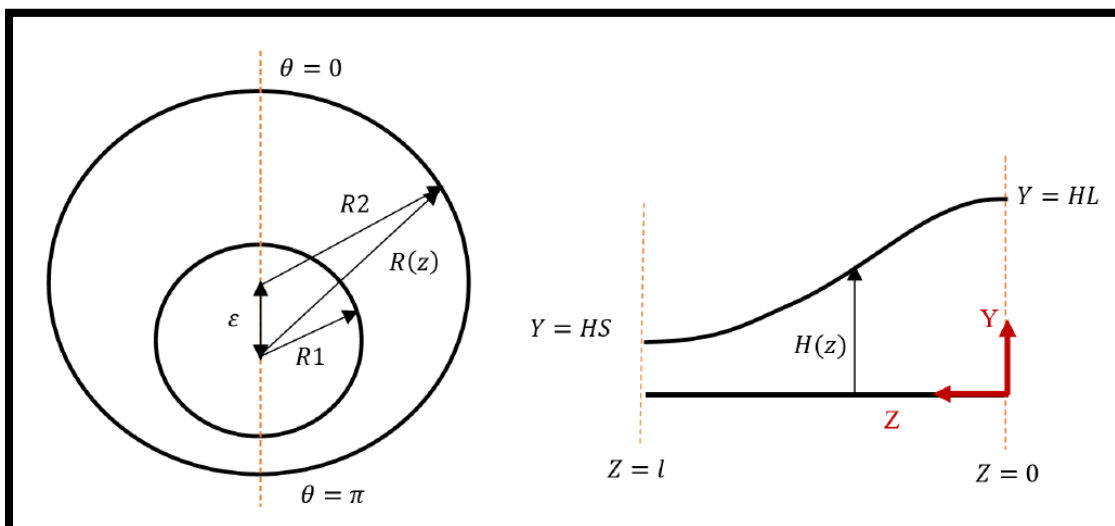


Figure 19. Eccentric annulus (left), Unwrapped eccentric annulus (right) (Foroushan et al, 2018)

The model was developed by solving the governing transport equations in this unwrapped eccentric annulus. The method consisted of solving a Poisson differential equation with irregular boundaries by modifying the differential equation and making the boundary conditions homogeneous. This provided a Laplace differential equation with homogeneous boundaries with the final solution to the single fluid in the unwrapped eccentric annulus. After that, the solution is extended to include the displacement of one fluid by another accounting for both density and viscosity differences and their effects. The transport equations were solved simultaneously for a system of two fluids with proper boundary conditions. No slip condition is applied at the walls for the displaced fluid, maximum velocity is at the center of the annulus for the displacing fluid, and the velocities and shear stresses are continuous at the interface. Fig. 20 shows an illustration of the fluid domain and the interface for a hypothetical case where the flow rates for the fluids can be calculated, and their summation provides the percentage of each fluid at a certain location. The calculations of this analytical model were compared to the results obtained from Computational Fluid Dynamics (CFD) for a few cases. The topic of CFD is of great importance for this thesis and will be discussed in more detail in the next section.

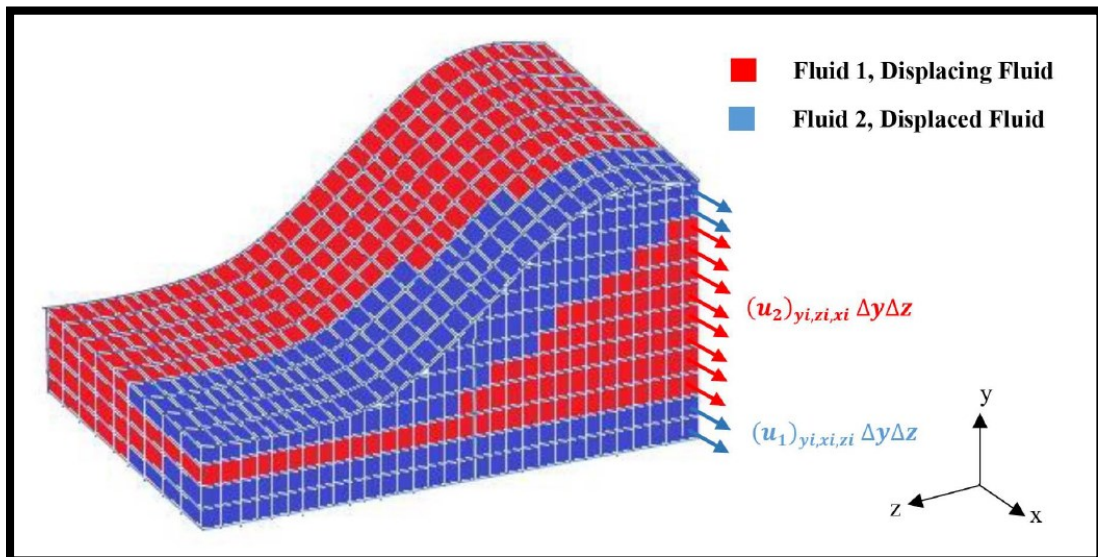


Figure 20. Illustration of fluid domain and interface (Foroushan et al, 2018)

Chapter 3

Computational Fluid Dynamics

Computational fluid dynamics, or CFD, is the simulation of fluid flows using a combination of physics, numerical mathematics, and computer science. It started in the 1970s where it was driven by the rapidly evolving technology, and the availability of more powerful computers (Blazek, 2015). From that time onwards, numerical methods have improved drastically with the evolution of modern computers and supercomputers. The use of numerical methods today allows us to solve complex fluid dynamics problems involving complex geometries in a relatively short time. Furthermore, computers can be clustered together to obtain solutions even faster. Thus, CFD offers a quick and cost-efficient method to study complex flow problems. These problems were typically studied using analytical model or experimental methods. However, the analytical models are often limited to specific cases due to the simplifying assumptions made to reach a solution. On the other hand, the experimental methods often require large resources (facilities, equipment, material...etc.) and can be more time consuming. That is why CFD is gaining more popularity as it is able to solve complex flow problems in a quick and efficient manner. However, CFD still relies heavily on experimental and analytical methods for validation due to its numerical nature.

The process of using CFD consists of three main stages as shown in Fig. 21 below:

1. Pre-processing
2. Solving
3. Post-processing

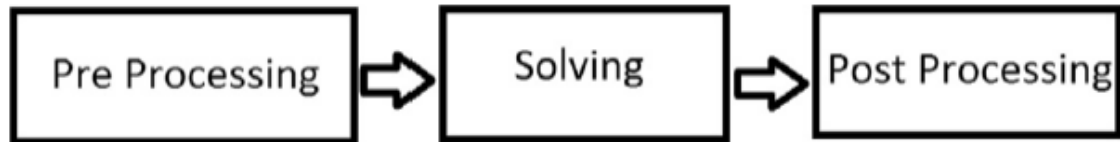


Figure 21. CFD process (Blazek, 2015)

The pre-processing stage consists of the meshing activities and is usually where most of the effort is put in CFD. In this phase, the user needs to create an understandable and realistic geometry. Then, the user needs to create a good quality mesh of this geometry to have a chance of converging the solution. A bad quality mesh is easy to identify, but it is much harder to judge if the mesh is of good quality. Next in the solving phase, the computer will solve the governing equations of flow. It be noted that ramifications of a poor-quality mesh and errors in it will be carried on to the solving phase, which can make it very difficult to obtain a converging solution. It only takes one problematic cell to diverge the solution. The final stage after solving is post-processing. This is where the results, that were obtained from the input and solution are analyzed. To validate these results, they are typically compared against experimental data for similar problems. Another method to ensure the consistency of the solution is a grid convergence study. In this study, the mesh is refined several times where the solution is obtained for each refinement. The grid convergence is obtained when the solution obtained is not changing with further mesh refinement, which means an asymptotically converged solution is obtained (Jamshed, 2015). Post-processing is also where the interesting graphics are created. One can create colorful contours, streamlines, plots and animations to show the flow solution and characteristics. These graphics come quite in handy to create interesting and understandable presentations to highlight the work done.

3.1 Governing Equations:

The term fluid dynamics is defined by Blazek, 2015, as “the investigation of the interactive motion of a large number of individual particles”. These particles in a fluid are the molecules and atoms. The fluid can be assumed to be a continuum considering it has a high enough density. This means that any infinitesimally small element in the fluid holds enough particles which have specific properties. Thus, we can study each fluid particle and define its important properties such as pressure, temperature, velocity, density...etc. The behavior of the fluid is governed by set of equations that describe the fluid flow. The main equations that are at the heart of fluid dynamics are

the Navier-Stokes equations. The Navier-Stokes equations have not been explicitly solved except for some specific cases. So, CFD was created as a means to convert these partial differential equations into simple algebraic ones, and then solve them numerically. By creating a well posed problem with a specific geometry and conditions, these solutions can yield meaningful results. These equations assume that fluid particles deform under shear stress. They are derived from the fundamental conservation laws namely:

1. Conservation of mass
2. Conservation of momentum
3. Conservations of energy

The conservation of a flow parameter means that its variation inside any volume is conserved. The variation can be expressed as the net amount of a certain quantity being transported into and out of the volume's boundaries, in addition to internal and external forces and sources acting on the volume. This amount of quantity being transported through the boundaries is called a flux. The flux can be divided into 2 main constituents, one caused by convective transport, and the other by diffusive transport which is due to the molecular motion of the fluid. The conservation laws allowed the development of a method by which the flow field is divided a number of volumes, and to model the fluid behavior in these individual finite volumes. Thus, the finite control volume was defined, and its physical properties were modelled using mathematical descriptions. Fig. 22 below shows a finite control volume fixed in space in a flow field represented by streamlines.

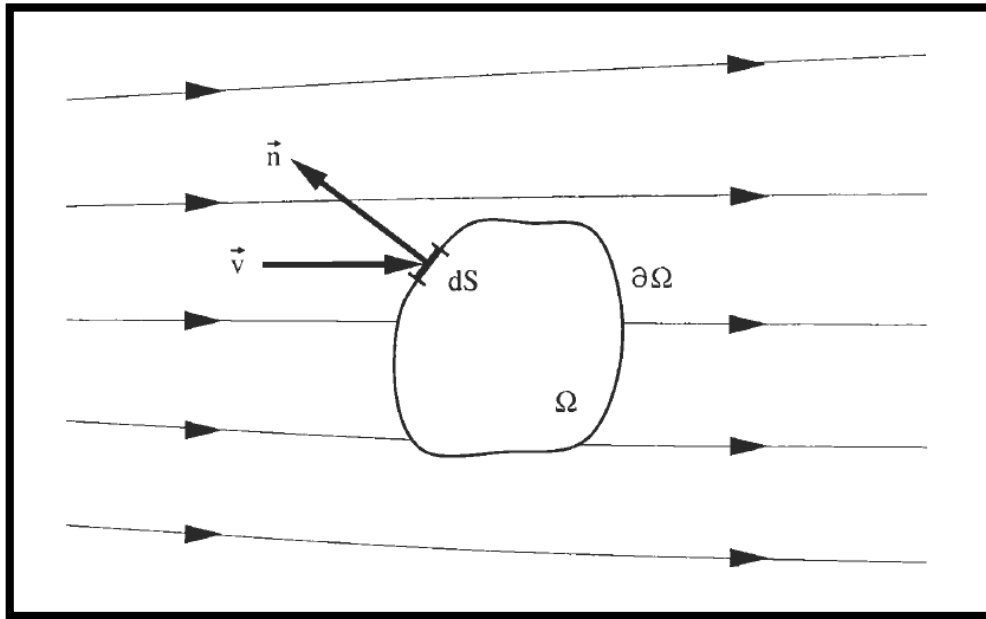


Figure 22. Finite control volume in a flow field ((Blazek, 2015))

3.1.1 Conservation of Mass:

The conservation of mass equation is also known as the continuity equation. It dictates that the temporal rate of change of mass in the control volume must be equal net rate of flow of mass into the control volume. The continuity equation is expressed as:

$$\frac{\partial \rho}{\partial t} + \nabla \cdot (\rho \mathbf{u}) = 0$$

where the divergence operator is represented by the symbol nabla-dot which can be expressed as:

$$\nabla \cdot \mathbf{a} = \text{div}(\mathbf{a}) = \frac{\partial a_x}{\partial x} + \frac{\partial a_y}{\partial y} + \frac{\partial a_z}{\partial z}$$

3.1.2 Conservation of Momentum:

The conservation of linear and angular momentum equations dictate that the rate of change of momentum in the control volume must be equal to the sum of forces acting on the control volume. The forces acting on the control volume can be split into body forces (such as gravity, electromagnetic forces, centrifugal forces...etc.) and surface forces transformed into stress tensors (such as stresses and static pressures). The conservation of linear momentum is based on Newton's second law of motion. The momentum equations are expressed as follows:

$$\frac{\partial}{\partial t}(\rho \mathbf{u}) + \nabla \cdot (\rho \mathbf{u} \mathbf{u}) = \nabla \cdot \boldsymbol{\sigma} + f_b$$

$$\frac{\partial}{\partial t}[\rho(\mathbf{r} \times \mathbf{u})] + \nabla \cdot [\rho \mathbf{u}(\mathbf{r} \times \mathbf{u})] = (\mathbf{r} \times \nabla \cdot \boldsymbol{\sigma}) + (\mathbf{r} \times f_b)$$

The linear momentum equation consists of 3 equations for the x,y, and z directions. These equations can be expressed as:

$$\text{x-direction: } \frac{\partial \rho u}{\partial t} + \frac{\partial \rho u u}{\partial x} + \frac{\partial \rho u v}{\partial y} + \frac{\partial \rho u w}{\partial z} = -\frac{\partial p}{\partial x} + \mu \frac{\partial}{\partial x} \left(\frac{\partial u}{\partial x} + \frac{\partial u}{\partial y} + \frac{\partial u}{\partial z} \right) + \rho f_x$$

$$\text{y-direction: } \frac{\partial \rho v}{\partial t} + \frac{\partial \rho v u}{\partial x} + \frac{\partial \rho v v}{\partial y} + \frac{\partial \rho v w}{\partial z} = -\frac{\partial p}{\partial y} + \mu \frac{\partial}{\partial y} \left(\frac{\partial v}{\partial x} + \frac{\partial v}{\partial y} + \frac{\partial v}{\partial z} \right) + \rho f_y$$

$$\text{z-direction: } \frac{\partial \rho w}{\partial t} + \frac{\partial \rho w u}{\partial x} + \frac{\partial \rho w v}{\partial y} + \frac{\partial \rho w w}{\partial z} = -\frac{\partial p}{\partial z} + \mu \frac{\partial}{\partial z} \left(\frac{\partial w}{\partial x} + \frac{\partial w}{\partial y} + \frac{\partial w}{\partial z} \right) + \rho f_z$$

where u,v, and w represent the velocity in the x,y and z directions respectively.

3.1.3 Conservation of Energy:

The conservation of energy is basically the first law of thermodynamics. It dictates that the rate of change of energy in the control volume must be equal to: the net rate of heat added to the control volume + the net rate of work done on the control volume. The conservation of energy equation is expressed as:

$$\frac{\partial}{\partial t}(\rho e) + \nabla \cdot (\rho \mathbf{u} e) = -\nabla \cdot \mathbf{q} + \rho Q + \nabla \cdot (\boldsymbol{\sigma} \mathbf{u}) + f_b \mathbf{u}$$

where e is the specific total energy (in J/kg) expressed as: $e = \frac{E}{m}$

The physical properties of a system can be classified into different categories (Vita, 2020):

- Intensive properties: are properties that are independent of the size of the system such as pressure and temperature.
- Extensive properties: are properties that are not isolated from the system size and thus depend on it such as mass.
- Specific properties: are extensive properties that have been normalized by mass to decouple them from the system size such as the specific total energy mentioned in the above equation.

3.1.4 Constitutive Relations:

Constitutive relations are equations derived from established laws of physics. They serve to describe the properties and behavior of materials where they establish dependencies between certain physical quantities of the material. In CFD, constitutive relations are needed as mathematical closure to be able to solve the governing equations of fluid flow. Some examples of these relations would be Hooke's law, stress in fluids, Fourier's law, equations of state, and rheological models. The modelling of rheological properties is of importance for this work because we will be dealing with wellbore fluids (drilling fluid, spacer, cement) that are typically non-Newtonian fluids. So, we will dive a bit into the different rheological models typically used which include inviscid fluids, Newtonian fluids, and non-Newtonian fluids.

Inviscid fluid: are ideal fluids that exhibit no viscosity.

Newtonian fluid: are fluids where the shear stress (τ) is directly proportional to the shear rate (γ). The viscosity (μ) of the fluid is the constant of proportionality and is calculated as the slope of shear stress/shear rate plot. The shear stress is also equal to zero in the absence of shear rate. The Newtonian model can be expressed using this equation:

$$\tau = \mu \cdot \gamma$$

Non-Newtonian Fluid: this type of fluid is characterized by the non-proportionality between shear stress and shear rate. Drilling fluids, spacer and cement slurries are non-Newtonian due to their complex rheological behavior. The aforementioned fluids

are considered as shear thinning fluids which means that their apparent viscosity decreases with increasing shear rate. There are numerous models that describe the relationship between shear stress and shear rate for non-Newtonian fluids. The three most common rheological models used in the oil and gas industry are the Bingham Plastic model, Power Law model, and Herschel-Bulkley model. Fig. 23 below shows the plot of shear stress vs shear rate for these models.

- **Bingham Plastic Model:** this model designates a linear relationship between shear stress and shear rate, and an initial yield stress that has to be overcome for the fluid to flow. The model is represented by the equation:

$$\tau = YP + PV(\dot{\gamma})$$

where YP is the yield stress, PV is the plastic viscosity.

- **Power Law Model:** this model designates a power law relationship between shear stress and shear rate. However it doesn't involve any yield stress. It is represented by the equation:

$$\tau = K(\dot{\gamma})^n$$

where K is the consistency index which represents the pumpability of the fluid, and n is the power law index which indicates the degree to which the fluid is Newtonian or non-Newtonian.

For n=1: the fluid is Newtonian.

For n<1: the fluid is shear-thinning.

For n>1: the fluid is dilatant.

- **Herschel-Bulkley Model:** this model can be considered as a combination of Bingham Plastic and Power Law models, and it is considered to present the behavior of drilling fluids, spacers, and cement slurries most accurately. It is represented by the equation:

$$\tau = \tau_0 + K(\dot{\gamma})^n$$

where τ_0 is the yield stress.

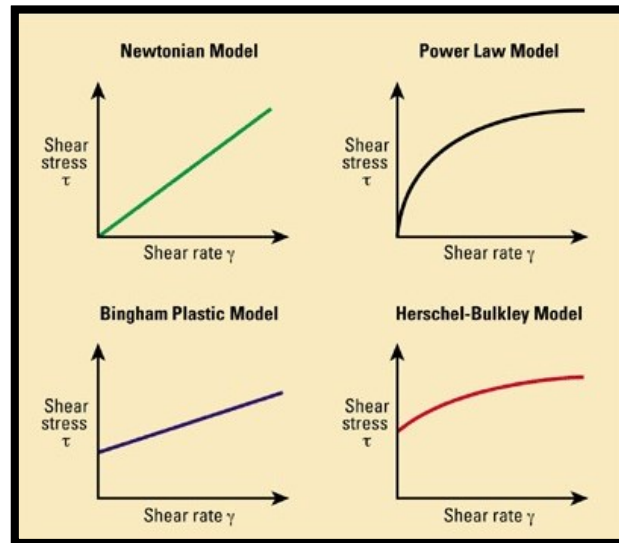


Figure 23. Shear stress vs shear rate for different rheological models (Schlumberger Oilfield Glossary)

3.2 Discretization Methods:

The fluid dynamics equations cannot be solved analytically, thus a numerical solution must be calculated. The partial differential equations (PDEs) form a continuous distribution of variables over the solution domain. These PDEs have to be discretized to generate a set of discrete values at nodes that form a grid over the solution domain. This is done by implementing approximations. There are different methods of discretization, however the most commonly used in CFD are Finite Difference Method (FDM) and Finite Volume Method (FVM).

3.2.1 Finite Difference Method (FDM):

The FDM is the oldest method and was the first to be used in CFD. It represents a class of numerical methods that are able of solving ordinary and partial differential equations. The geometry of interest must be discretized to create a numerical computational grid. Fig. 24 below shows a comparison between the geometrical domain of interest and the equivalent numerical grid.

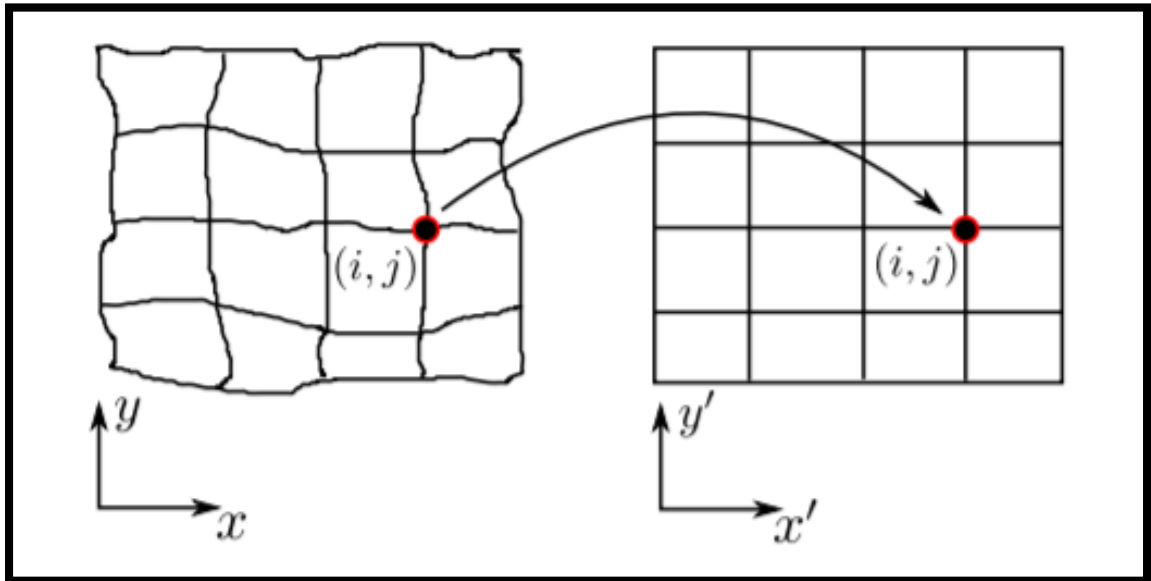


Figure 24. Schematic for comparison of a geometrical domain against its equivalent numerical grid.

The discretization here basically means that the differential equations are replaced by difference equations hereby converting the continuum into a discretized form, for example:

$$\frac{\partial y}{\partial t} \rightarrow \frac{\Delta y}{\Delta t}$$

This creates an algebraic system of equations where there exists an equation for each grid point. This equation has to be solved along with the equations of the neighboring grid points. The number of equations generally must be equal to the number of unknowns for the system of equations to be solved. Each grid point is identified by an index, and the partial derivatives at each point are replaced by approximations based on the nodal values. This transition is done by using the definition of a derivative as follows (Stoevesandt et al, 2017):

$$\left(\frac{\partial u}{\partial x}\right)_{x_i} = \lim_{\Delta x \rightarrow 0} \frac{u(x_i - \Delta x) - u(x_i)}{\Delta x}$$

The Finite Difference Method can solve a problem using three different schemes:

1. Forward Difference Scheme
2. Backward Difference Scheme
3. Central Difference Scheme

Taylor Series Approximation:

The concept of finite difference approximations relies on the Taylor series expansions. So, if we expand $u(x + \Delta x)$ around $u(x)$:

$$u(x + \Delta x) = u(x) + \Delta x \frac{\partial u}{\partial x} + \frac{\Delta x^2}{2} \frac{\partial^2 u}{\partial x^2} + \frac{\Delta x^3}{3!} \frac{\partial^3 u}{\partial x^3} + \dots + \frac{\Delta x^n}{n!} \frac{\partial^n u}{\partial x^n} + \dots$$

This equation can be re-written as:

$$\frac{u(x + \Delta x) - u(x)}{\Delta x} = \frac{\partial u}{\partial x} + \underbrace{\frac{\Delta x}{2} \frac{\partial^2 u}{\partial x^2} + \frac{\Delta x^2}{3!} \frac{\partial^3 u}{\partial x^3} + \dots}_{\text{Truncation Error}}$$

Thus, the first derivative at x can be approximated. The remaining terms on the right-hand side of the equations are grouped together as the truncation error. The order of accuracy of the finite difference approximation is represented by the power of Δx in the truncation error. The higher the number of points in the grid, the more accurate the numerical results which means that reduced Δx will improve accuracy. Thus, when higher-order terms are neglected, a first order scheme can be obtained as follows:

$$\frac{u(x + \Delta x) - u(x)}{\Delta x} \cong \frac{\partial u}{\partial x} + \frac{\Delta x}{2} \frac{\partial^2 u}{\partial x^2} = \frac{\partial u}{\partial x} + O(\Delta x)$$

Forward Difference Scheme:

For a forward difference scheme, we develop the approximation at point i and $i+1$. Thus, the value at $i+1$ for a function u would be:

$$u_{i+1} = u_i + \Delta x \frac{\partial u}{\partial x} + \frac{\Delta x^2}{2} \frac{\partial^2 u}{\partial x^2} + \frac{\Delta x^3}{3!} \frac{\partial^3 u}{\partial x^3} + \dots$$

By re-arranging the equation to evaluate the derivative and to obtain a first-order forward difference scheme, meaning that the error term contains the term Δx in the first order, we get:

$$\frac{\partial u}{\partial x} = \frac{u_{i+1} - u_i}{\Delta x} + O(\Delta x)$$

Backward Difference Scheme:

The first-order backward difference scheme follows the same logic as the forward difference expect we develop the approximation at point i and $i-1$ and get:

$$u_{i-1} = u_i - \Delta x \frac{\partial u}{\partial x} + \frac{\Delta x^2}{2} \frac{\partial^2 u}{\partial x^2} - \frac{\Delta x^3}{3!} \frac{\partial^3 u}{\partial x^3} + \dots$$

Re-arranging we get:
$$\frac{\partial u}{\partial x} = \frac{u_i - u_{i-1}}{\Delta x} + O(\Delta x)$$

Central Difference Scheme:

The central difference scheme combines the forward and backward schemes by subtracting their equations. This leads to the following equation:

$$\frac{\partial u}{\partial x} = \frac{u_{i+1} - u_{i-1}}{2\Delta x} - \frac{\Delta x^2}{6} \left(\frac{\partial^3 u}{\partial x^3} \right) + \dots$$

$$\frac{\partial u}{\partial x} = \frac{u_{i+1} - u_{i-1}}{2\Delta x} + O(\Delta x^2)$$

The central difference scheme is second-order accurate as can be seen from the final term in the equation. Thus, it is widely used as a higher accuracy differencing scheme.

The second-order derivative can also be obtained, but it involves more terms and is more mathematically complex. The resulting equation becomes:

$$\frac{\partial^2 u}{\partial x^2} = \frac{u_{i+1} - 2u_i + u_{i-1}}{\Delta x^2} + O(\Delta x^2)$$

3.2.2 Finite Volume Method (FVM):

The finite volume method works by dividing the computational domain into a finite number of control volumes. The values of interest are typically calculated at cell centers. Then, by interpolating these values at cell centers, the values of fluxes at cell interfaces are calculated. An algebraic equation is obtained for each control volume, and then all the generated equations are solved numerically. Thus, the FVM divides the domain into control volumes, whereas the FDM uses discrete points. Both schemes are capable of handling 2D and 3D fluid flows. However, FVM offers some advantages over FDM. For instance, FVM can be used for any type of grid whether structured or un-structured. Additionally, FVM can handle cases where there exists a discontinuity in the flow, whereas FDM fails to calculate such cases. On the other hand, a disadvantage of FVM would be that it is difficult to handle 3D cases with schemes that are higher than second order. This is due to the interpolation of the cell interfaces and surfaces with the cell centers.

Gauss's divergence theorem is considered here on the control volume. The mesh can be structured or unstructured as mentioned earlier. For example, the continuity

equation can be discretized using FVM for a 2D mesh shown in Fig. 25 below. The resulting continuity equation would become:

$$\left(\frac{u_E - u_W}{2\Delta x}\right) + \left(\frac{v_N - v_S}{2\Delta y}\right) = 0$$

The above equation indicates a second-order accuracy scheme because the denominator has $2\Delta x$ and $2\Delta y$. Let us compare the resulting equation with that obtained from using the central difference scheme of FDM. The resulting x-component equation would be:

$$\frac{u_E - u_W}{2\Delta x}$$

Similarly, the y-component would be:

$$\frac{v_N - v_S}{2\Delta y}$$

To get the continuity equation, we sum both terms and equate to zero. We get exactly the same result as FVM. Both schemes produce a second-order accurate result.

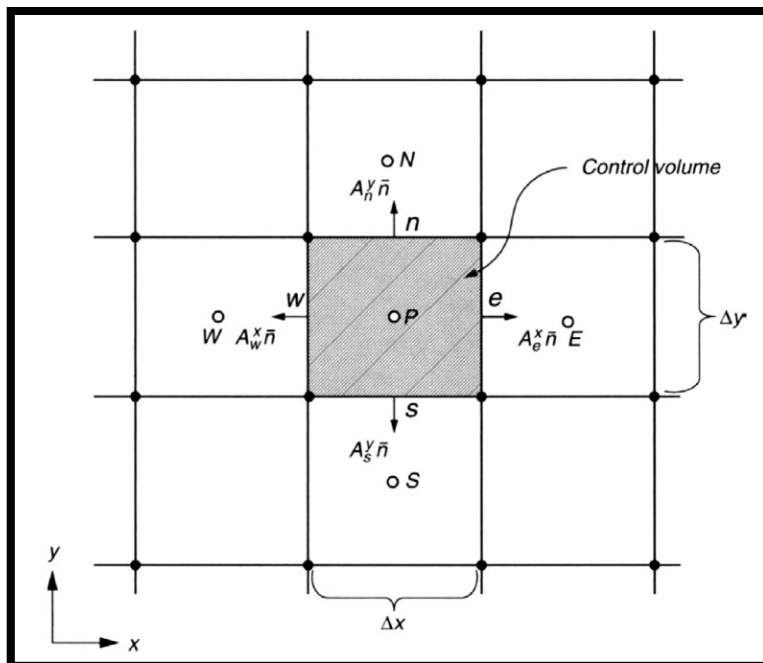


Figure 25. FVM of 2D grid (Stoevesandt et al, 2017)

Chapter 4

Computational Domain

The computational grid, or mesh, is used to describe the geometry of interest in a discretized manner. This mesh becomes the location where the solution for the equations describing the problem will be obtained. It also defines the zones where the boundary conditions will be applied (Blazek, 2015). It is of utmost importance to create a mesh that produces proper results in terms of convergence, accuracy, and computational time. The following chapter will discuss some basic of mesh generation and quality control. The computational grid, or mesh, falls under two main categories or a combination of these two:

- Structured grids
- Unstructured grids
- Hybrid grids

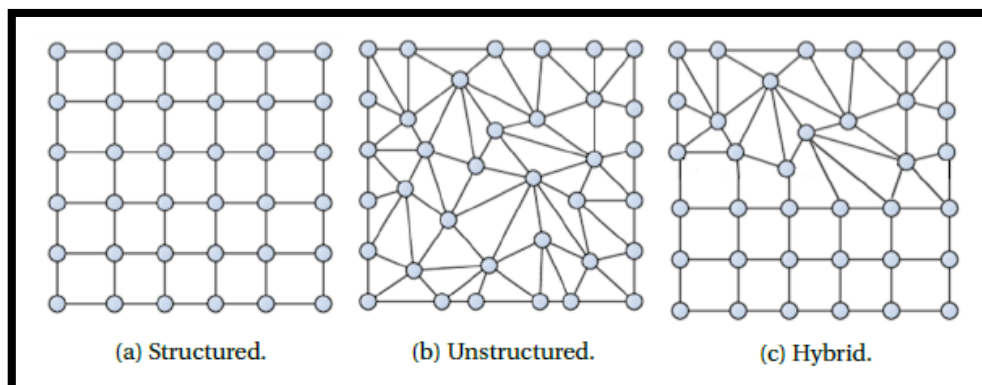


Figure 26. Mesh Classifications (Vita, 2020)

4.1 Mesh Nomenclature:

There exist a few terms that should be well understood for meshing operations. This ensures proper mesh generation and control. These terms include:

- Node: a grid point.
- Cell: smallest volumetric unit of the domain.

- Cell Centre: centroid of a cell.
- Face: boundary of a cell.
- Edge: boundary of a face.
- Zone (Patch): grouping of nodes, cells, and faces.
- Domain (Region): group of nodes, cells, and faces.

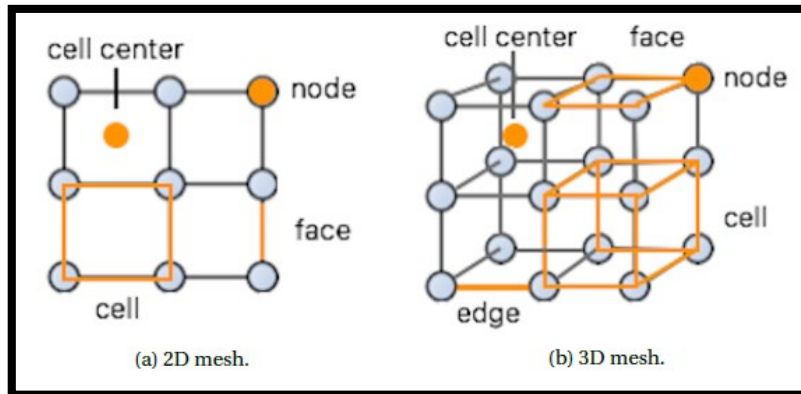


Figure 27. Mesh nomenclature (Vita, 2020)

4.2 Structured Grids:

This type of grid follows a logical structure where the grid points are identified by indices that correspond to the directions of the cartesian coordinates system. There exists different types of mesh cells or elements. For 2D, the main types are triangle, quadrilateral (quad), and polygon. For 3D meshes, these become tetrahedron (or prism, pyramid), hexahedron and polyhedral. The structured grids are typically generated using quads in 2D and using hexahedrons in 3D. The main advantage of structured grids is that the grid cells are properly indexed in the computational space. This allows quick and easy access to neighboring cells or points of any grid point. This leads to the simplification of evaluating the gradients, fluxes, boundary conditions and other required physical quantities. Fig. 28 below shows an example of a structured mesh generated for a cylindrical pipe.

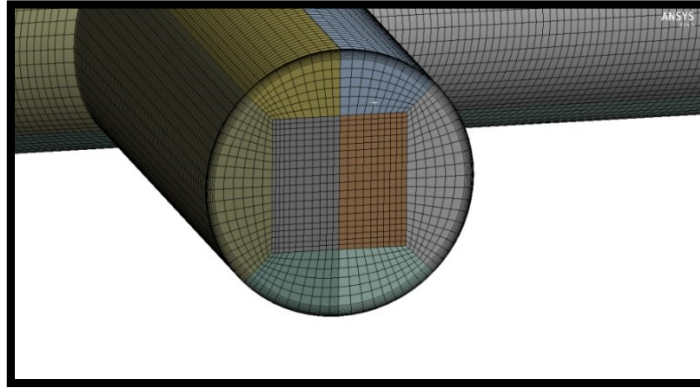


Figure 28. Cylindrical pipe structured mesh. (Mesh Generation & Pre-processing, CFD Online)

4.3 Unstructured Grids:

The grid cells and points in this type of mesh have no logical structure. Thus, the neighboring grid cells and points cannot be indexed. The cell types are triangles and polygons in 2D, and tetrahedrons and hexahedrons in 3D. These triangles and tetrahedrons can typically be generated automatically regardless of the complexity of the geometry. Therefore, unstructured grids are particularly useful for problems with complex geometries as they offer the most flexibility. However, there still needs to be some defined parameters for the automatic generation to ensure a good mesh quality. On the other hand, these arbitrary grid cells might require higher memory and CPU resources. Fig. 29 below shows an example of an unstructured mesh.

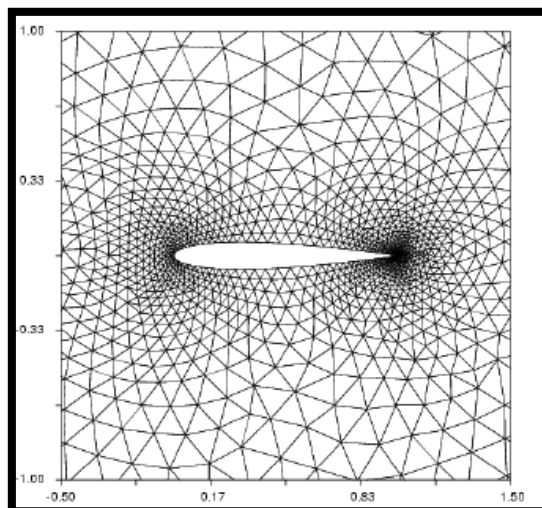


Figure 29. Unstructured mesh (Cusdin & Mueller, 2003)

Hybrid grids are combination of the two grid classifications mentioned above. They are composed of different zone of which some are structured, and the other unstructured.

The idea behind hybrid grids is to employ the most suitable mesh type for each flow region which can in turn lead to better accuracy and faster computational time (Vita, 2020).

4.4 Mesh Quality:

There exist highly varying levels of good quality meshes. A bad mesh is easy to identify, but a good one is difficult to judge. However, there exists some general guidelines that can assist in obtaining a good quality mesh. Some of these rules include that the grid lines of the mesh must be aligned with the flow. The mesh must consider boundary layers at the walls. The mesh also should have an adequate resolution to capture the relevant flow characteristics where more cells can provide improved accuracy. However, more cells also mean higher computational costs. So, a middle ground has to be found to keep cell count under control while also providing sufficient accuracy. An important parameter to be mentioned here is the Courant Number (C) which represents how quickly the information spreads inside the mesh. It can also be used the other way around to calculate the minimum mesh resolution or the required time step size for solution stability (typically $C=1$). The Courant Number must be kept under control to obtain a converged solution. The Courant Number is described by the following equation:

$$C = \frac{u\Delta t}{\Delta x}$$

In addition to these guidelines, there exist several geometrical mesh metrics that can give an indication about the quality of the mesh. Some of the main mesh metrics will be discussed here.

Orthogonal Quality (OQ):

Orthogonal Quality is calculated for each cell using the face vectors from the cell centroid, the face area vector, and the vector from the cell centroid to neighboring cell centroids. The orthogonal quality is in the range 0-1, where the worst cells will have a value of 0 and the best cells will have a value of 1. The minimum orthogonal quality for any type of cell should always be above 0.01, with the average OQ being considerably higher.

Skewness:

Skewness is a measure of the difference between the shape of an equilateral cell and the shape of the actual cell. Cells with high skewness can lead to decreased accuracy and stability, and it might also lead to a diverging solution. Skewness also ranges between 0 and 1, 0 being the best and 1 being the worst. A rule of thumb is to keep the maximum skewness of any cell below 0.95, with average skewness being much lower. A maximum skewness higher than 0.95 can lead to convergence problems.

Aspect Ratio and Smoothness:

Aspect ratio represents the stretching of a cell. It is generally recommended to avoid sudden changes in aspect ratio of adjacent cells especially where the flow is rapidly changing. The ideal aspect ratio would be 1.

Smoothness is a measure of the changes in size of adjacent cells. It is also best not to have sudden and large changes in cell size between adjacent cells. This can lead to larger errors.

However, these geometrical mesh metrics cannot guarantee a high-quality mesh. They can provide general direction about the quality of the mesh, but it might not be able to correlate directly with the solution accuracy of the mesh. Thus, the mesh must be further validated to ensure it provides realistic physical solutions. The table below provides best practices about mesh quality for CFD based on important mesh metrics.

Table 2. Mesh quality based on Min OQ and Max Skewness (Ansys Inc., 2017)

	Excellent	Very Good	Good	Acceptable	Bad	Unacceptable
Min OQ	0.95-1	0.7-0.95	0.2-0.7	0.15-0.2	0.01-0.14	0-0.01
Max Skewness	0-0.25	0.25-0.5	0.5-0.8	0.8-0.95	0.95-0.97	0.98-1

4.5 Mesh Generation:

The computational mesh was generated using Ansys Meshing to represent an annulus with an outer pipe representing the borehole wall, and an inner pipe representing the casing. The dimensions of the setup are presented in table 3. Fluids will be pumped through an inlet on the bottom to an outlet at the top. The fluids simulated are shear-thinning fluids and their properties are in the ranges presented in table 3 below. In

addition, various flowrates were used in the simulations which are represented by the Reynold's number range in table 3. The eccentricity of the inner pipe was of major interest. Thus, the mesh was generated for 4 different cases including a concentric annulus and 3 eccentric annuli. An eccentricity factor was introduced and is calculated using the following equation:

$$e = \frac{\text{center-to-center distance}}{\text{outer diameter} - \text{inner diameter}}$$

where the eccentricity could vary between 0 and 1, 0 being a concentric case, and 1 being the most severe eccentricity where the inner pipe is laying on the outer pipe. For the eccentric cases, the 3 generated meshes correspond to eccentricity of 0.25, 0.5 and 0.75. The 4 different meshes are shown in the figures below.

These dimensions and properties were chosen to create a digital twin of the state-of-the-art experimental flow loop setup at the DPE in Leoben. The flow loop will be used to accurately validate the multiphase displacement model in future works. This will provide a powerful tool for accurately studying and optimizing the displacement process in cementing operations.

Table 3. Annulus dimensions and fluid and flow properties.

	Value/Range	Unit
Outer Pipe ID	90	mm
Inner Pipe OD	65	mm
Annulus Length	5	m
Fluid Density	1000-2000	kg/m ³
Fluid Apparent Viscosity	10-100	cP
Reynold's number	200-4000	-
Eccentricity e	0-0.75	-

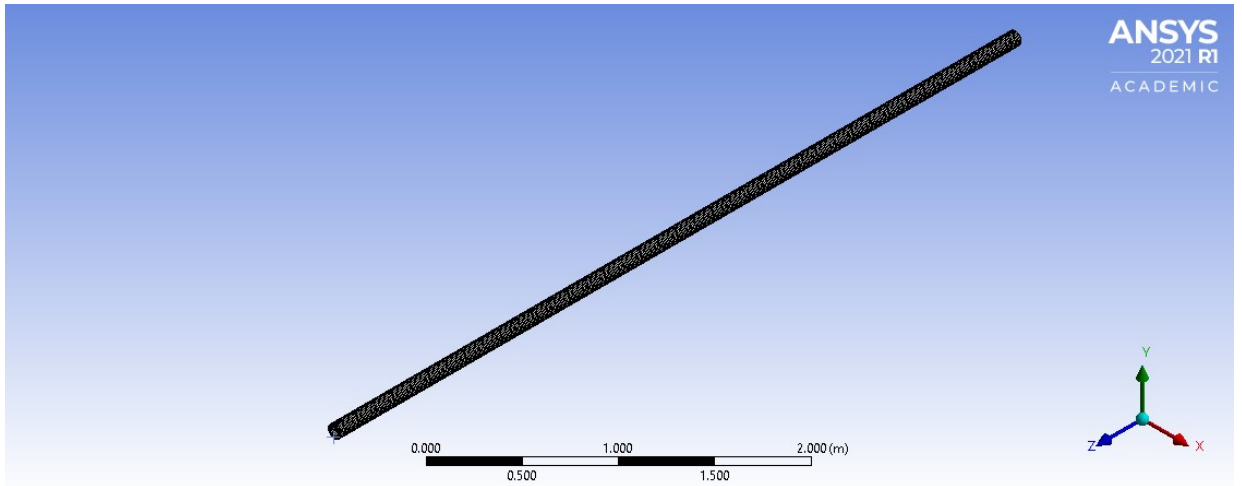
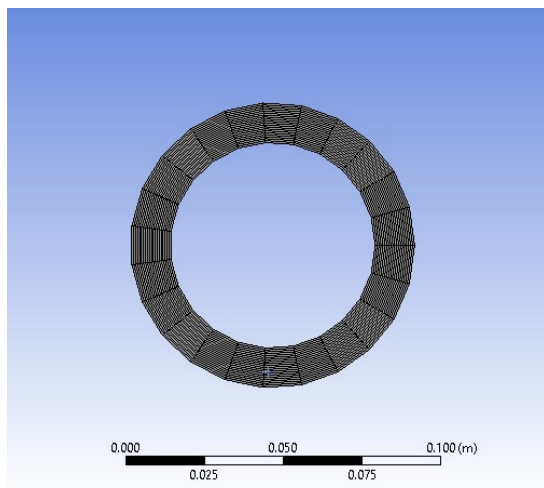
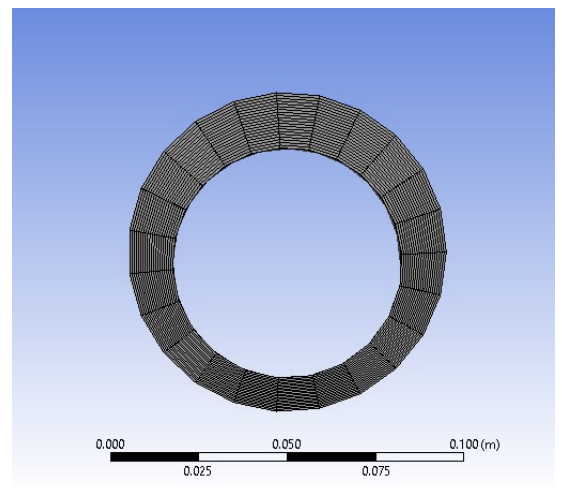


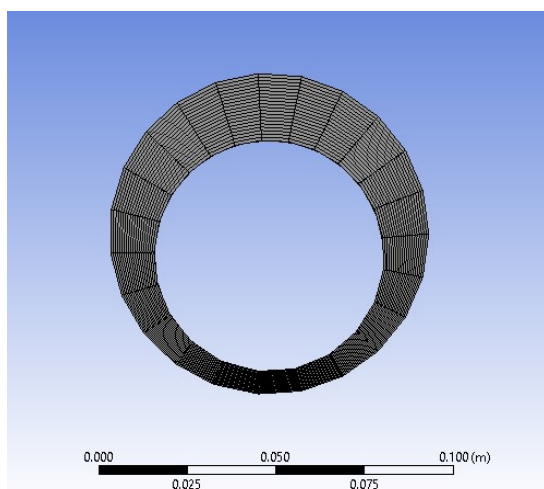
Figure 30. Computational mesh for 5-meter annulus.



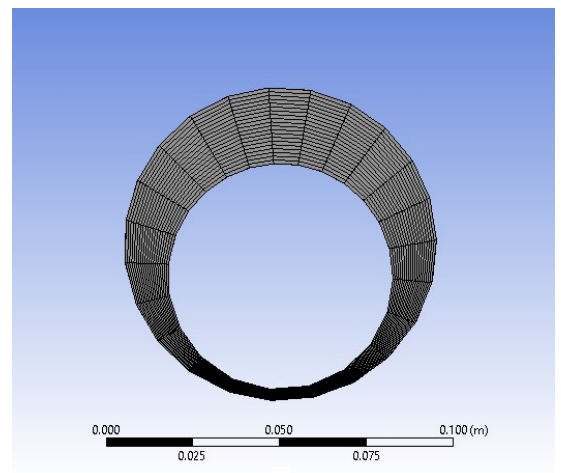
a



b



c



d

Figure 31. Generated mesh for different eccentricities: a) concentric, b) $e=0.25$, c) $e=0.5$, d) $e=0.75$.

The quality of these meshes was assessed using the mesh metrics previously mentioned, and it was found that they have good to excellent quality. The highest eccentricity possible using this mesh generation technique was $e=0.75$, further increasing the eccentricity resulted in a bad mesh. Thus the study was limited to a maximum eccentricity of $e=0.75$. A summary of the mesh metrics and quality is shown in Table 4 below.

Table 4. Assessment of mesh quality using mesh metrics

Mesh	Minimum Orthogonal Quality	Maximum Skewness
Concentric	0.99 (excellent)	0.08 (excellent)
$e=0.25$	0.71 (very good)	0.45 (very good)
$e=0.5$	0.64 (good)	0.32 (very good)
$e=0.75$	0.25 (good)	0.34 (very good)

4.6 Grid Convergence Study

A grid convergence study was performed to determine the number of cells required for accurate and reliable simulation runs as well as to ensure their consistency. Six simulations were run, starting from a cell count of 20,000 cells and reaching up to 500,000 cells. The base case for this study was the mesh of a concentric annulus mentioned previously, with a Herschel-Bulkley rheology fluid being pumped at a flow rate of 350 Lpm (92 gpm). The properties of the fluids 1 and 2 are respectively as follows:

- $\rho = 1100 \text{ kg/m}^3$
- $n = 0.43$
- $K = 0.89 / 0.5289 \text{ Pa}\cdot\text{s}$
- $\tau_y = 5 / 1 \text{ Pa}$

The pressure drop was used as an indicator for the convergence of the solution with a varying number of cells. As can be seen in Figure 32 below, the solution converges at

a cell count of 350,000 cells. Further increasing the cell count would not affect the simulation results as the maximum variation of the solution is within 0.5%. However, using a mesh with less than 350,000 cells can have an adverse effect on the solution accuracy and reliability as can be seen in Figure 32, where the values of pressure drop are changing considerably between each data point. Thus, a mesh of 350,000 cells will be used for the subsequent simulations and studies which will provide reliable results while ensuring the computational time is kept within acceptable limits.

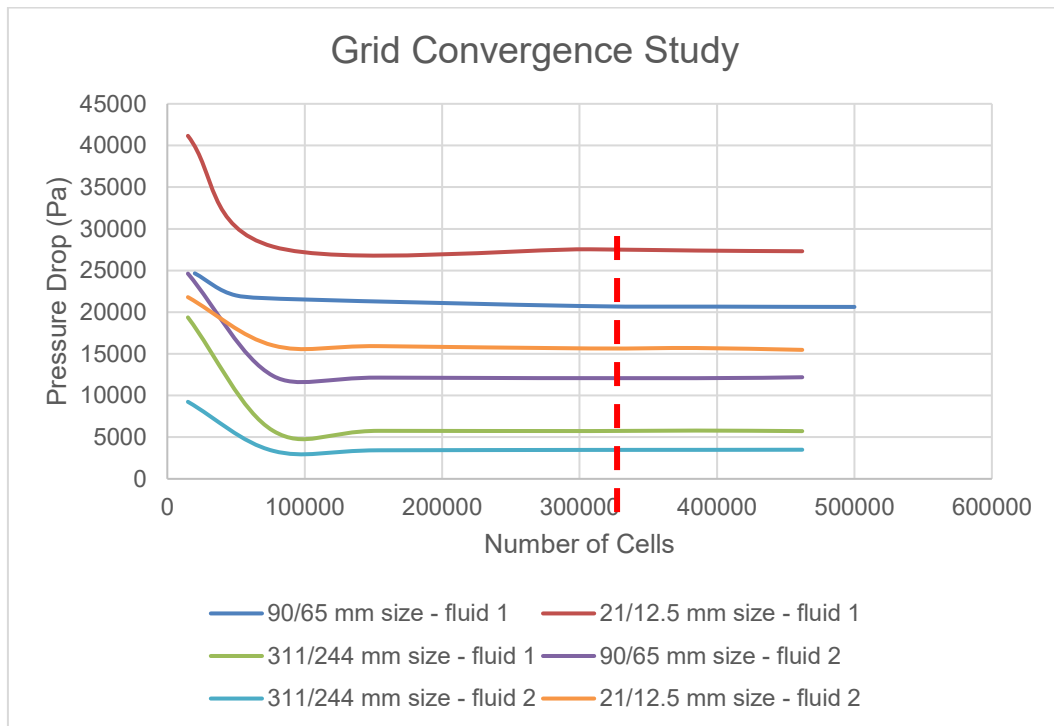


Figure 32. Grid convergence study, pressure drop vs mesh cell count.

Chapter 5

Single Phase Validation Simulations

5.1 Model Validation: Pressure Drop

The motto Garbage In Garbage Out is quite popular in the field of CFD. That is why, CFD models must be validated against experimental data to ensure they are working in the real world. If the model is not validated, the results are not reliable and might as well be fancy guess work. Thus, the validation of the CFD model in use in this work was done by a series of simulations that replicate the experimental work done by Zhigarev et al, 2011.

The experiments done by Zhigarev et al. consisted of three drilling fluids with different rheological properties. The density of all three fluids was 1100 kg/m³. The rheological properties are summarized in the Table 5 below.

Table 5. Rheological properties of drilling fluids used in Zhigarev et al. (2011)

Rheological Properties			
	Flow Behaviour Index, n	Consistency Index, K (Pa.s ⁿ)	Yield Stress, τ_y (Pa)
Fluid 1	0.4871	0.224	1.00E-05
Fluid 2	0.4317	0.5289	1.00E-05
Fluid 3	0.43	0.89	1.00E-05

The experiments consisted of pumping each fluid with a series of five flow rates and measuring the pressure drop for each flow rate. The flow rate sequence is shown in Table 6 below. The computational mesh to simulate these experiments was created using Ansys Meshing and consisted of a concentric annulus with an 21 mm outer diameter and a 12.5 mm inner diameter. A representation of the mesh is shown in Figure 33 below.

Table 6. Flow rate sequence of experiments done by Zhigarev et al. (2011)

Flow Rate Sequence		
mass flow rate (kg/s)	volume flow rate (lpm)	v (m/s)
0.057	3.11	0.23
0.161	8.78	0.65
0.264	14.40	1.07
0.369	20.13	1.50
0.473	25.80	1.92

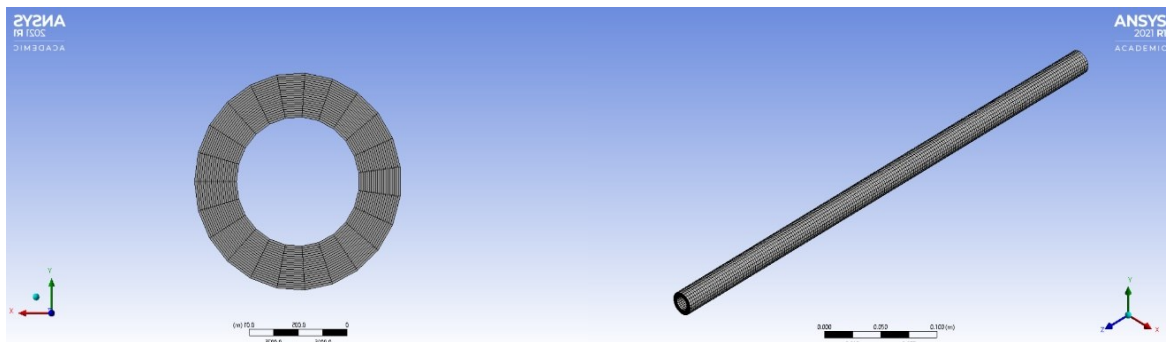


Figure 33. Computational mesh generated for the validation simulations with experimental data from Zhigarev et al.

Five simulations were run for each fluid with the varying fluid properties and flow rate sequence. The results from the CFD simulations were then compared to the experimental results obtained by Zhigarev et al. The results can be seen in Figure 34 below. The CFD results and the experimental data show very comparable results with an average error less than 5%, and a maximum error of 10% for the lower flow rates of Fluid 1. This shows that the simulation model is valid and can yield realistic and reliable results.

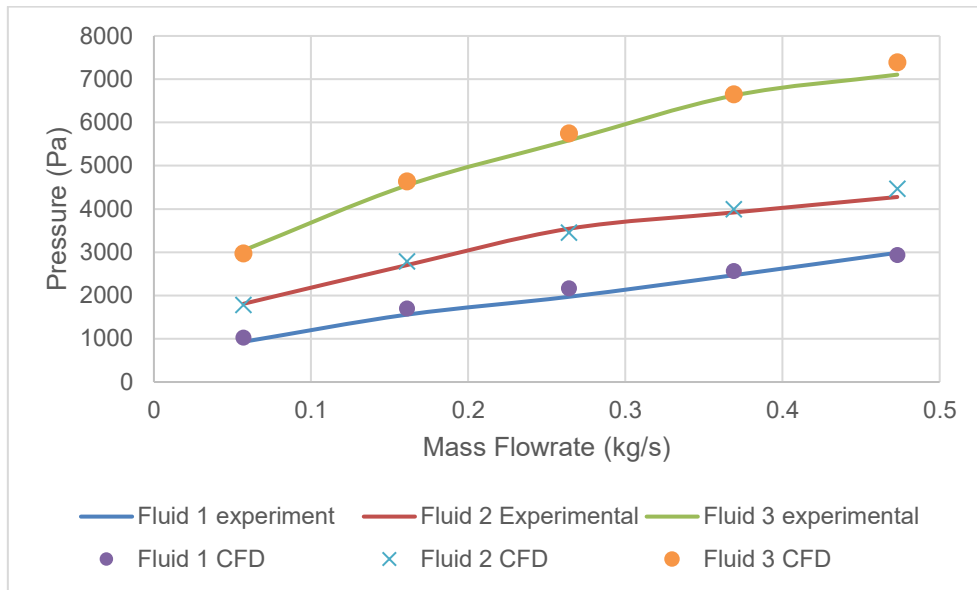


Figure 34. Pressure drop comparison of experimental data vs the CFD results for 3 different fluids at varying flowrates.

It was also necessary to examine the effect of eccentricity on the accuracy of the CFD simulations. Thus, simulations were also run for the same Fluid 3 shown above with a flow rate of 0.473 kg/s while varying the eccentricity. The results can be seen in Figure 35 below. The CFD model yields comparable results with the experimental data with a maximum error of 8% at the highest eccentricity case. Therefore, the computational model is validated for concentric and eccentric cases. Now, further studies and simulations can be run to study the displacement process of multiple fluids, and the results can be confidently assumed to be reliable and accurate.

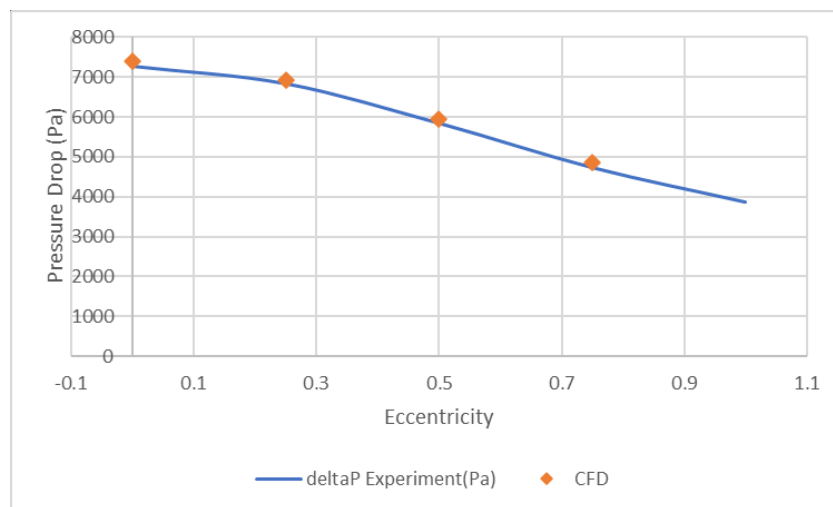


Figure 35. Pressure drop vs eccentricity comparison between experimental and CFD results for fluid 3 at a flowrate of 0.473 kg/s

5.2 Model Validation: Velocity

The CFD model was validated not only in terms of pressure drop, but also in terms of velocity. Moran & Savery conducted a series of experiments on eccentric annuli. They used annular sizes and materials typically employed in primary cementing operations. In these experiments, they were able to measure velocity difference between the wide and the narrow sides of the annulus by dividing the flow area at the top as shown in figure 36 below. The measurement method consisted of placing a barrel situated on a scale under each side's outlet. The time during which the fluid flowed into the barrel was measured using a manual timer, and the fluid volume was calculated based on the scale readings. Thus, the flowrate and subsequently the velocity could be calculated for the wide and narrow sides individually. The experimental setup can be seen in figure 36 below.



Figure 36. Experimental setup and measurement method for wide and narrow side velocities

CFD simulations were conducted using the same parameters used in these experiments. The geometry used consisted of typical industry casing sizes as seen in table below. Three different configurations were used to simulate different eccentricities seen in table below. In addition, the tests were conducted with three different fluids of varying rheological properties. The fluid properties are shown in table below. The tests were run for each fluid at every annular configuration with a flowrate sequence of 1 bpm to 5 bpm.

Table 7. Setup used consisting of typical industry casing sizes

	in	mm
OD	8.5	215.9
ID	7	177.8
length	84	2133.6

Table 8. Annular configurations used with different Standoffs

Standoff	82.10%	67.30%	54.60%
Center to center distance (mm)	3.41	6.23	8.65

Table 9. Fluid properties for the 3 test fluids used

Type	Density (ppg)	Density (kg/m³)	YP (Pa)	PV (cP)	PV (Pa.s)
Low Viscosity	13.1	1569.8	1.7	20.7	0.0207
Medium Viscosity	13.2	1581.8	5.9	43.2	0.0432
High Viscosity	13.2	1581.8	15.8	74.5	0.0745

In total, 45 simulations were run to obtain the results for all different models in the mentioned flowrate range. The velocity ratio was calculated and is defined as the ratio of wide side velocity to narrow side velocity. The velocities on the wide (V_w) and narrow (V_n) side were calculated as a steady-state, area-weighted average velocity. The results are compiled and shown in figures 37-38 below. The same trends and observations can be seen in the experimental results and the CFD simulations. However, the exact values of velocity and velocity ratios vary because of the different shape of the outlet as well as the experimental measurement technique which is highly prone to manual error. The CFD model was made as a normal annulus of the same dimensions as the experimental setup, but it did not include the apparatus created on the outlet to divide the flow. This was not necessary as the CFD model can give the wide and narrow side velocities without the need of complicating the geometry. This

change in geometry at the outlet certainly has a significant impact on the velocity magnitudes being measured in the experiments. And thus, there exists a difference in the velocity magnitudes between the experimental and CFD results.

Starting with figure 37, the results shown represent the velocity ratios for the 3 different fluids at 3 different eccentricities. The trends and observations are in agreement between the experimental and CFD results. Here, we can see that the effect of eccentricity on the velocity ratio is similar for all 3 fluids. As the eccentricity increases (i.e the standoff decreases), the velocity ratio will increase significantly as the fluid favors the wider side more pronouncedly. We can also see that this sharp variation in velocity ratio happens at low flowrates. As the flowrate increases, the velocity ratio stabilizes and the deviation caused by eccentricity effects becomes less pronounced.

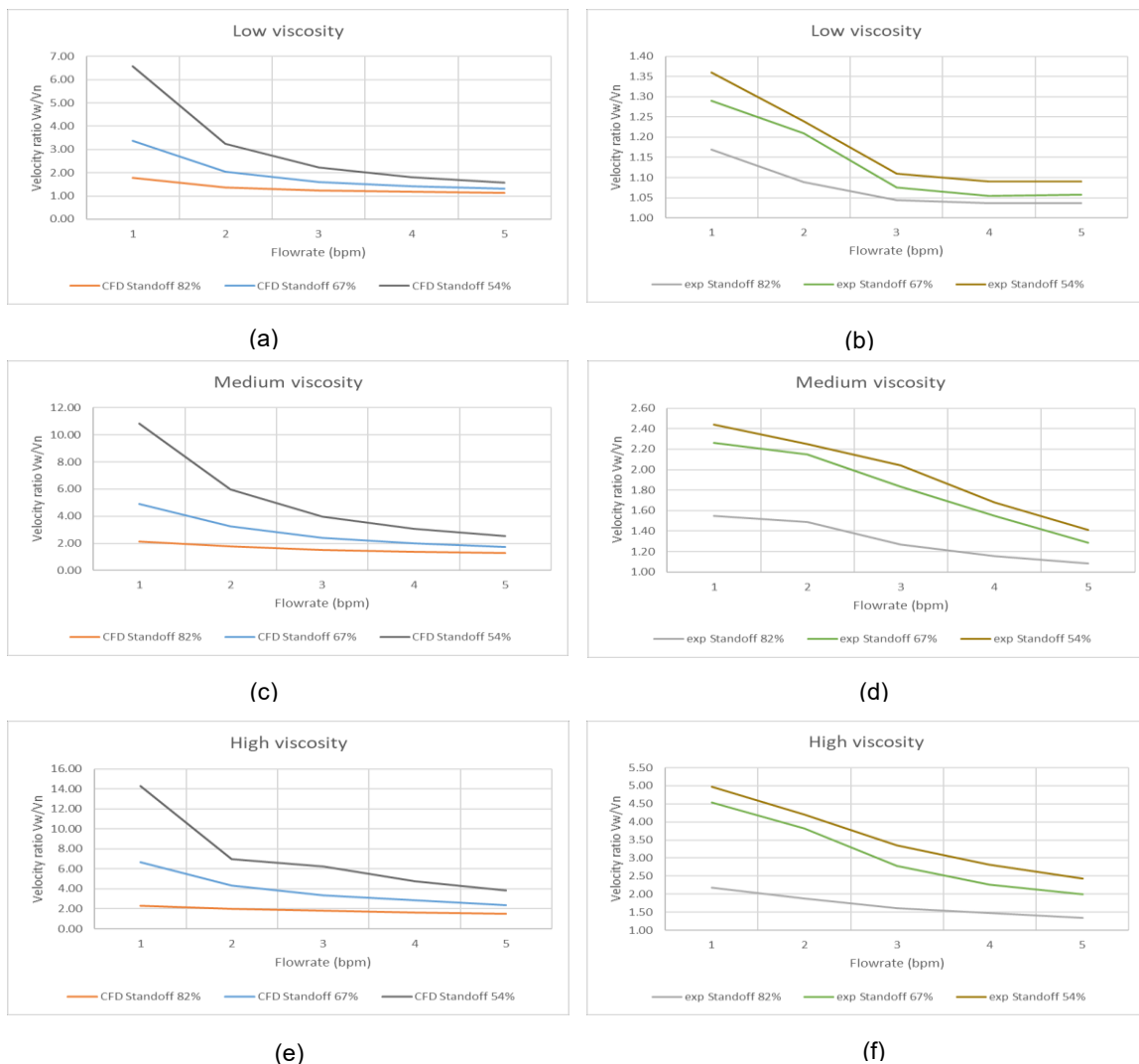
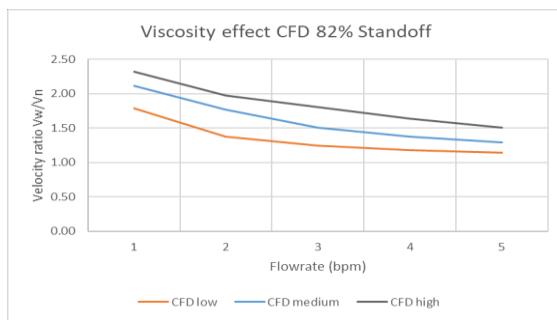
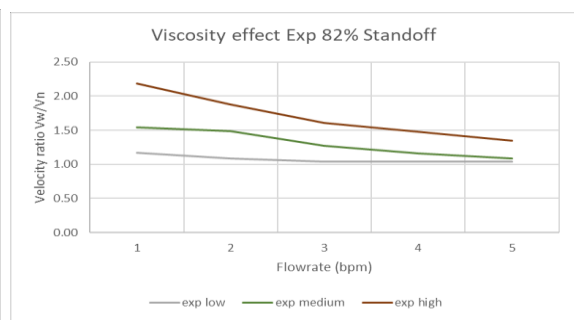


Figure 37. Eccentricity effect on velocity ratio for CFD and experimental results. a) low viscosity fluid CFD, b) low viscosity fluid experimental, c) medium viscosity fluid CFD, d) medium viscosity fluid experimental, e) high viscosity fluid CFD, f) high viscosity

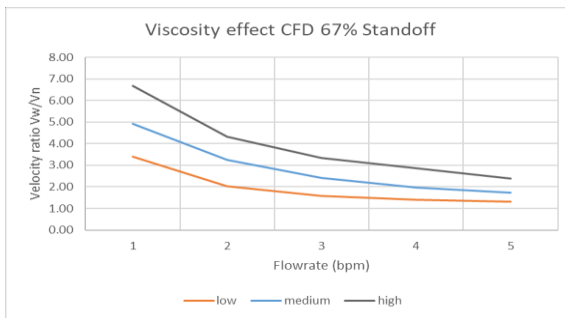
In figure 38 below, we can see the effect of the fluid viscosity at each annular configuration. Again we see the same trends and observations in the CFD and experimental results. The fluid viscosity has a big impact on the velocity ratio between the wide and narrow annular sides. As the fluid viscosity increases, the velocity ratio also increases because the viscous forces make it more difficult for the fluid to flow in the narrow side of the annulus. We also see that the effect of viscosity is amplified by the increase in eccentricity. The deviation in velocity ratio between the low viscosity and high viscosity fluids is much higher in the higher eccentricity configuration. We see here again that as the flowrate increases, the velocity ratio stabilizes, and the deviation caused by viscosity and eccentricity effects is reduced.



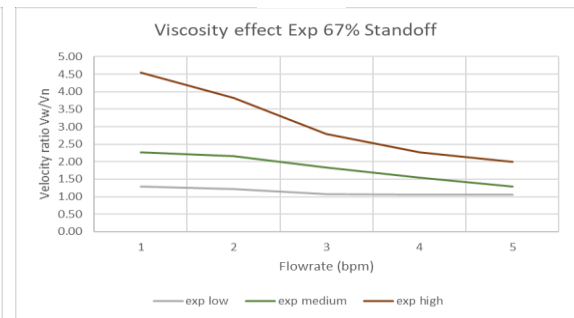
(a)



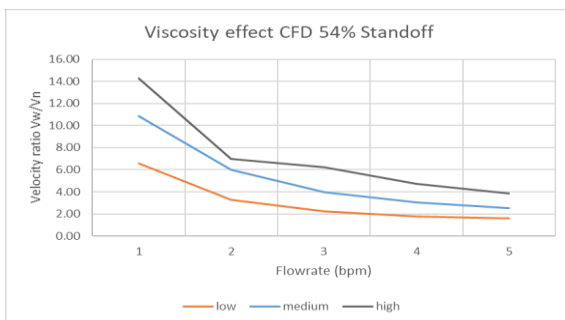
(b)



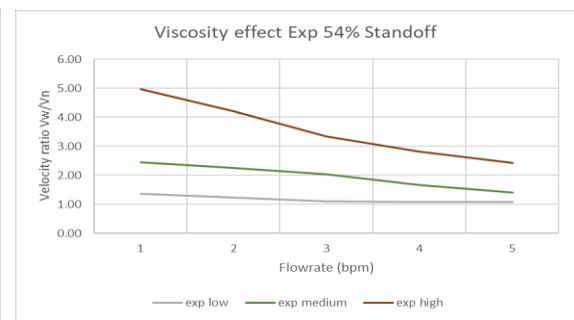
(c)



(d)



(e)



(f)

Figure 38. Viscosity effect on velocity ratio for CFD and experimental results. a) 82% standoff CFD, b) 82% standoff experimental, c) 67% standoff CFD, d) 67% standoff experimental, e) 54% standoff CFD, f) 54% standoff

Chapter 6

Multiphase Displacement Results & Discussion

The multiphase fluid displacement simulations were run as a transient model to capture the evolution of the fluid interface and displacement efficiency with time. The fluids were modelled using the Herschel-Bulkley rheology model and the flow regime was laminar. Turbulent flow was briefly studied but was not included in the scope of this thesis because of the many challenges it poses in real cementing operations such as ECD limitations, as well as the high uncertainty in turbulence modelling using CFD. The multiphase solver used for these simulations was the Volume of Fluid (VOF). The VOF solver models the two fluids as immiscible and solves a single set of momentum equations to track the volume fraction of each fluid in the computational domain. The VOF is used in cases where the fluid interface is of interest which is one of the main topics of this work. The simulations were run for the eccentric annuli presented in section 4.5 of this work. The density of the fluids used was in the range of 1000-2000 kg/m³, and the apparent viscosity was in the range of 10-100 cp. The main results and findings are presented and discussed in the following sections.

6.1 Eccentricity:

To further study the effect of eccentricity on fluid displacement in cementing operations, multiphase simulations were run for models with increasing eccentricity. These multiphase simulations represented a displacing fluid flowing through the inlet and displacing another fluid already present in the annulus referred to as a displaced fluid. As discussed before, the fluid favors the wide side of an eccentric annulus. This effect is exacerbated as eccentricity increases as we can see in the results shown in

figure 39 below. As the eccentricity increases, the fluid flows much more easily in the wide side of the annulus and the velocity difference between the wide and narrow sides increases drastically. We can see the homogenous distribution of the velocity in the concentric annulus. Then with increasing eccentricity, the velocity on the wider side increases, and that on the narrow side decreases until it reaches levels close to zero in highly eccentric cases.

This velocity difference will cause the interface between the displacing and displaced fluids to be elongated. This elongated interface can cause significant problems in the cement placement process. An elongated interface creates uncertainty in the position of the top of the cement. This can lead to improper placement and a lack of zonal isolation. Furthermore, an elongated interface can cause long mud channels to remain undisplaced on the narrow side of the annulus. This can create pathways for the formation fluids and causes the cement to fail as a well barrier element. We can see in figure 40 below how the interface between the fluid changes with increasing eccentricity. In the concentric case, the interface is short, and the fluid moves with the same velocity on both sides. However, in highly eccentric annuli, we can see that the fluid interface is much longer. The fluid on the narrow side is trailing that on the wide side by a long distance thus creating a large channel of undisplaced fluid on the narrow side.

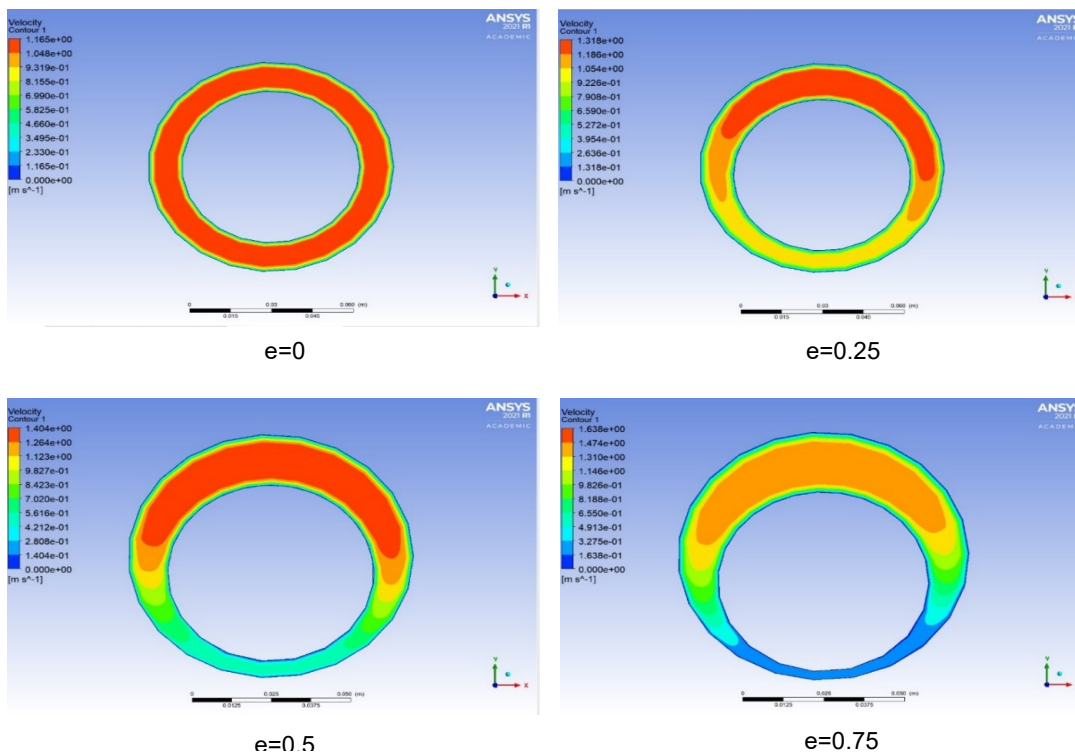


Figure 39. Velocity profile in cross section of models with different eccentricities

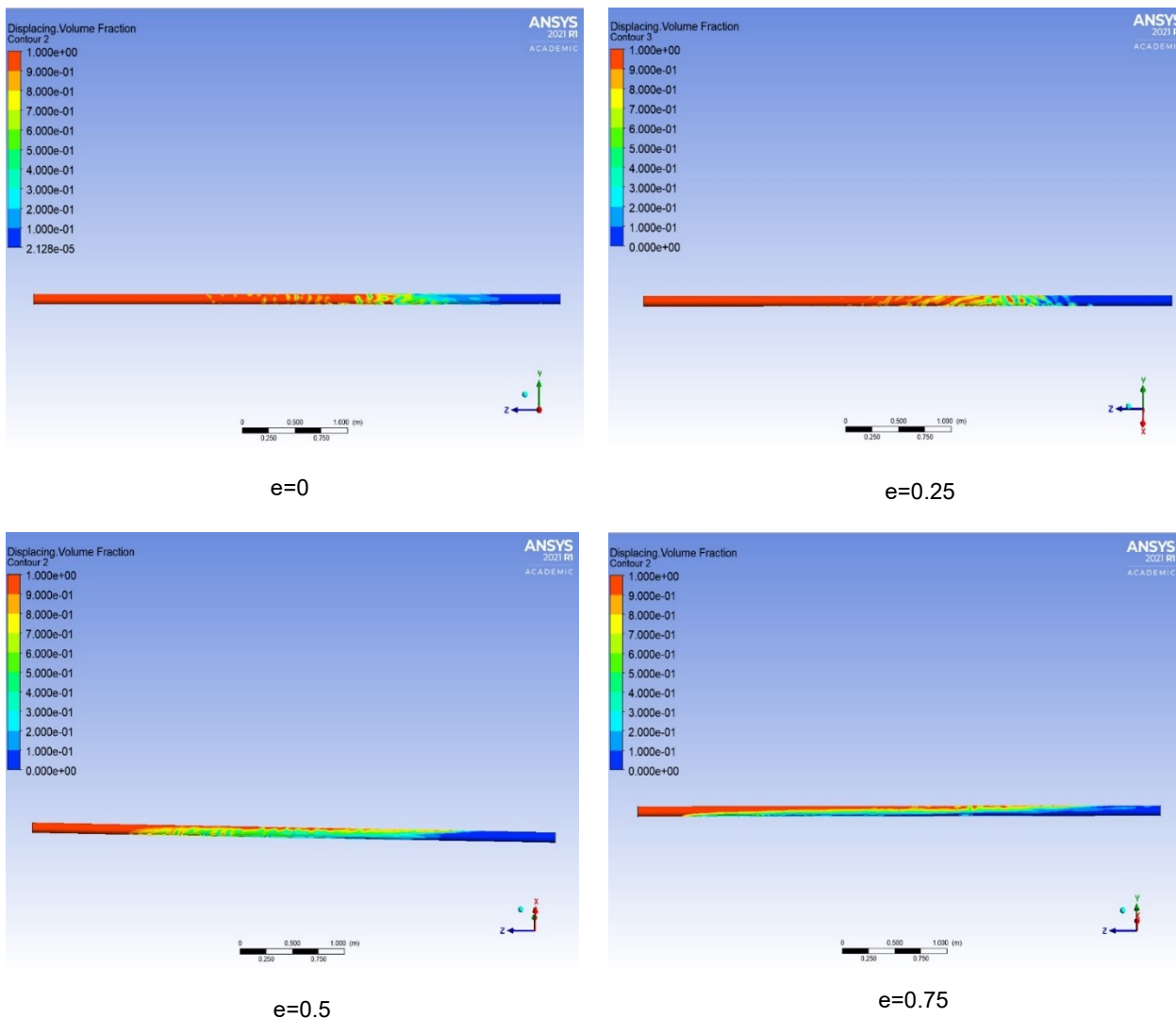


Figure 40. Fluid Interface in annuli with different eccentricities

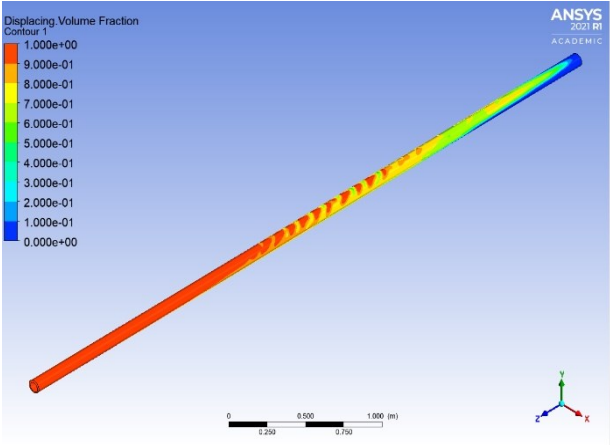
6.2 Density Vertical:

Another set of simulations was run to study the influence of density on the displacement process. A density ratio was defined as the density of the displacing fluid to that of the displaced fluid. All other fluid and flow parameters were left constant, and the density ratio was varied for numerous runs. The results of five main simulation runs are presented in table 10 below. This section covers the effect of density in a vertical annulus with gravity acting along the axis of the wellbore. Another measure was defined to test the success of the displacement which is the annular volume required to reach a 95% displacement efficiency. The annular volume is equivalent to the

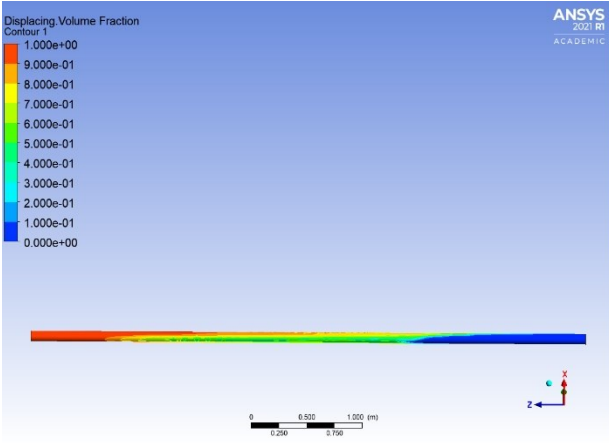
volume of 1 filled annulus corresponding to the geometry used. The displacement efficiency is defined as the volume percentage of displacing fluid in the annulus. We can see that the velocity difference between the wide and narrow sides does not change with density except when the displacing fluid is less dense than the displaced fluid. We can see that the volume of displacing fluid required to reach a 95% displacement efficiency is highest when the density ratio is below unity. Once the density ratio is higher than unity, the volume required remains constant. We can also see the effect of density on fluid intermixing and much channeling in figure 41 below. Increasing the density ratio from 0.92 to 1.2 significantly reduces fluid intermixing at the interface. Furthermore, we can see that the mud channel is also smaller on the narrow side of the annulus for a density ratio of 1.2 although the velocity difference between the wide and narrow sides is higher. On the other hand, we don't see any significant changes in the displacement when we increase the density ratio from 1.2 to 1.75. This illustrates the importance of maintaining a density hierarchy i.e. the displacing fluid must have a higher density than the fluid it displaces. This density hierarchy allows for reduced intermixing at the interface and ensures that the displacing fluid is dense enough to sweep the displaced fluid from the annular walls.

Table 10. Simulation results for studying the effect of density on the displacement process in a vertical annulus

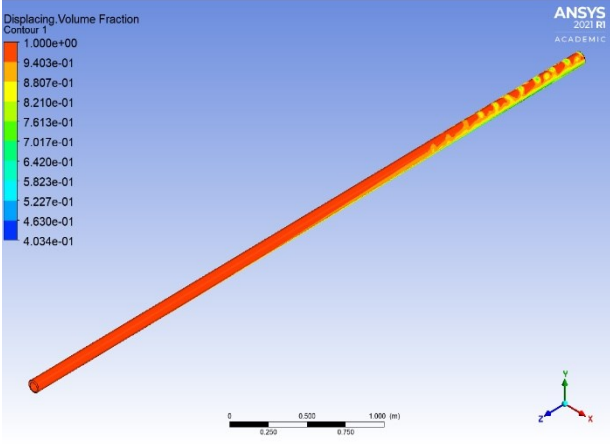
Density Ratio	Velocity Ratio V_w/V_n	Annular Volume to reach 95% DE
0.92	2.19	1.00
1.2	3.37	0.96
1.35	3.29	0.96
1.50	3.22	0.96
1.75	3.15	0.96



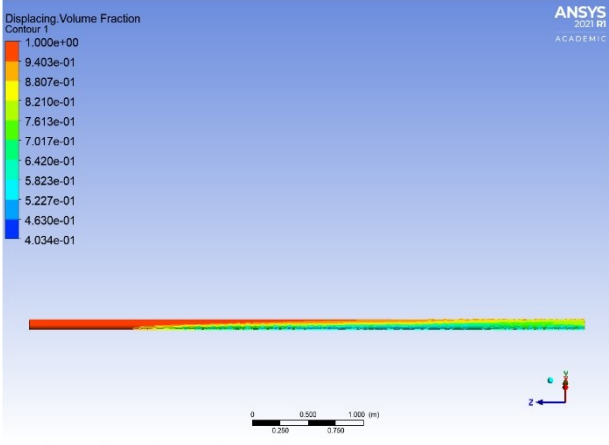
Density ratio = 0.92



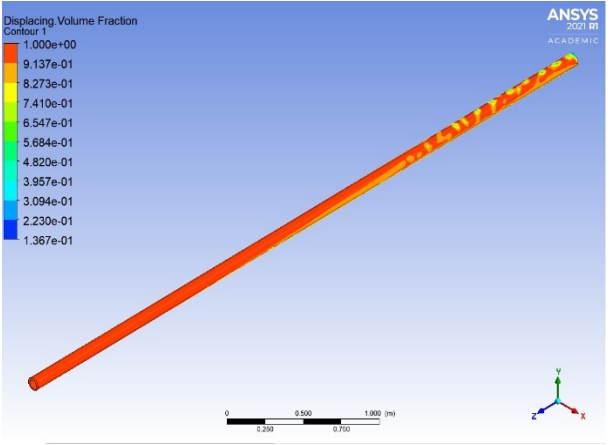
Density ratio = 0.92



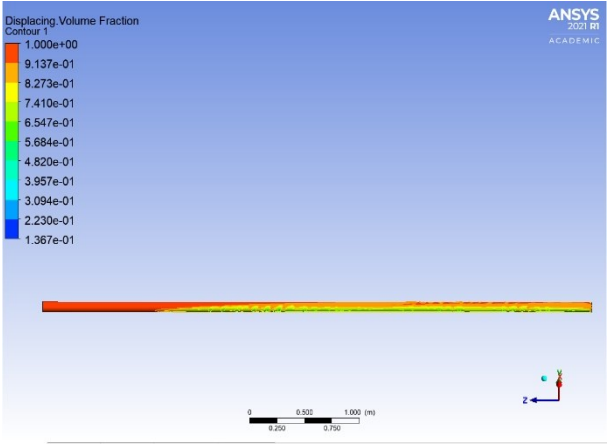
Density ratio = 1.2



Density ratio = 1.2



Density ratio = 1.75



Density ratio = 1.75

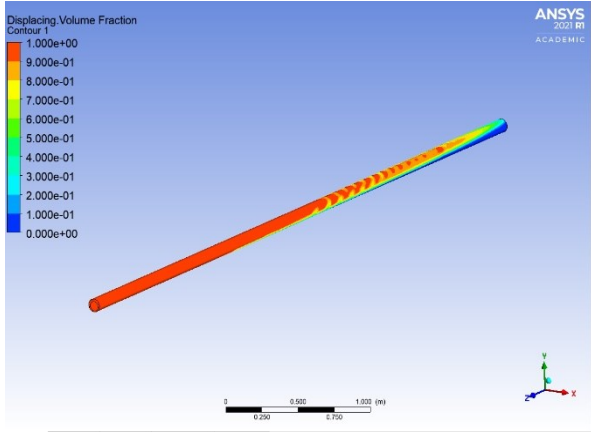
Figure 41. 3D graphic of the fluid displacement interface for varying densities in a vertical annulus.

6.3 Density Horizontal:

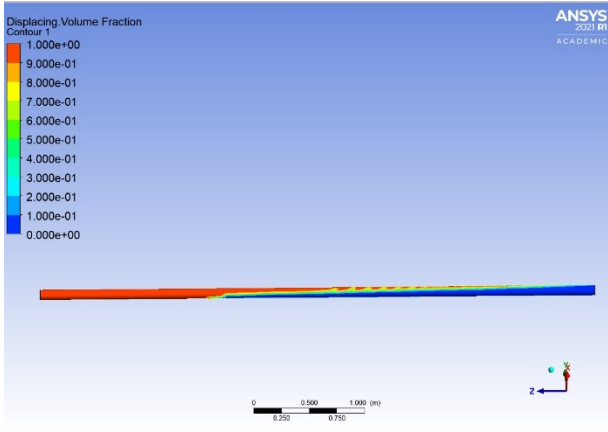
The effect of density was also studied in a horizontal annulus where buoyancy effects are much more pronounced. The same simulation cases were run as with the vertical annulus case to be able to compare the results. The same parameters were also used for analysis i.e., the velocity ratio between wide and narrow sides and the annular volume required to reach 95% displacement efficiency. The results for the horizontal case can be seen in table 11 below. For the calculated parameters, the exact same results are seen as the vertical case. However, the real difference can be seen when examining the fluid interface in the annulus in figure 42 below. We see here that the density contrast between the displacing and displaced fluids has a much more pronounced effect. Increasing the density contrast can allow the displaced fluid on the lower narrow side of the annulus to be more efficiently displaced as can be seen in figure 42 on the right-hand side. This effect is present because the flow in a horizontal annulus is typically buoyancy-dominated. Thus, as the density contrast between the displacing and displaced fluid gets higher, the denser displacing fluid will tend to move downward due to buoyancy into the narrow side of the annulus and the lighter fluid will move upward towards the wider side. This can offset the negative effect of eccentricity on the fluid interface and allow the denser displacing fluid to efficiently remove channels of displaced fluid that typically remain on the narrow side.

Table 11. Simulation results for studying the effect of density on the displacement process in a horizontal annulus

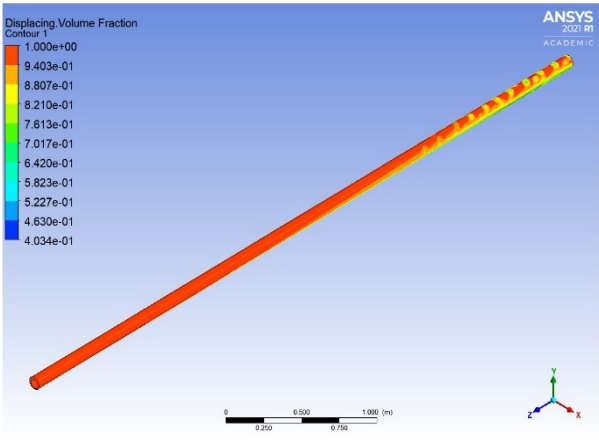
Density Ratio	Velocity Ratio V_w/V_n	Annular Volume to reach 95% DE
0.92	2.13	1.00
1.2	3.49	0.96
1.35	3.44	0.96
1.50	3.39	0.96
1.75	3.30	0.96



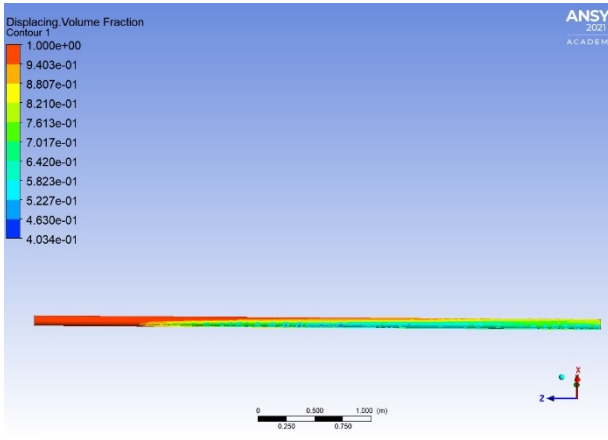
Density ratio = 0.92



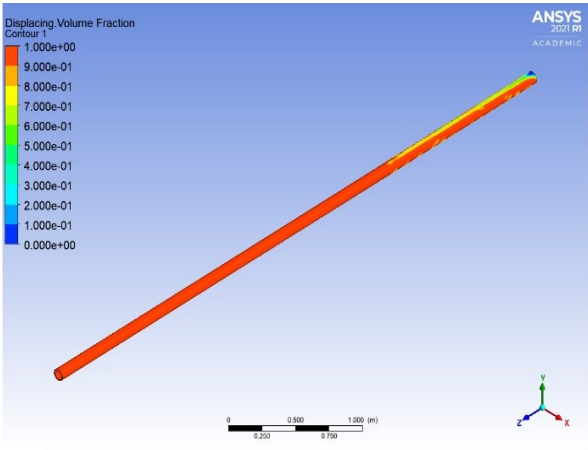
Density ratio = 0.92



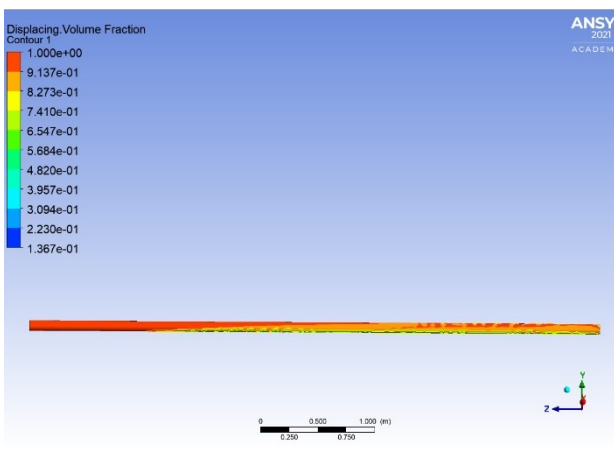
Density ratio = 1.2



Density ratio = 1.2



Density ratio = 1.75



Density ratio = 1.75

Figure 42. 3D graphic of the fluid displacement interface for varying densities in a horizontal annulus

6.4 Viscosity:

Another set of simulations was run to study the influence of viscosity on the displacement process. A viscosity ratio was defined as the apparent viscosity of the displacing fluid to that of the displaced fluid. All other fluid and flow parameters were left constant, and the viscosity ratio was varied for numerous runs. Similarly, the results of five main simulation runs are presented in table 12 below. The same parameters were used as before for comparison i.e., velocity ratio and annular volume required to reach 95% displacement efficiency, as well as visual analysis of the fluid interface. As we have seen before, as the viscosity of the fluids increases, the velocity difference between the wide and narrow sides of the annulus will also increase. So here we can see that higher viscosity ratios (which translate into more viscous displacing fluids) lead to higher velocity ratios and low fluid mobility on the narrow side of the annulus. We can see that the volume of displacing fluid required to reach a 95% displacement efficiency is very comparable for all cases. However, an important effect of viscosity is seen when we examine the fluid interface. We can see in figure 43 that the fluid interface is unstable and broken in the case of a 0.97 viscosity ratio. On the other hand, we see much more intermixing on the annulus wall in the case of a 2.5 viscosity ratio because the high viscosity is creating an instability and preventing the fluid from flowing completely at the wall. Thus, there needs to be a tradeoff between maintaining a stable interface, preventing intermixing, and avoiding very high velocity ratios. For the middle case of viscosity ratio equal to 1.5, we can see that the fluid interface is fairly stable, and the velocity ratio has still not drastically increased. Therefore, a viscosity hierarchy must be maintained first to create a stable interface, but the viscosity should not be increased to a level where it starts to create a very elongated interface and intermixing problems. It is difficult to provide exact ranges for viscosity to optimize the fluid displacement because each cementing job is unique, and a multitude of different parameters play a role in its success. Consequently, CFD can be an important tool as it allows specialized solutions and guidelines for individual cases which leads to better overall understanding and design.

Table 12. Simulation results for studying the effect of viscosity on the displacement process in an eccentric annulus

Viscosity Ratio	Velocity Ratio V_w/V_n	Annular Volume to reach 95% DE
0.97	1.11	1.28
1.5	1.22	1.26
2	1.91	1.29
2.5	3.02	1.32
3.00	3.63	1.31

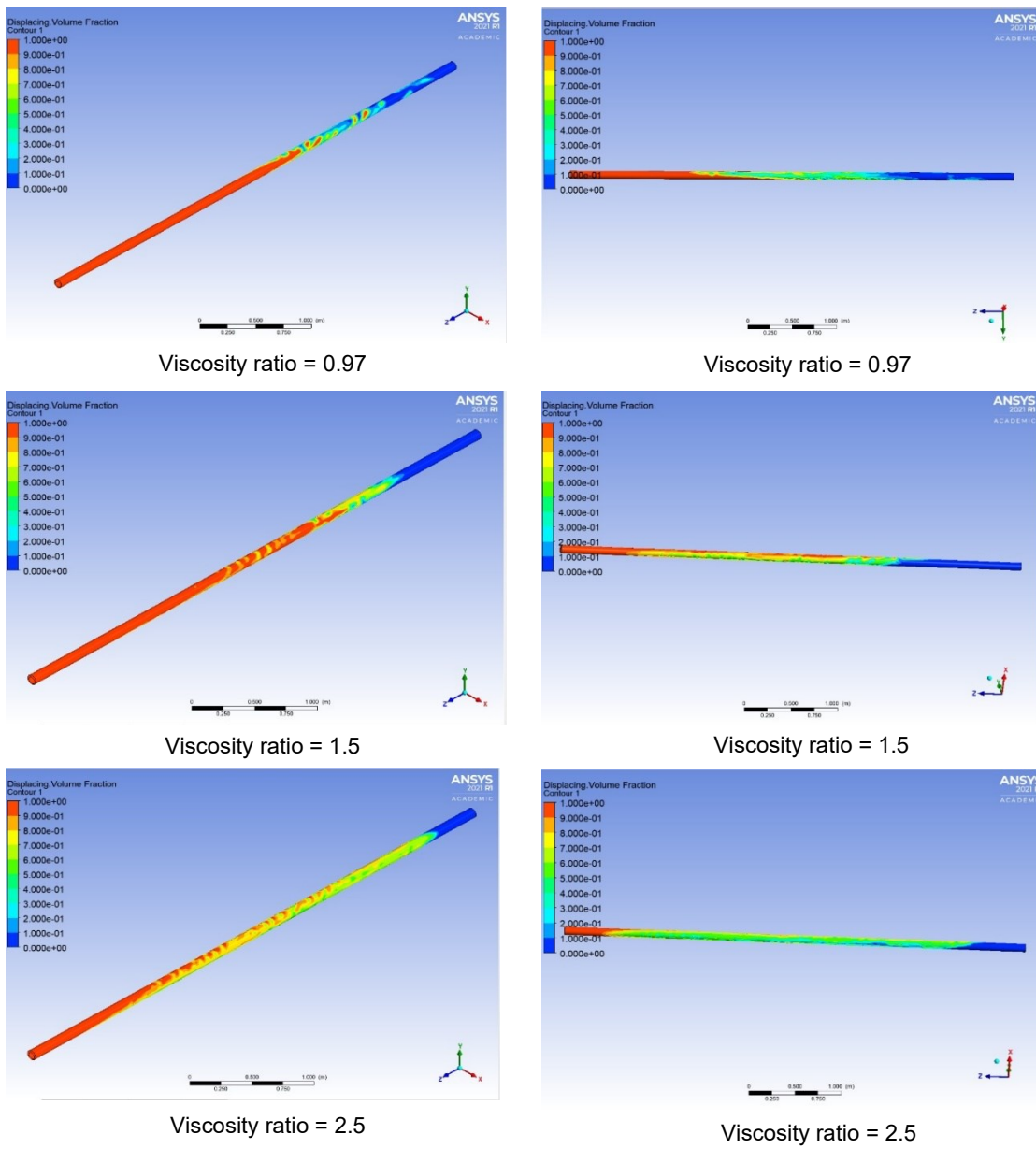


Figure 43. 3D graphic of the fluid displacement interface for varying viscosities in an eccentric annulus

6.5 Flowrate:

Another set of simulations was run to study the influence of flowrate or pump rate on the displacement process. A set of flow rates equivalent to ones typically used in the industry for cementing operations were used for the study. All other fluid and flow parameters were left constant, and the flowrate was varied for numerous runs. The results of the simulation runs are presented in table 13 below. The same parameters were used as before for comparison i.e., velocity ratio and annular volume required to reach 95% displacement efficiency, visual analysis of the fluid interface, and Reynold's number was introduced as a dimensionless parameter would be a better fit for comparison and establishing guidelines.

Table 13. Simulation results for studying the effect of flowrate on the displacement process in an eccentric annulus

Flowrate (gpm)	Reynold's Number Re	Velocity Ratio Vw/Vn	Annular Volume to reach 95% DE
6.71	241	4.87	1.19
13.41	844	3.27	1.01
16.77	1262	2.63	1.02
20.12	1752	2.11	1.05
26.82	2938	1.52	1.26
30.18	3630	1.40	1.25

We can see that the velocity ratio decreases as the flowrate increases which is in line with the observations made in Moran & Savery (2007) mentioned in the velocity validation section. We also see that the optimum annular volume required to reach 95% displacement efficiency is for Reynold's number in the range of 750-2000. Flowrates lower or higher than this range tend to require more volumes to reach 95% displacement efficiency. Furthermore, we notice that the flowrate has an important effect on the intermixing of the fluids at the interface. As the flowrate increases, the interface tends to become more unstable, and more intermixing occurs. So yet again, a tradeoff must be made between an optimum velocity ratio and minimizing intermixing of the fluids. Too low flowrates are not desirable as they require more time and volume to complete the job successfully. Thus, the flowrates in the range mentioned previously

are a good starting point for the design and more studies can be made on individual cases to further optimize the displacement process.

As for turbulent flow, research has not shown any significant improvement in the displacement process by pumping the fluids in a turbulent flow regime. In this work, turbulent flow has not been explicitly studied but we have seen that increasing the flow rate above a certain threshold deteriorated the displacement process. Furthermore, increasing flowrates to reach a turbulent flow regime poses ECD and fracture pressure issues as the fluids pumped are usually highly dense and viscous. Regarding CFD, a universal turbulence model cannot be established and still remains a topic of debate in the CFD community. This leads to the use of different turbulence models that require rigorous validation and verification studies which raises many questions about the accuracy and reliability of these turbulent solvers. Therefore, the use of turbulent flow in the displacement process was not extensively studied in this work.

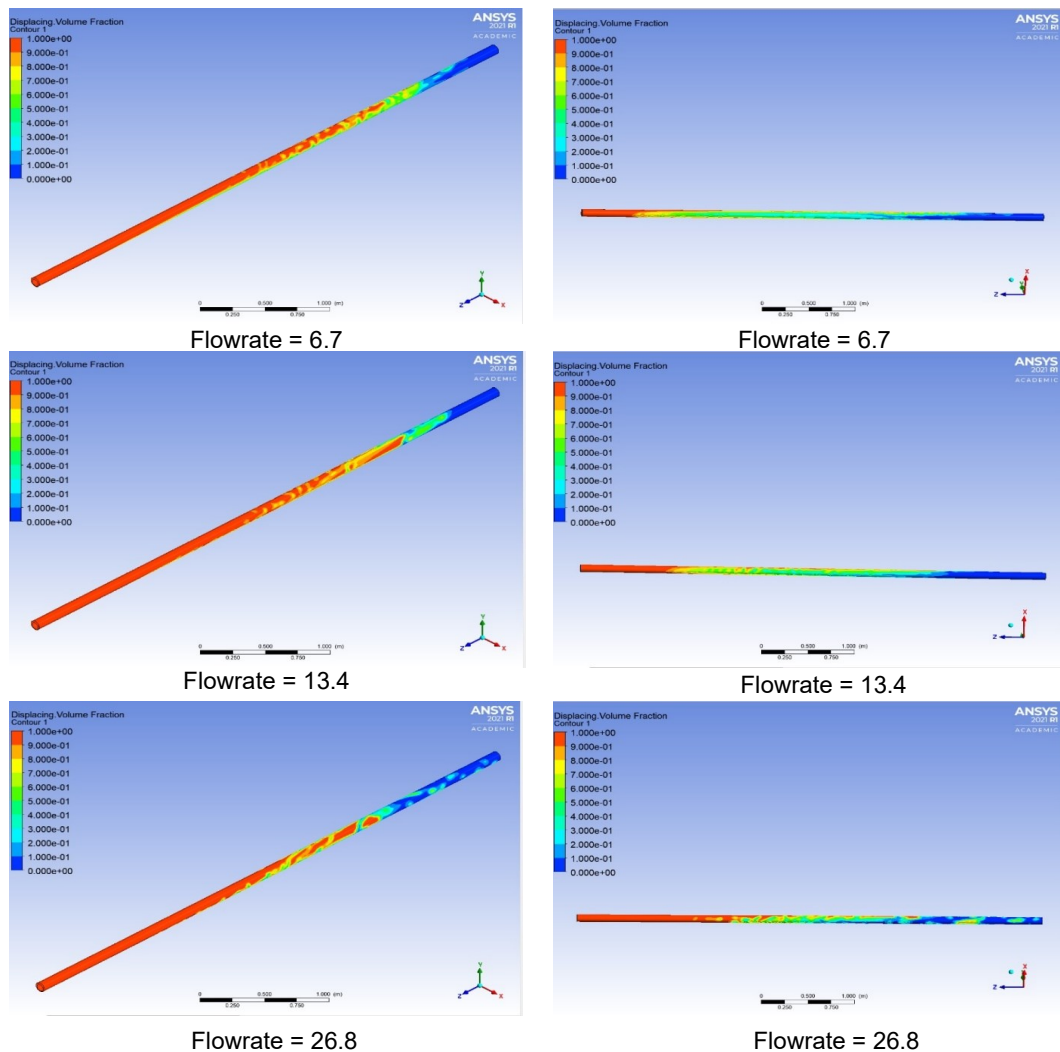


Figure 44. 3D graphic of the fluid displacement interface for varying flowrates in an eccentric annulus

6.6 Casing Rotation:

Another set of simulations was run to study the influence of casing rotation on the displacement process. A rotational speed was introduced to the inner pipe. All other fluid and flow parameters were left constant, and the casing rotational speed was varied for numerous runs. The results of the simulation runs are presented in table 14 below. The same parameters were used as before for comparison i.e., velocity ratio and annular volume required to reach 95% displacement efficiency, and visual analysis of the fluid interface. We can see that the velocity ratio decreases as casing rotation is introduced. The rotation offsets the velocity profile and establishes a more homogeneous velocity distribution between the wide and narrow sides of the annulus as can be seen in figure 45. This effect has a positive influence on the displacement process as it allows the displaced fluid in the narrow side of the annulus to be displaced effectively as can be seen in figure 46. Thus, casing rotation is an important parameter that can be utilized to counteract, to a certain extent, the effect of eccentricity and allow for a more efficient displacement process.

Table 14. Simulation results for studying the effect of casing rotation on the displacement process in an eccentric annulus

Rotation (rpm)	Velocity Ratio V_w/V_n	Annular Volume to reach 95% DE
0	2.07	1.01
10	1.92	0.96
20	1.67	0.96
50	1.36	0.96

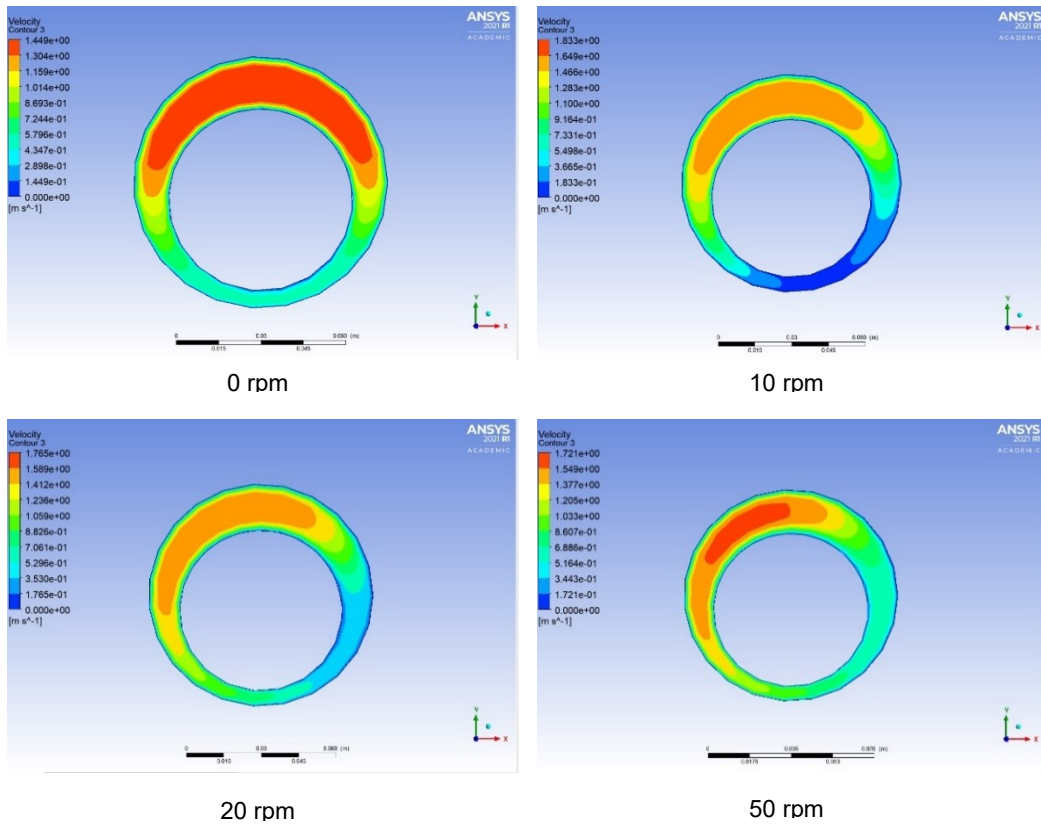


Figure 45. Velocity profile for varying casing rotation speeds in an eccentric annulus

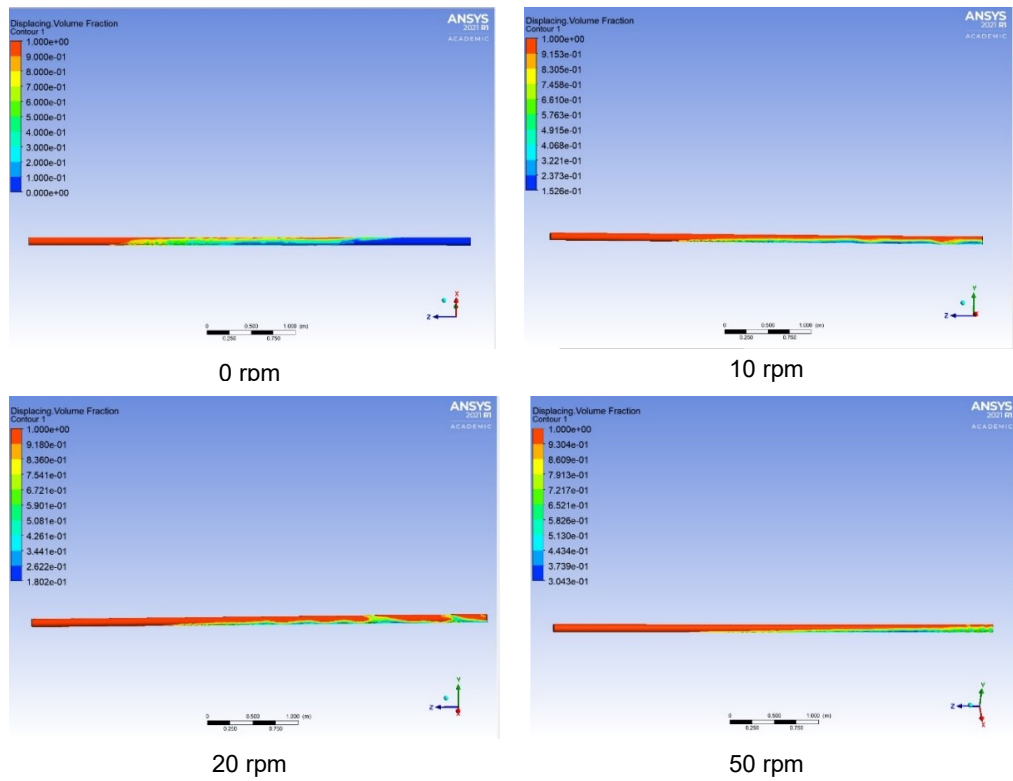


Figure 46. 3D graphic of the fluid displacement interface for varying casing rotation speeds in an eccentric annulus

Chapter 7

Conclusion

7.1 Summary

This work presented the development of a state-of-the-art CFD model for fluid displacement in cementing operations which can simulate 3D laminar flow of non-Newtonian wellbore fluids in an eccentric annulus. This CFD model was validated against two sets of experimental data which proved that it could create a reliable representation of pressure, velocity, and flow characteristics in eccentric annuli. The main findings presented in this work are as follows:

1. Casing eccentricity has a large impact on the success of the cementing job. The eccentricity should be minimized to tolerable limits wherever possible using centralizers. The complexity of the cementing job increases with increasing eccentricity as larger portions of drilling fluid remain undisplaced on the narrow side of the annulus.
2. The displacing and displaced fluids' properties also play an important role in the displacement process. An improper design of the fluid properties results in excessive mixing and channeling and would require substantially more volumes of displacing fluid to reach the high levels of displacement efficiency. Maintaining density and viscosity hierarchy between the displacing and displaced fluids is also of utmost importance. The fluid properties are also able to counteract the negative effects of high eccentricity to a certain extent.
3. The flowrate rate of the displacing fluid needs to be optimized as well. There must be a tradeoff between fluid intermixing and the velocity ratio between the wide and narrow sides of the annulus. Higher flow rates yield velocity ratios closer to unity which results in a less elongated fluid interface. However, higher

flow rates can increase fluid intermixing to a large extent. Thus, an optimum flow rate should be established as a tradeoff between these two effects.

4. Casing rotation proved to be a beneficial tool for increasing the success of the cementing job. This casing rotation greatly assists in reducing the contrast in velocity profiles between the wide and narrow sides of the annulus. Thus, it can result in a more homogenous and less elongated fluid interface and a better displacement in eccentric annuli.

7.2 Future Work

Additional work can be done in the future to further increase the accuracy and applicability of this CFD model including:

1. The multiphase displacement simulations can be validated using experimental data. This work is already in progress as part of a digital flow loop project at the DPE. The simulations here represent a digital model of the experimental flow loop to be used, which provides a highly accurate and reliable one-to-one validation of the CFD multiphase model.
2. Increasing the complexity of the geometry by adding casing roughness and wellbore tortuosity can result in a more realistic representation of wellbore conditions compared to the smooth wellbore assumption made in this work.
3. After the multiphase validation work is complete, the CFD model can be scaled up to typical wellbore sizes and lengths. This would allow highly accurate and reliable planning and optimization of cementing jobs using a one-to-one digital representation of the displacement process through a wellbore.

References

- ANSYS Inc., Ansys fluent 12.0/12.1 documentation. 2017.
- Beirute, R. M., & Flumerfelt, R. W. (1977). Mechanics of the displacement process of drilling muds by cement slurries using an accurate rheological model. *All Days*. <https://doi.org/10.2118/6801-ms>
- Benge, G. (2015). Cement evaluation—A risky business. *SPE Drilling & Completion*, 30(04), 322-326. <https://doi.org/10.2118/170712-pa>
- Biezen, E., Van der Werff, N., & Ravi, K. (2000). Experimental and numerical study of drilling fluid removal from a horizontal Wellbore. *All Days*. <https://doi.org/10.2118/62887-ms>
- Blazek, J. (2015). *Computational fluid dynamics: Principles and applications*. Butterworth-Heinemann.
- Couturler, M., Guillot, D., Hendriks, H., & Callet, F. (1990). Design rules and associated spacer properties for optimal mud removal in eccentric annuli. *All Days*. <https://doi.org/10.2118/21594-ms>
- Crain, E. R. (2006). *Crain's Petrophysical handbook*.
- Cusdin, P., & Mueller, J. D. (2003). Automatic differentiation and sensitivity analysis methods for computational fluid dynamics.
- Dai, H. (2021). Displacement efficiency. *Applied Well Cementing Engineering*, 435-480. <https://doi.org/10.1016/b978-0-12-821956-0.00006-7>
- Drilling fluids rheological models*. (2020, April 14). Drilling Course. <https://www.drillingcourse.com/2020/04/drilling-fluids-rheological-models.html>
- Drilling Manual. (2021, November 23). *Cement bond log guide for cementing evaluation*. <https://www.drillingmanual.com/cement-bond-log/>

- Foroushan, H. K., Lund, B., Ytrehus, J. D., & Saasen, A. (2021). Cement placement: An overview of fluid displacement techniques and modelling. *Energies*, 14(3), 573. <https://doi.org/10.3390/en14030573>
- Foroushan, H. K., Ozbayoglu, E., Gomes, P. J., Miska, S., & Yu, M. (2018). Mud-cement displacement in eccentric annuli: Analytical solution, instability analysis, and computational fluid dynamics simulations. *Day 1 Tue, March 06, 2018*. <https://doi.org/10.2118/189646-ms>
- Harris, K. (2021). Cement job evaluation. *Applied Well Cementing Engineering*, 523-567. <https://doi.org/10.1016/b978-0-12-821956-0.00010-9>
- Jamshed, S. (2015). Introduction to CFD. *Using HPC for Computational Fluid Dynamics*, 1-20. <https://doi.org/10.1016/b978-0-12-801567-4.00001-5>
- K. Foroushan, H., M. Ozbayoglu, E., & J. Gomes, P. (2020). How realistic is the calculated cementing displacement efficiency? *Day 1 Tue, March 03, 2020*. <https://doi.org/10.2118/199553-ms>
- Kroken, W., Sjaholm, A., & Olsen, A. (1996). Tide flow: A low rate density driven cementing technique for highly deviated wells. *All Days*. <https://doi.org/10.2118/35082-ms>
- Liu, G. (2021). *Applied well cementing engineering*. Gulf Professional Publishing.
- Lockyear, C. F., Ryan, D. F., & Gunningham, M. M. (1990). Cement channeling: How to predict and prevent. *SPE Drilling Engineering*, 5(03), 201-208. <https://doi.org/10.2118/19865-pa>
- McLean, R., Manry, C., & Whitaker, W. (1967). Displacement mechanics in primary cementing. *Journal of Petroleum Technology*, 19(02), 251-260. <https://doi.org/10.2118/1488-pa>
- Mesh generation & pre-processing*. (n.d.). CFD Online. <https://www.cfd-online.com/Forums/mesh-generation/>
- Mitchell, R. F., & Lake, L. W. (2006). *Petroleum engineering handbook. Vol.2. Drilling engineering*.
- Moran, L. K., & Savery, M. R. (2007). Fluid movement measurements through eccentric annuli: Unique results uncovered. *All Days*. <https://doi.org/10.2118/109563-ms>
- Nelson, E. B. (2012). *Well Cementing Fundamentals*. Schlumberger.
- NORSOK D-010, 2013. *Well Integrity in Drilling and Well Operations*. Standard Norge, Oslo.

- Parker, P., Ladd, B., Ross, W., & Wahl, W. (1965). An evaluation of a primary cementing technique using low displacement rates. *All Days*. <https://doi.org/10.2118/1234-ms>
- Ravi, K., Beirute, R., & Covington, R. (1992). Erodability of partially dehydrated gelled drilling fluid and filter cake. *All Days*. <https://doi.org/10.2118/24571-ms>
- Rheology*. (n.d.). The Schlumberger Oilfield Glossary | Oilfield Glossary. <https://glossary.oilfield.slb.com/en/terms/r/rheology>
- Sevillano, L. C., De Andrade, J., Sangesland, S., & Stanko, M. (2016). Thermal effects on Subsea Wellhead fatigue during Workover operations. <https://doi.org/10.2118/180065-ms>
- Stoevesandt, B., Steinfeld, G., & Höning, L. (2017). Computational Fluid Dynamics.
- Vita, P. Computational Continuum Mechanics Lecture Notes
- Zhigarev, V. A., Neverov, A. L., Guzei, D. V., & Pryazhnikov, M. I. (2017). Studying laminar flows of power-law fluids in the annular channel with eccentricity. *Journal of Physics: Conference Series*, 899(9), 092016. <https://doi.org/10.1088/1742-6596/899/9/092016>

List of Figures

Figure 1. Typical Well Schematic (Sevillano et al., 2016)	14
Figure 2. Primary cementing job with two-plug technique (Nelson, 2012).....	18
Figure 3. Pressure test (Harris, 2021).....	23
Figure 4. Cement Bond Log (Drilling Manual, 2021)	25
Figure 5. Temperature Log (Crain, 2006)	25
Figure 6. Displacement efficiency illustration (Dai, 2021).....	26
Figure 7. Effect of power law index on velocity profile and displacement efficiency (Foroushan et al, 2021)	28
Figure 8. Pipe Stand-Off Ratio Definition (Liu, 2021)	28
Figure 9. Visualization on the effect of casing eccentricity on displacement efficiency (Liu, 2021).....	29
Figure 10. Effect of casing rotation on displacement efficiency (Liu, 2021).....	30
Figure 11. Forces acting on the fluids during displacement in an eccentric inclined annulus (Lockyear et al, 1990)	33
Figure 12. Illustration of channeling and mixing during displacement between a denser fluid (Fluid A) and a lighter fluid (Fluid B) (Lockyear et al, 1990).....	34
Figure 13. Illustration of testing facility (a) and test section (b) (Foroushan et al., 2020)	36
Figure 14. Illustration of experimental setup for measurement of erodability of PDG drilling fluid (Ravi et al, 1992).	38
Figure 15. Schematic of conductivity measurement experimental setup (Biezen et al, 2000).....	39
Figure 16. Sector division of an eccentric annulus (Mclean et al, 1967).....	40
Figure 17. Displacement process as depicted by Beirute and Flumerfelt, 1977.	41
Figure 18. Unwrapped eccentric annulus (Foroushan et al, 2018).....	42
Figure 19. Eccentric annulus (left), Unwrapped eccentric annulus (right) (Foroushan et al, 2018).....	42
Figure 20. Illustration of fluid domain and interface (Foroushan et al, 2018).....	43
Figure 21. CFD process (Blazek, 2015).....	46
Figure 22. Finite control volume in a flow field ((Blazek, 2015)	48
Figure 23. Shear stress vs shear rate for different rheological models (Schlumberger Oilfield Glossary).....	52
Figure 24. Schematic for comparison of a geometrical domain against its equivalent numerical grid.....	53
Figure 25. FVM of 2D grid (Stoevesandt et al, 2017).....	56
Figure 26. Mesh Classifications (Vita, 2020).....	57
Figure 27. Mesh nomenclature (Vita, 2020).....	58
Figure 28. Cylindrical pipe structured mesh. (Mesh Generation & Pre-processing, CFD Online).....	59
Figure 29. Unstructured mesh (Cusdin & Mueller, 2003)	59
Figure 30. Computational mesh for 5-meter annulus.	63
Figure 31. Generated mesh for different eccentricities: a) concentric, b) $e=0.25$, c) $e=0.5$, d) $e=0.75$	63
Figure 32. Grid convergence study, pressure drop vs mesh cell count.	65
Figure 33. Computational mesh generated for the validation simulations with experimental data from Zhigarev et al.....	68
Figure 34. Pressure drop comparison of experimental data vs the CFD results for 3 different fluids at varying flowrates.....	69
Figure 35. Pressure drop vs eccentricity comparison between experimental and CFD results for fluid 3 at a flowrate of 0.473 kg/s.....	69

Figure 36. Experimental setup and measurement method for wide and narrow side velocities	70
Figure 37. Eccentricity effect on velocity ratio for CFD and experimental results. a) low viscosity fluid CFD, b) low viscosity fluid experimental, c) medium viscosity fluid CFD, d) medium viscosity fluid experimental, e) high viscosity fluid CFD, f) high viscosity 72	
Figure 38. Viscosity effect on velocity ratio for CFD and experimental results. a) 82% standoff CFD, b) 82% standoff experimental, c) 67% standoff CFD, d) 67% standoff experimental, e) 54% standoff CFD, f) 54% standoff.....	73
Figure 39. Velocity profile in cross section of models with different eccentricities.....	76
Figure 40. Fluid Interface in annuli with different eccentricities.....	77
Figure 41. 3D graphic of the fluid displacement interface for varying densities in a vertical annulus.....	79
Figure 42. 3D graphic of the fluid displacement interface for varying densities in a horizontal annulus.....	82
Figure 43. 3D graphic of the fluid displacement interface for varying viscosities in an eccentric annulus	83
Figure 44. 3D graphic of the fluid displacement interface for varying flowrates in an eccentric annulus	85
Figure 45. Velocity profile for varying casing rotation speeds in an eccentric annulus	87
Figure 46. 3D graphic of the fluid displacement interface for varying casing rotation speeds in an eccentric annulus	87

List of Tables

Table 1. Test section specifications.	36
Table 2. Mesh quality based on Min OQ and Max Skewness (Ansys Inc., 2017).....	61
Table 3. Annulus dimensions and fluid and flow properties.....	62
Table 4. Assessment of mesh quality using mesh metrics	64
Table 5. Rheological properties of drilling fluids used in Zhigarev et al. (2011)	67
Table 6. Flow rate sequence of experiments done by Zhigarev et al. (2011)	68
Table 7. Setup used consisting of typical industry casing sizes	71
Table 8. Annular configurations used with different Standoffs.....	71
Table 9. Fluid properties for the 3 test fluids used	71
Table 10. Simulation results for studying the effect of density on the displacement process in a vertical annulus	78
Table 11. Simulation results for studying the effect of density on the displacement process in a horizontal annulus	80
Table 12. Simulation results for studying the effect of viscosity on the displacement process in an eccentric annulus.....	83
Table 13. Simulation results for studying the effect of flowrate on the displacement process in an eccentric annulus.....	84
Table 14. Simulation results for studying the effect of casing rotation on the displacement process in an eccentric annulus.....	86